Biodegradable magnesium matrix composites for bone fixation devices

Naddaf Dezfuli, Sina

DOI
10.4233/uuid:2c127d9b-17ab-449e-8e16-f93b10f55158

Publication date
2018

Document Version
Final published version

Citation (APA)
Naddaf Dezfuli, S. (2018). *Biodegradable magnesium matrix composites for bone fixation devices*. [Dissertation (TU Delft), Delft University of Technology]. https://doi.org/10.4233/uuid:2c127d9b-17ab-449e-8e16-f93b10f55158

Biodegradable magnesium matrix composites for bone fixation devices

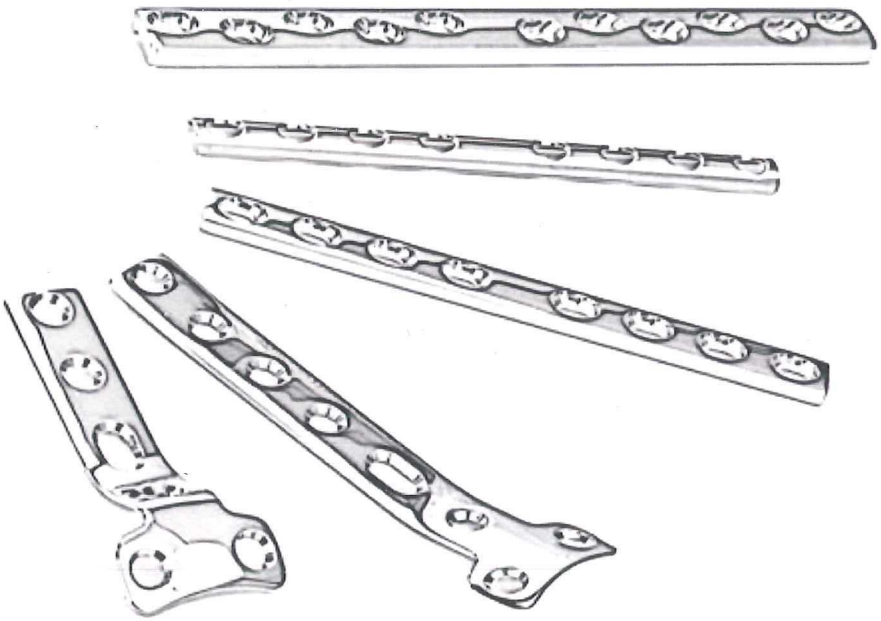

Sina Naddaf Dezfuli

Propositions

Accompanying the thesis

By Sina NaddafDezfuli

1. Future research projects should focus on in-vivo behavior of existing Mg-based composites before attempting to design and fabricate new ones.
2. Having a daily routine is important to be productive and breaking one is important to be inventive.
3. A mandatory educational program for PhDs would improve their knowledge and skills more than an elective educational program.
4. PhD candidates should not be evaluated based on the number but on the quality of their publications.
5. Ambition is the key element of being a renowned scholar.
6. Project-based research improves technology but does not do justice to curiosity-driven science.
7. Open-access journal publishers should shift their library to a block-chain based platform to make their articles available to everyone everywhere.
8. Morality is a result of human experience of immorality.
9. The only way to intellectually compete with AI in the future is to integrate our brain with AI.

These propositions are regarded as opposable and defendable, and have been approved as such by the supervisor and promoter, Dr. Jie Zhou and Prof.dr. F.C.T van der Helm.

Biodegradable magnesium matrix composites for bone fixation devices

Sina NADDAF DEZFULI

Biodegradable magnesium matrix composites for bone fixation devices

Proefschrift

ter verkrijging van de graad van doctor aan de Technische Universiteit Delft, op gezag de Rector Magnificus Prof.dr.ir. T.H.J.J. van der Hagen voorzitter van het College voor Promoties, in het openbaar te verdedigen op woensdag 13 juni 2018 om 10.00 uur

door

Sina NADDAF DEZFULI

Master of Science in Biomaterials

Sharif University of Technology, Teheran, Iran

geboren te New Delhi, India

Dit proefschrift is goedgekeurd door de promotoren:

Prof. dr. F.C.T. van der Helm
Dr. J. Zhou

Samenstelling promotiecommissie:

Rector Magnificus,	TU Delft, voorzitter
Prof.dr. F.C.T. van der Helm,	TU Delft, promotor
Dr. J. Zhou,	TU Delft, promotor

Onafhankelijke leden:

Prof.dr. K. Ito,	TU Eindhoven
Prof.dr. A.A. Zadpoor,	TU Delft
Prof.dr. R.G.H.H. Nelissen,	LUMC Leiden
Prof.dr.ir. J. Sietsma,	TU Delft
Prof.dr.ir. H.A. Terryn,	VU Brussel/TU Delft
Prof.dr.ir. H.H. Weinans,	TU Delft, reservelid

This research was funded by The Netherlands Organization for Health Research and Development (ZonMw) under the project 1163500004.

ZonMw

ISBN: 978-94-6186-938-8

Keywords: magnesium, composite, degradation, mechanical properties, biocompatibility

Book and cover design: Sina NADDAF DEZFULI

Printed in the Netherlands

To my loving parents

Table of contents

CHAPTER 1

Introduction

1.1. Background

Bone related diseases such as osteoporosis affect millions of people worldwide, causing more than 9 million fractures annually, which means an osteoporotic fracture every 3 seconds [1]. In 2010, about 30 million women and 7.5 million men in the European Union and the United States had osteoporosis [2-4]. By 2050, osteoporosis and its associated fragility fractures such hip and vertebral fractures in men and women are expected to increase by 310% and 240% compared to year 1990, respectively [5]. Osteoporosis-related fragility fractures impose a major public health burden in industrial and developed countries. In 2010, for example, public health burden related to fragility fractures in Belgium, Netherlands and Germany was about € 10 billion, which is estimated to increase by 25% in 2025, exceeding € 12 billion [6].

Numerous bone fractures need to be treated by using either permanent or temporary (biodegradable) fixtures. For load-bearing applications, metallic materials play an important role as biomaterials to provide necessary support for the damaged bone tissue to repair and remodel itself [7]. Compared to their ceramic- and polymer-based counterparts, metallic biomaterials are more suitable choices due to their excellent combination of high mechanical strength and fracture toughness [7]. Commonly used permanent metal-based biomaterials include stainless steels, titanium and cobalt–chromium alloys, which are nearly inert in vivo, meaning that they do not actively interact with biological systems and they remain as permanent fixtures. Although some animal and clinical studies suggest the effectiveness of these materials for orthopedic applications [8-10], other retrieval studies demonstrated sever cases of corrosion, generating toxic metal ions in the vicinity of these implants, which enables inflammatory cascades of the body, involving macrophages in the process, causing bone resorption and osteolysis, which ultimately results in implant loosening and tissue loss [11-16]. Thereby, permanent fixtures must be removed by a second surgical procedure after the tissue has healed sufficiently.

During the past 20 years, orthopedic implants, based on biodegradable metals [17], have been developed and studied as potential alternatives to permanent fixtures, hoping to achieve the desired ability of providing temporary support for fractured bone and simultaneously, dissolving at a rate that matches new tissue formation [18].

Magnesium has become popular as a biodegradable implant material due to its biodegradable nature, high strength-to-density ratio, and mechanical properties similar to those of the human bone, which makes it superior to existing biodegradable materials such as polymers and ceramics in load-bearing applications [19].

1.2. Problem statement and hypothesis

Despite numerous advantages of Mg-based materials, extremely high degradation rate of commercially pure magnesium in the physiological environment imposes severe limitations in clinical applications. Magnesium dissolves readily in aqueous solutions, especially those containing chloride ion, leading to rapid release of hydrogen gas and resulting in the formation of subcutaneous bubbles and deterioration of the mechanical integrity of the implant before complete healing of injured bone tissue [17].

Commonly known magnesium alloys, including AZ31, AZ91 and WE43, have been investigated for bone implant applications as alternatives to monolithic magnesium metal, because of their relatively lower degradation rates and higher mechanical strengths. It has been demonstrated that all the above mentioned alloys were in direct contact with the surrounding bone tissue after implantation, and bone mass surrounding the implants was found to be enhanced during degradation [20]. Despite the encouraging preliminary outcomes of the in-vivo studies on guinea pigs, it has been shown that common alloying elements of magnesium such as aluminum might have latent toxic effects on the human body, causing neurological disorder or even cancer [21, 22].

Magnesium-based composites, having bioactive ceramic particles incorporated into the monolithic magnesium matrix could be an excellent alternative to their alloyed counterparts. As a new generation of biomaterials, magnesium-based composites can provide a combination of unique characteristics including adjustable mechanical properties (i.e., strength, ductility and elastic modulus), corrosion resistance and bioactivity by the appropriate selection of the reinforcement material without the need of using alloying elements so as to avoid any known or uncertain clinical side effects [23-25]. The superior bioactivity of magnesium-based composites as compared with their alloyed counterparts has been proven in previous studies by demonstrating the ability of the composites to induce the formation of bioactive calcium- and phosphate-containing compounds, which leads to enhanced proliferation and differentiation of osteoblastic cells [26, 27].

When choosing a ceramic reinforcement, it is critically important to consider and fulfill the basic, and at the same time, essential requirements of a bioceramic phase in magnesium matrix composites for orthopedic purposes, which are biocompatibility, biodegradability, bioactivity and mechanical properties. To date, most of the chosen bioceramics, such as hydroxylappetite (HA) and ß-Tricalcium phosphate (ß-TCP) have one or more deficiencies. For example, HA is a osteoconductive ceramic however, often regarded as a permanent biomaterial because it poorly resorbs in the body, limiting the process of biomaterial integration with the surrounding bone tissue, especially within a few weeks after implantation,

which could lead to the formation of fibrous tissue around the implant, being susceptible to long-term failure [28]. ß-TCP on the other hand resorbs much faster than HA but partially converts to HA when implanted in the body [29], leaving slowly absorbing fragments of HA at implantation site. Moreover, HA and ß-TCP both are not osteoinductive, meaning that they cannot induce the process of new bone formation, mainly because they lack silicon that is directly involved in the mineralization process of bone growth [30]. The bioceramic of choice in our research (Bredigite-Ca7MgSi4O16) is a biodegradable Si-containing ceramic in the $CaO{\cdot}MgO{\cdot}SiO_2$ family, with a proven stimulating effect on osteoblast proliferation [31, 32] and mechanical properties close to those of cortical bone [33]. The superior bioactivity and mechanical properties of bredigite compared to traditionally used calcium-phosphate-based compounds makes it a more suitable option for orthopedic applications, where mechanical load is applied on the implant [33]. Additionally, bredigite has a potential ability to form a chemical bonding with the magnesium matrix [24], which differentiates the bioceramics in the $CaO\text{-}SiO_2\text{-}MgO$ system from the other magnesium-matrix composites that have so far been studied potentially for orthopedic applications.

Fabrication method of bioceramic-reinforced magnesium matrix composites is as critically important as the choice of a suitable reinforcement. To date, most of the magnesium-based composites have been manufactured by powder metallurgy methods [23, 34]. Powder metallurgy is a unique low-temperature manufacturing process, which allows effective control over fabrication parameters, conserves energy and enables homogenous dispersion of reinforcing particles in the metallic matrix, thereby improving the mechanical properties as well as the corrosion resistance. However, most of powder metallurgy processed Mg-matrix composites suffer from excessive porosity and inter-particle fracture under loading [23, 35] – an issue that we attempted to address in this research. This issue is of critical importance because porosity and mechanical cracks could lead to intense localized corrosion and premature mechanical failure, producing broken pieces and debris, damaging the surrounding tissue and increasing the risk of clinical complications [19].

For load-bearing biodegradable implants, it is considered ideal if the mechanical strength of the fabricated material gradually decreases as bone defects are replaced by new tissue. In this process, the fabricated Mg-bredigite composite should be able to withstand the applied mechanical loads during the healing process (3 - 6 months). To achieve mechanical function as long as clinically required, there is a strong need to understand the degradation mechanisms in relation to the gradual losses of the mechanical properties of magnesium-bredigite composites in order to draw a comprehensive outlook on the composite's behavior during the course of degradation.

1.3. Objectives of the research

Taking the abovementioned issues about the current Mg-based composites into account, our main objective was first to fabricate biodegradable magnesium-based composites using a powder metallurgy method with careful selection of the bioceramic part of the composites as a reinforcing phase to satisfy the abovementioned requirements, and then aiming at optimizing the process parameters for powder metallurgy magnesium-based composites to limit the problem of excessive porosity and avoid premature interparticle fracture, while improving the degradation behavior. Subsequently, we aimed at determining the relationship between the degradation behavior and the loss of the mechanical properties of magnesium-bredigite composites.

When bioactive particles are added to the magnesium matrix to produce magnesium matrix composites, they participate in chemical reactions, in addition to magnesium, by continuously releasing bioactive agents into the surroundings, which will ideally result in forming a protective layer and stimulating appetite formation throughout the whole course of degradation [36].

To clarify the underlying roles of each part of the composite (magnesium+bredigite), we first investigated the mechanisms affecting the degradation of monolithic magnesium in a pseudo-physiological solution and then, the composite as a whole was investigated with particular attention to understanding the role that silicon-containing bredigite played in corrosion and bioactivity mechanisms.

1.4. Outline of the research

This thesis tries to address the current issues regarding the applicability of biodegradable magnesium-based composites for successful clinical trials.

In this regard, chapter 2 explores the degradation behavior of powder metallurgy processed monolithic magnesium in a pseudo-physiological solution.

Chapter 3 explores the degradation behavior of magnesium-bredigite composites, with particular attention to the role of the bredigite bioceramic in degradation and bioactivity mechanisms.

Chapter 4 attempts to establish a clear correlation between the corrosion mode and rate, and the loss of the mechanical properties during degradation in a pesuedo-physiological solution.

Chapter 5 aims at addressing the common issues of magnesium-based composites, i.e., interparticle fracture under loading and intense localized corrosion, by exploring the feasibility of establishing a chemical bonding between powder particles, as an additional bonding mechanism to the mechanical interlocking.

Chapter 6 critically examines the findings in the light of the previous chapters and provides practical guidelines for further research on the subject.

CHAPTER 2

Influence of HEPES buffer on the local pH and formation of surface layer during in vitro degradation of magnesium in DMEM

This chapter is published as:

NaddafDezfuli, S., Huan, Z., Mol, J.M.C., Chang, J., Zhou, J., 2014. Influence of HEPES buffer on the local pH and formation of surface layer during in vitro degradation of magnesium in DMEM. Progress in Natural Science: Materials International 24, 531-538.

Abstract

The human body is a buffered environment where pH is effectively maintained. HEPES is a biological buffer often used to mimic the buffering activity of the body in in vitro studies on the degradation behavior of magnesium. However, the influence of HEPES on the degradation behavior of magnesium in the DMEM pseudo-physiological solution has not yet been determined. The research aimed at elucidating the degradation mechanisms of magnesium in DMEM with and without HEPES. The morphologies and compositions of surface layers formed during in vitro degradation tests for 15 – 3600 s were characterized. The effect of HEPES on the electrochemical behavior and corrosion tendency was determined by performing electrochemical tests. HEPES indeed retained the local pH, leading to intense intergranular/interparticle corrosion of magnesium made from powder and an increased degradation rate. This was attributed to an interconnected network of cracks formed at the original powder particle boundaries and grain boundaries in the surface layer, which provided pathways for the corrosive medium to interact continuously with the internal surfaces and promoted further dissolution. Surface analysis revealed significantly reduced amounts of precipitated calcium phosphates due to the buffering activity of HEPES so that magnesium became less well protected in the buffered environment.

2.1. Introduction

Biodegradable ceramics or polymers are not really suitable implant materials for applications at the load-bearing sites of the human body, because of a lack of sufficient mechanical properties [37, 38], and therefore they are often used to fill up the cavities of the damaged bone tissue [39]. More suitable biodegradable materials for the repair of load-bearing defects are the metallic ones that have higher fracture toughness and ductility than bio-ceramics and higher strength and elastic modulus than bio-polymers. Magnesium and its alloys represent the most interesting biodegradable materials. These materials possess densities and elastic moduli closer to those of the human bone than other metallic biomaterials for permanent implants such as stainless steel, cobalt-chromium alloys and titanium alloys [40], which makes them promising candidates for orthopedic applications at the load-bearing sites of the human body [41, 42]. However, advances towards the clinical applications of these materials have been seriously hampered by too rapid degradation and premature loss of mechanical integrity in physiological environments. Although a great deal of research has been directed toward understanding their corrosion behavior and seeking measures to slow down degradation, the underlying corrosion mechanisms of magnesium and its alloys in relation to complex physiological media under *in vitro* and *in vivo* test conditions have not been fully understood. Clearly, further efforts are needed to reveal the nature of the interactions between magnesium and physiological media.

In *in vitro* studies on the degradation behavior of magnesium and its alloys, the choice of a suitable test medium is of critical importance. Many types of pseudo-physiological solutions that mimic the composition of body fluids, such as 0.9 wt.% NaCl solution, conventional simulated body fluid (c-SBF), revised simulated body fluid (r-SBF), Hank's balanced salt solution, Dulbecco's modified Eagle's medium (DMEM) and phosphate buffered saline (PBS) have been used. Among these, DMEM is one of the cell culture solutions that has been proven to produce an appropriate physiological condition for *in vitro* degradation tests of magnesium [43-45]. Major inorganic salts in DMEM, such as sodium bicarbonate, turn magnesium ions into magnesium carbonates, resulting in surface passivation [46]. Carbon dioxide also triggers the formation of magnesium carbonates. In the presence of carbon dioxide in aqueous solutions, carbonic acid forms, which is the ingredient for $MgCO_3$ formation [46-48]. The formation of a carbonated layer is thought to encourage further precipitation of the most important inorganic constituents of biological hard tissues - calcium phosphate phases [47], which is of biological and medical significance.

As soon as magnesium is in contact with a simulated physiological solution, corrosion takes place, leading to the changes in the chemistry of the magnesium surface and the surrounding solution. It has been observed during *in vitro* immersion tests that corrosion of magnesium leads to the local formation of hydroxyl ions and their leaching into the surrounding solution, which alters the pH of the solution through local alkalization [19]. In the human body, however, pH cannot increase significantly, as it is actively regulated through various biochemical reactions [49]. Therefore, the addition of a buffer to the immersion solution provides magnesium with a realistic degradation environment, as it closely mimics the *in vivo* situation.

In the *in vivo* situation, the pH of body fluids is regulated 39 % by the respiratory system, i.e., the CO_2/bicarbonate system, and 61 % by biochemical buffers, e.g., proteins (excluding the kidneys that have a long-term buffering effect on pH). In other words, the biochemical buffers play a dominant role in regulating the pH of the physiological environments in the body, relative to the bicarbonate buffering system [50]. Thus, to mimic the *in vivo* environments, the buffer chosen for *in vitro* tests should have a greater buffering capacity than the CO_2/bicarbonate system.

In preceding *in vitro* degradation tests of magnesium and its alloys, different buffering agents of various concentrations have been added to different pseudo-physiological solutions. As the corrosion behavior of magnesium and its alloys is highly sensitive to the aggressive environment, the type and concentration of buffering agents can dramatically change their degradation behavior. Due to the use of different pseudo-physiological solutions and buffering agents, many inconsistent results have been obtained from *in vitro* and *in vivo* studies on the degradation behavior of magnesium and its alloys, which makes the comparisons between *in vitro* test results and between *in vitro* and *in vivo* test results difficult. HCl-containing buffer systems, for example, have shown their abilities to introduce chloride ions into the solution, which in turn attack the surface layer of magnesium [51]. Phosphate-based buffers alter the chemical properties of the corrosion layer, as they provide phosphate ions in aqueous solutions, thereby producing insoluble salts with magnesium ions and eventually precipitating on the surface [48, 52]. In addition, phosphate-based buffers contribute to regulating the pH of the body, although this contribution is often neglected due to their small concentrations in the blood plasma [50]. HEPES (N-2-Hydroxyethylpiperazine-N'-2-ethanesulfonic Acid) is one of Good's biological buffers that offers a greater buffering capacity than the bicarbonate buffers [53] and thus could be a suitable candidate to be coupled with the bicarbonate buffers that are present in DMEM. HEPES is water-soluble and atmosphere-independent. It has shown to have negligible affinity to metallic ions found in the blood plasma [54]. Previous studies have provided a basic understanding of the influence of HEPES on the degradation of magnesium in

sodium chloride solutions [55, 56], but this understanding may not necessarily be applicable to the DMEM solution, because of the differences in the surface layer formed as a result of the interactions between magnesium and the test solution. A better understanding of the influence of HEPES buffering on the degradation behavior of magnesium in the DMEM cell culture medium is of fundamental importance for understanding the correlations between the experimental results obtained from *in vitro* and *in vivo* tests, because body fluids themselves are a buffered environment.

The present research aimed at elucidating the corrosion mechanisms of pure magnesium in the DMEM solutions with and without the HEPES buffer. Degradation tests in a pseudo-physiological condition (Electrolyte = DMEM; T = 37 °C; pH = 7.45) for 15 s and for up to 3600 s were performed. The morphologies and compositions of surface layers formed were characterized and their correlations with the degradation rate were determined. Potentiodynamic Polarization (PDP) and Open Circuit Potential (OCP) tests were carried out to evaluate the influence of the HEPES buffer in DMEM on the electrochemical behavior and corrosion tendency of magnesium.

2.2. Materials and methods

2.2.1. Material

Magnesium powder (of 99.98% purity) with a medium particle size of 90 µm was uni-axially pressed in a cylindrical die at 350 °C and under a pressure of 500 MPa to yield fully consolidated specimens for the research, instead of cast magnesium specimens with inevitable porosity that would affect corrosion behavior. Compacted magnesium pellets with a diameter of 13 mm were cut into slices with a thickness of 8 mm. A copper wire with a waterproof isolation layer was attached to the slices. The conductive specimens were then mounted in an epoxy resin with only the top surface being exposed to the immersion media for degradation tests. The mounted specimens were then ground using SiC grinding paper to 2400 grit and ultrasonically cleaned in acetone for 3 min.

2.2.2. Degradation tests

A corrosion cell operating at 37 °C was used to carry out all the degradation tests. The temperature of the cell was maintained using a thermostatic water bath. DMEM

(D1145, Sigma-Aldrich) was used as the base immersion medium. HEPES (391338, Calbiochem) was added to DMEM to reach a concentration of 25 mM (referred to as the HEPES-buffered solution hereafter) to determine the influence of the buffering agent on the degradation behavior of magnesium. The ratio of solution volume to specimen surface area (SV/SA) was 378 ml/cm^2, being much larger than the critical value of 67 ml/cm^2 [57] in order to prevent ions in the solution from accumulation and the bulk solution from alkalization. Local pH changes during the immersion tests were registered by using a micro pH meter (S220 SevenCompact, Mettler Toledo) placed approximately 1 mm above the specimen surface. Another pH meter was placed over a lateral distance of 90 mm away from the specimen surface to measure the bulk pH, considering the possibility that the bulk pH might not be representative of the pH at the specimen surface and might vary by several pH units [19, 58]. Data logging was carried out every 60 s.

2.2.3. Surface analysis

Magnesium specimens were immersed in the DMEM solution and in the HEPES-buffered solution for 15, 300 and 3600 s to determine the effect of the buffer on the morphology and composition of surface layer formed. At these time points, specimens were removed from the solutions, rinsed in ethanol for 30 s and then air dried. The morphologies and chemical compositions of surface layers formed were characterized using a JEOL JSM-6500F Scanning Electron Microscope (SEM) working at an accelerating voltage of 15 kV and equipped with an Energy Dispersive Spectrometer (EDS).

2.2.4. Electrochemical tests

The three electrode configuration was adopted to perform the polarization tests. A Saturated Calomel Electrode (SCE) was used as the reference electrode and a platinum mesh as the current electrode. The electrochemical activity of magnesium specimens in the DMEM solutions with and without HEPES at 37 °C were determined by measuring the Open Circuit Potential (OCP) during immersion using a Solartron 1250/1255 potentiostat. Potentiodynamic Polarization (PDP) tests were performed immediately after the OCP tests at an initial potential of - 0.2V vs OCP increasing to +0.5V vs OCP at a scan rate of 0.2 mV/s.

2.3. Results and discussion

2.3.1. Effect of HEPES on the $Mg(OH)_2$ layer formed

Fig. 1 shows the morphologies of specimen surfaces after immersion in the HEPES-buffered solution for 15, 300 and 3600 s. After immersion for 15 s, the original grinding marks were still visible, indicating that the initial surface layer was yet very thin at this stage (Fig. 1a). In the surface layer, the original powder particle boundaries and grain boundaries, indicated by white arrows in Fig. 1a (backscattered image), were outlined. Observation of the square box in Fig. 1a at a higher magnification revealed that a nanostructured layer with grain sizes between 10 – 100 nm was formed on the surface and the surface layer contained nano-sized cracks with lengths of less than 100 nm. EDS point scans showed the presence of the elements of magnesium and oxygen on the surface, suggesting that the nano-structured layer was mainly composed of $MgO/Mg(OH)_2$.

After immersion for 300 s, the thickness of the surface layer slightly increased and larger cracks (with a maximum length of 1 μm) appeared mostly at the grain boundaries (Fig. 1b). Obviously, such a cracked surface layer could not effectively protect the surface from further corrosion, because in effect it provided pathways for the immersion solution to stay in direct contact with the magnesium surface and thus accelerated the degradation [59]. As a result, the dissolution of magnesium continued, in spite of the formation of the surface layer. During further immersion tests till the final time point (3600 s), these cracks significantly grew almost 500 times (up to a maximum length of 50 μm) from their initial sizes. These grown surface cracks were mostly developed along the original powder particle boundaries and grain boundaries where an interconnected network of cracks throughout the surface was formed (Fig. 2a). Aung and Zhou [60] considered the formation of surface cracks as an indication of a higher dissolution rate in some regions on the surface. A grain boundary can be regarded as an area of defects in the crystal structure with a configuration of dislocations. It is well known that anodic metal dissolution would be accelerated in the vicinity of dislocations [61]. During the immersion tests of magnesium made from powder, the original powder particle boundaries and grain boundaries became anode and preferentially corroded, building up local galvanic coupling with the surrounding grains. Subsequently, magnesium grains became cathode relative to the original powder particle boundaries and grain boundaries and galvanically protected (Fig. 2a). This explanation is yet to be confirmed by using the electrochemical microcell technique and scanning vibrating electrode technique to reveal local galvanic coupling between the internal structural boundaries and neighboring grain interior on a micro scale.

In contrast, after immersion tests in DMEM without the buffer for 3600 s, the original powder particles could still be identified using SEM backscattered imaging. These are highlighted in Fig. 2b for comparison with the surface morphology after immersion in the HEPES-buffered solution also for 3600 s (Fig. 2a). From the comparison, it is clear that in DMEM without HEPES, interparticle and intergranular corrosion did not take place and the surface was less electrochemically active. It also suggests that the degradation of magnesium in the HEPES-buffered solution would proceed considerably faster than that in DMEM.

It is well known that the pH of a solution strongly influences the nature and stability of the protective hydroxide layer [47, 51]. The hydroxide layer is more stable in an alkaline solution [16]. The higher degradation rate of magnesium in the HEPES-buffered solution could be associated with the limited alkalization of the solution on account of the buffering activity of HEPES. During the immersion tests, the bulk pH of both of the electrolytes (DMEM and HEPES-buffered DMEM) remained constant at 7.45, confirming that the very large SV/SA ratio indeed prevented the solutions from bulk alkalization, as observed by Yang and Zhang [57]. Of more interest were the changes of the local pH. It was found that while the bulk pH remained stable during the immersion tests, the local pH changed to alkaline values, as shown in Fig. 3. The local pH of DMEM continuously increased from 7.45 to 7.65 in 3600 s, exceeding the pH range of 7.4 - 7.6 in the normal physiological environments, while only a short positive shift with a maximum pH value of 7.55 in the local pH of the HEPES-buffered solution occurred and quickly the local pH returned to the initial value of 7.45. It demonstrated that the local alkalization indeed took place despite the large SV/SA ratio and the alkalization remained local throughout the tests without affecting the pH of the whole solution. It is likely that the local pH measurements are affected by the distance between the pH electrode placement and the corroding surface. In other words, the local pH measurements of the solution at closer spots, e.g., a few micrometers away from the surface, might have shown even higher values [19]. The exact correlation of the local pH with the distance from the magnesium surface, yet to be established by means of pH micro-sensors, is of major significance, because it is the microenvironment at the solid-liquid interface that mainly determines the corrosion behavior of magnesium.

From Fig. 3, it is clear that the local alkalization was less severe for magnesium in the HEPES-buffered solution than in DMEM. This suggests that HEPES neutralized an excess number of local OH^- ions in the solution and provided a neutral environment, which would enhance the degradation rate. Other researchers proposed that a complex might have formed between Mg^{2+} and HEPES, which effectively removed Mg cations from the solution, thereby disturbing the equilibrium and leading to further dissolution [47], although such a complex probably would not form at the

physiological concentration of Mg^{2+} ions [47]. Therefore, the lower local pH in the HEPES-buffered solution might have had a dominant effect on the degradation of magnesium. In the present immersion experiments, adding HEPES to DMEM increased the degradation rate of magnesium through intense dissolution at the original power particle boundaries and grain boundaries, causing the formation of initially nano-sized and then micro-sized cracks in the surface layer, as the degradation proceeded further. The hierarchy of the cracks built up an open structure of the surface layer, which allowed the immersion solution to stay in direct contact with the magnesium surface, thereby promoting further degradation. As a result, the magnesium surface became less protected and exhibited a stronger tendency of corrosion in the HEPES-buffered solution.

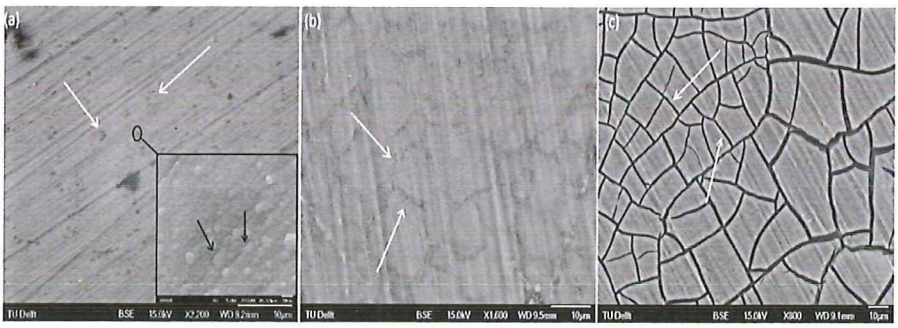

Fig. 1 Surface morphologies of magnesium specimens after immersion in the HEPES-buffered solution for (a) 15, (b) 300 and (c) 3600 s. Black arrows in Fig. 1a show the presence of nano-sized cracks in the initial surface layer, while white arrows indicate the formation (Fig. 1a) and growth of cracks (Fig. 1b and c) in the surface layer along the original powder particle boundaries and grain boundaries.

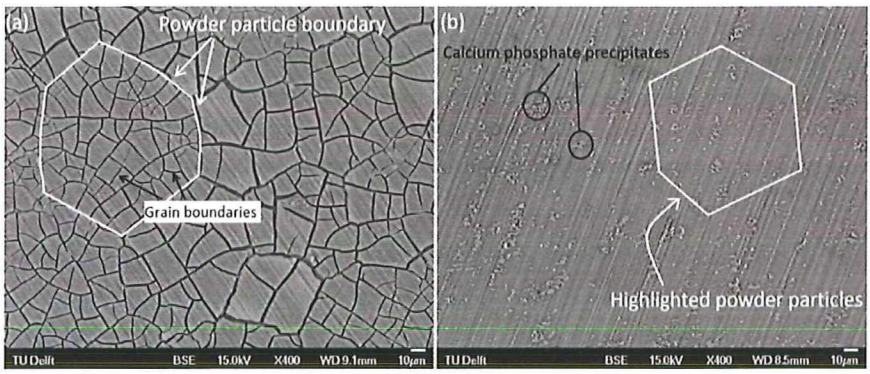

Fig. 2 Surface morphologies of specimens after immersion in (a) the HEPES-buffered solution and (b) the DMEM solution for 3600 s. Black and white arrows in Fig. 2a show an interconnected network of cracks along the grain boundaries and original powder particle boundaries, respectively.

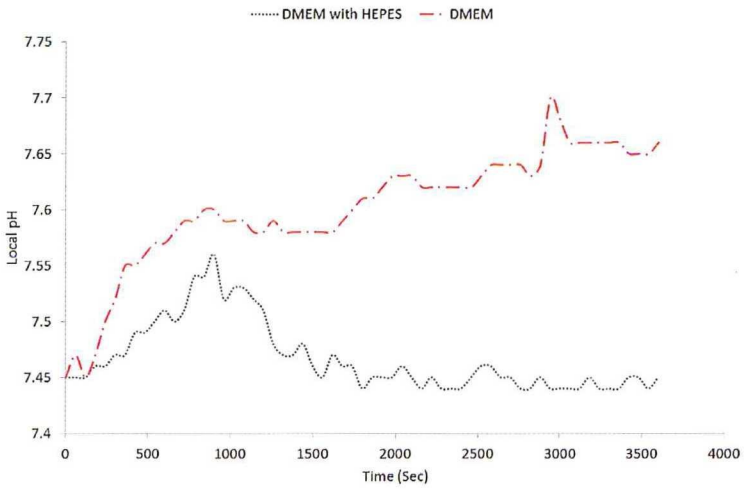

Fig. 3 Local pH variations with time during immersion tests in the DMEM solution and in the HEPES-buffered solution.

2.3.2. Effect of HEPES on the precipitation of calcium phosphates

After immersion in DMEM for 3600 s, colonies of agglomerated spherical precipitates were observed on specimen surfaces (Fig. 2b). EDS line scan analysis

revealed that the spherical precipitates contained the elements of calcium and phosphorus (Fig. 4). Physiological solutions are known for inducing the formation of calcium phosphate precipitates on the magnesium surface owing to super-saturation [62]. These precipitates are thought to be mainly amorphous calcium phosphate phases agglomerated to form spherical particles [63]. The calculated Ca/P ratio of spherical precipitates was around one, meaning that these precipitates were deficient in calcium. The contribution of magnesium cations in the DMEM solution to spherical agglomerates might be the cause for the calcium deficiency, as magnesium cations could react with calcium and phosphate ions in the solution to form insoluble precipitates [57]. These precipitates have shown to improve the biocompatibility and osteoconductivity of magnesium-based implants, in comparison with hydroxyapatite [64].

By contrast, the surfaces of specimens after immersion in the HEPES-buffered solution for 3600 s showed no visible calcium phosphate precipitates (Fig. 2a). It is generally acknowledged that the alkalization of the solution as a result of an increase in OH^- concentration through reduction reactions at the specimen surface encourages the precipitation of calcium phosphate phases [57, 65]. Therefore, the lower local pH almost without solution alkalization, caused by the HEPES buffer, must have prevented the calcium phosphate precipitation from taking place. The Tris buffer, often used to regulate the pH of the simulated body fluid (SBF), is notorious for limiting the precipitation of calcium phosphates [66]. It is believed that the Tris buffer lowers the local pH and also forms soluble complexes with calcium ions, which further reduces the concentration of free Ca^{2+} required to form calcium phosphate precipitates [66]. In the HEPES-buffered solution used in the present study, however, such complexes with calcium ions would unlikely form [67]. Thus, the tendency of the HEPES-buffered solution to precipitate calcium phosphates was reduced, as the local pH of the solution was maintained at a lower level by the buffer [68].

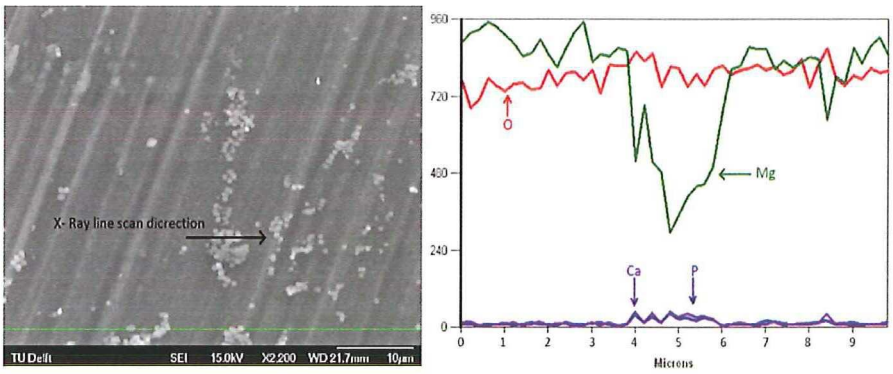

Fig. 4 EDS line scan on magnesium specimen surface after immersion in DMEM for 3600 s. White spherical particles (left image) were calcium phosphate agglomerates precipitated directly from the solution.

2.3.3. Corrosion behavior of magnesium during PDP and OCP tests

The corrosion tendencies of magnesium in the DMEM with and without the HEPES buffer was determined by performing OCP tests for 3600 s (Fig. 5a). The OCP value of magnesium in DMEM was considerably elevated to more positive values, shortly after immersion (from -1.76 V to -1.62 V after 500 s) and increased with time (-1.54 V after 3600 s), indicating the immediate formation and maturation of the protective layer. Such a strong shift to positive values was however not observed for magnesium in the HEPES-buffered solution; OCP increased smoothly and gradually from -1.86 V to -1.83 V after 3600 s. After 500 s, the OCP value of magnesium in the HEPES-buffered solution was 200 mV smaller than that in the DMEM solution and after 3600 s the difference became even larger (300 mV). It suggested that magnesium surface was better protected by a hydroxide layer in DMEM at the early stage of immersion and the initially formed layer was more rapidly matured, as compared to that in the HEPES-buffered solution [55]. This is in line with the observations of the surface layer of magnesium in the presence of HEPES (Figs. 1 and 2), where cracks appeared such that the surface was continuously exposed to the immersion solution. The multiple fluctuations of the OCP curve of magnesium in DMEM (Fig. 5a) could be an indication of metastable surface breakdown. A previous study conducted by Xin and Chu [69] on the effect of the TRIS buffer on magnesium corrosion showed a similar indication for pitting at the early stages of immersion. However, such an indication was absent in the OCP curve of magnesium in the HEPES-buffered solution, as shown in Fig. 5a.

Fig. 5b shows the potentiodynamic polarization curves of magnesium in the DMEM solution and in the HEPES-buffered solution. The corrosion potential of magnesium in DMEM (-1.53 V) showed a more positive value than in the HEPES-buffered solution (-1.77 V), meaning that the surface was more effectively protected by the initially formed surface layer. As a consequence, the corrosion current densities in both cathodic and anodic regions (before surface breakdown) were higher in the HEPES-buffered solution (Fig. 5d). In DMEM, however, the corrosion current density suddenly increased drastically at relatively low anodic over-potentials (+50 mV vs corrosion potential), as a result of the surface breakdown. On the contrary, no such surface breakdown occurred for magnesium when HEPES was added as a buffer to DMEM and with increasing over-potential the corrosion current remained at a higher but constant level. Fig. 5c depicts the measured values of the local pH as a function time in the PDP tests. With increasing anodic potential, a local acidic environment developed over the surface of magnesium and its magnitude was significantly higher in DMEM. Increasing anodic potential caused the rapid dissolution of magnesium, leading to a large amount of Mg^{2+} migrating to the solution. Baes and Masmer [70] showed that the high concentration of Mg^{2+} cations would eventually react with water and produce protons that would acidify the local environment (Eq. 1).

$$4Mg^{2+}_{(aq)} + 4H_2O_{(l)} \rightarrow Mg_4(OH)_4{}^{4+}_{(aq)} + 4H^+_{(aq)} \qquad \text{Eq.1}$$

Subsequently, the surface layer would become more unstable in the presence of a higher concentration of protons and eventually breakdown would take place according to the following reaction

$$Mg(OH)_{2\,(S)} + 2H^+_{(aq)} \rightarrow 4H_2O_{(l)} + Mg^{2+}_{(aq)} \qquad \text{Eq. 2}$$

The local acidification as a result of the hydrolysis of magnesium cations was first mentioned by Robinson and George [71] and then adopted to explain the degradation mechanisms of magnesium [72]. However, other studies suggested that the possible anodic acidification of magnesium surface would not be significant enough to influence the pH of the solution [73]. In the present study, high acidification of the local environment was detected during anodic polarization. The cation hydrolysis could be even more significant inside an isolated pit or a crack where the anodic dissolution was dominant and therefore the concentration of Mg^{2+} might be extremely high. Fig. 5c shows that the cation hydrolysis became more significant with increasing anodic current density. This indicates that the magnitude of the local acidification is dependent on the activity of the local anodes, e.g., grain boundaries. In other words, the stronger the galvanic coupling, the greater the local acidification on the local anodes. HEPES neutralized an excess number of protons and thus limited the magnitude of surface acidification, as shown in Fig 5c. The

surface layer could be more immune to protons as a result of the buffering activity of HEPES. Highly aggressive anions such as chlorides could also be responsible for the surface breakdown, because they would eventually attack and destroy the protective layer [42]. Since the solutions used in the present study were identical with respect to the base chemical composition (e.g., chloride ions) and the only difference between the two solutions was the presence and absence of the HEPES buffer, it was most likely that the buffering activity of HEPES influenced the anodic dissolution of magnesium.

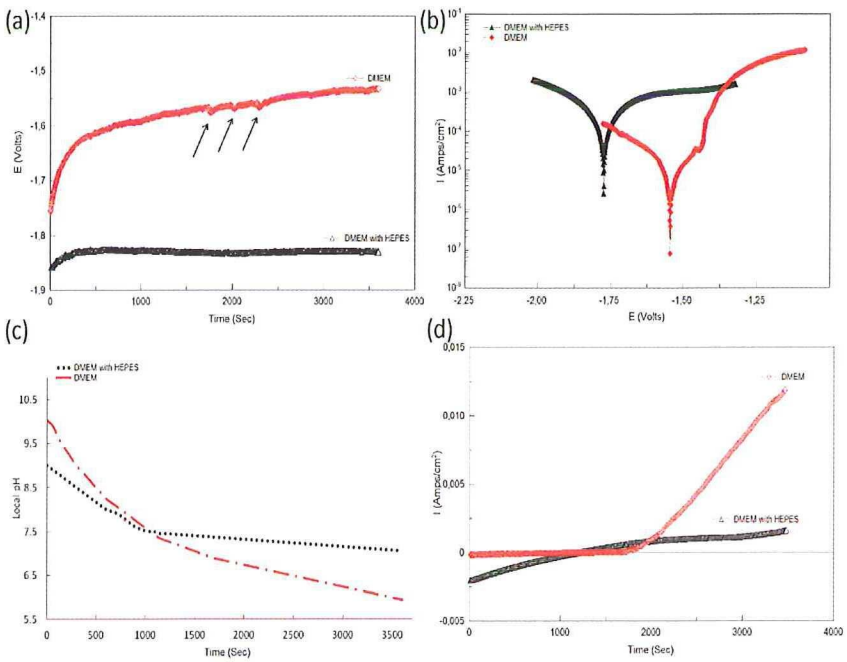

Fig. 5 (a) OCP, (b) potentiodynamic polarization curves of magnesium in the DMEM solution and in the HEPES-buffered solution, (c) changes in local pH and (d) corrosion current density during the PDP tests.

2.4. Conclusions

In the present research, immersion tests, electrochemical tests and surface characterization were performed to develop an understanding of the effect of the buffering activity of HEPES in DMEM on the degradation behavior of magnesium. This understanding is of fundamental importance, because it will help understand the correlations between experimental results obtained from in vitro and in vivo tests. It will allow the further research to be focused on other major factors, such as the circulation of pseudo-physiological solutions that continuously carry ions away in a dynamic manner to account for the differences between static in vitro test results and in vitro test results. The following conclusions have been drawn from the present research.

1. With the addition of the HEPES buffer to DMEM, the local pH close to the magnesium surface was largely maintained, leading to intense intergranular and interparticle corrosion and thus a higher degradation rate of magnesium.

2. A higher dissolution rate of magnesium at the original powder particle boundaries and grain boundaries resulted in an interconnected network of cracks in the surface layer, thereby providing pathways for the immersion solution to stay in direct contact with the magnesium surface and promoting further dissolution.

3. In the HEPES-buffered solution, the cathodic and anodic current densities in the PDP tests were higher and the OCP values were more negative due to the presence of surface cracks, as compared to those in DMEM without the buffer.

4. The precipitation of calcium phosphates in the HEPES-buffered was limited due to the buffering activity of HEPES.

5. The addition of the HEPES buffer to the DMEM solution used in in vitro studies on the biodegradation behavior of magnesium provided a harsher environment for magnesium to resist rapid corrosion, but it is necessary, as the body fluids are also a buffered environment.

CHAPTER 3

Advanced bredigite-containing magnesium-matrix composites for biodegradable bone implant application

This chapter is published as:

NaddafDezfuli, S., Huan, Z., Mol, J.M.C., Leeflang, S., Chang, J., Zhou, J., 2017. Advanced bredigite-containing magnesium-matrix composites for biodegradable bone implant application. Materials Science and Engineering C 79, 647-660.

Abstract

The present research was aimed at developing magnesium-matrix composites that could allow effective control over their physiochemical and mechanical responses when in contact with physiological solutions. A biodegradable, bioactive ceramic - bredigite was chosen as the reinforcing phase in the composites, based on the hypothesis that the silicon- and magnesium-containing ceramic could protect magnesium from fast corrosion and at the same time stimulate cell proliferation. Methods to prepare composites with integrated microstructures - a prerequisite to achieve controlled biodegradation were developed. A systematic experimental approach was taken in order to elucidate the in vitro biodegradation mechanisms and kinetics of the composites. It was found that the composites with 20–40% homogenously dispersed bredigite particles, prepared from powders, could indeed significantly decrease the degradation rate of magnesium by up to 24 times. Slow degradation of the composites resulted in the retention of the mechanical integrity of the composites within the strength range of cortical bone after 12 days of immersion in a cell culture medium. Cell attachment, cytotoxicity and bioactivity tests confirmed the stimulatory effects of bredigite embedded in the composites on the attachment, viability and differentiation of bone marrow stromal cells. Thus, the multiple benefits of adding bredigite to magnesium in enhancing degradation behavior, mechanical properties, biocompatibility and bioactivity were obtained. The results from this research showed the excellent potential of the bredigite-containing composites for bone implant applications, thus warranting further in vitro and in vivo research.

3.1. Introduction

Over the last decade, magnesium has attracted much attention in the field of biomaterials on account of its biodegradable nature and high strength-to-density ratio. In addition, magnesium in its ionic form (Mg^{2+}) is the most abundant bivalent cation within the cells and the fourth most abundant element in vertebrates [74]. Around 64% of the total Mg^{2+} can be found in bone, 35% in other tissue compartments and 1–2% in plasma and extracellular fluids [75]. Because of the good biocompatibility and mechanical compatibility of magnesium to human bone, extensive research has been performed to explore the possibilities of using magnesium-based materials for orthopedic implants [76-78]. However, up till now, clinical applications of magnesium-based implants have been rather scarce. Too fast degradation of magnesium-based materials in physiological solutions containing inorganic salts [79], leading to rapid release of hydrogen gas, premature loss of mechanical properties and implant failure, has remained to be a fundamental problem hindering their widespread applications.

Many research efforts have been made to reduce the degradation rate of magnesium by alloying. Although much progress has been made, almost all second phases formed as a result of exceeding solubility limits in the magnesium solid solution have been reported to promote micro-galvanic corrosion, causing localized anodic dissolution of the adjacent magnesium matrix [80]. Consequentially, most magnesium alloys exhibit corrosion rates even greater than pure magnesium [81]. In addition, constraints have been encountered in using alloying elements, because of known or uncertain long-term clinical effects of these elements. Aluminum, a commonly used alloying element to enhance the strength and corrosion resistance of magnesium, for example, has been reported to cause neurological disorder [22], when its concentration in plasma exceeds 3 μM [82]. Zirconium, an element in the ZK magnesium alloy family, has been found to be associated with liver cancer, lung cancer, breast cancer and nasopharyngeal cancer, when its presence in plasma exceeds 1 mM [21]. Undesirable effects of alloying elements as such have largely limited the adoption of the alloying approach. Surface coating to form a biodegradable layer has been tried as a useful approach to delaying the onset of the biodegradation of the magnesium substrate by preventing the corrosive liquid from reaching the substrate. Obviously, the functionality of the surface coating is limited only to the early stages of immersion in physiological solutions [83], but not during the whole course of degradation, because only the exposed surfaces of an implant can be treated while the bulk remains untreated. Moreover, most biodegradable coatings tend to flake off, once a coated implant is under mechanical loading, which results in localized corrosion of the substrate at an accelerated rate.

Ideally, a biodegradable orthopedic implant is also bioactive and can preserve its functionality over the whole healing period of defected bone (ideally 3–6 months) [84]. Magnesium matrix composites containing biodegradable and bioactive particles embedded in the bulk may be able to expose these particles, form a protective layer and stimulate appetite formation throughout the whole course of biodegradation. However, despite the promising potential of magnesium matrix composites for orthopedic applications, up till now, there have been only a few investigations on the subject [23].

Attempts have been made to use hydroxyapatite (HA) and β-tricalcium phosphate (β-TCP) [85, 86] as the reinforcing phases to slow down the degradation of magnesium alloys and improve their bioactivity, mainly considering the close chemical similarities of these bioceramics with the inorganic component of bone. It is the authors' point of view that the choices of these bioceramics were not firmly based on comprehensive considerations to fulfill the requirements of the bioceramic phase in magnesium matrix composites, including biocompatibility, biodegradability, bioactivity, mechanical properties and bondability with the magnesium matrix. As a result, the chosen bioceramics have one or more deficiencies. For example, HA lacks biodegradability, as clinical tests have shown that it does not degrade significantly in the body and remains as a permanent fixture, being susceptible to long-term failure [28]. β-TCP on the other hand is bioresorbable, but its bioactivity leaves much to be desired, mainly because it lacks silicon that is directly involved in the mineralization process of bone growth [30]. Thus, the incorporation of silicon into Ca-P bioceramics is considered a must, if enhanced bioactivity is desired [87, 88].

Bredigite ($Ca_7MgSi_4O_{16}$) is a biodegradable and bioactive ceramic in the CaO-SiO_2-MgO system. This silicon-containing bioceramic has shown rapid HA mineralization, excellent cytocompatibility [32], a strong stimulating effect on osteoblast proliferation [31] and high osteogenic potential [89]. The mechanical properties of bredigite are close to those of cortical bone [31, 33], enabling bredigite to bear mechanical load over a sustained period of time after implantation, which makes bredigite a more suitable option than the previously used calcium-phosphate-based compounds such as tricalcium phosphates (TCP). One unique property of bredigite lies in its ability to form chemical bonding with the magnesium matrix through a highly exothermic reaction between Si—O bonds of bredigite and magnesium [90], thereby producing MgO and Mg_2Si at the Mg-bredigite interface. It is this property that differentiates the composites with the bioceramics in the CaO-SiO_2-MgO system from the other magnesium-matrix composites that have so far been studied potentially for orthopedic applications and shown a lack of proper bonding between composite constituents [26]. In other words, bredigite was considered a better

choice than HA or TCP in meeting the five requirements of an ideal bioceramic phase for biodegradable magnesium-matrix composites.

In this study, we aimed at developing magnesium matrix composites containing homogenously dispersed bredigite particles and having integrated microstructures in order to (i) slow down the degradation of magnesium, (ii) to extend the duration of its mechanical functionality and (iii) to enhance its bioactivity at the same time. Particular attention was paid to understanding the role that silicon-containing bredigite played in biodegradation and bioactivity mechanisms.

3.2. Materials and methods

3.2.1. Material preparation

In this research, a powder metallurgy route was chosen to prepare monolithic magnesium and composite specimens. Magnesium (with a purity of 99.86%, 320 ppm Fe and 160 ppm Ni, determined by means of an X-ray Fluorescence Spectroscope - XRF) and bredigite ($Ca_7MgSi_4O_{16}$) powders with median particle sizes of 90 µm and 10 µm, respectively, were chosen as the starting materials. Irregular bredigite powder particles were mixed with spherical magnesium powder particles at 20 and 40 vol% using a rotary mixer for 12 h to obtain homogenous mixtures. Subsequently, the mixed powders with 20 and 40 vol% bredigite particles were heated in a cylindrical die to 350 °C under a pre-pressure of 100 MPa and then compacted at 500 MPa. A sintering step for 2 h under the compaction load was taken to ensure bonding between powder particles.

The value of bulk density (P) was derived from the measured weight and volume of each sample by using Archimedes' principle according to ASTM B962-15.

The microstructures and surface morphologies of the materials were characterized using a JEOL JSM-6500F Scanning Electron Microscope (SEM) working at an accelerating voltage of 15 kV and equipped with an Energy Dispersive Spectrometer (EDS). EDS elemental mapping was conducted to study the elemental compositions of sample surfaces before and after the immersion tests as described below.

3.2.2. Mechanical properties

Microhardness (Vickers hardness) values of the materials were obtained by micro-indentation with a square-based pyramidal-shaped diamond indenter having an

angle of 136° and with a dwelling time of 12 s, according to the standard test method (ASTM E384-99). Samples were indented at 1 kgf. Indentation was repeated at a minimum of 15 times to ensure a reliable mean value. The bulk mechanical properties of the materials were determined by performing compression tests at a crosshead speed of 0.5 mm/min. Compression tests were stopped when the compressive load dropped by > 20%. The height to diameter ratio of the samples was one, according to ASTM E9. Composite samples were subjected to compression tests before and after immersion in the Dulbecco's Modified Eagle's Medium (DMEM) solution for 1, 3, 6, 12 days.

3.2.3. In vitro degradation tests

To mimic the situations *in vivo*, degradation tests were conducted in a corrosion cell operating at 37 °C using DMEM (D1145, Sigma-Aldrich) as a corrosive environment. HEPES (4-(2-hydroxyethyl)-1-piperazineethanesulfonic acid - 391338, Calbiochem) - an atmosphere-independent biological buffer was added to DMEM (25 mM) to maintain a certain degree of electrolyte alkalinity during the degradation tests. An anti-bacterial and anti-fungus agent (A5955, Sigma-Aldrich) was added to DMEM by 1% to prevent bacterial and fungi growth. The ratio of solution volume to sample surface area (SV/SA) was 30 ml/cm^2, according to ASTM G31-72. Before the immersion tests, the exposing surfaces of magnesium and composite samples were ground using SiC sandpaper up to 2400 grit, washed in an ultrasonic ethanol bath for 5 min and dried by a hot air blower. The degradation rates of the materials were determined from the amounts of hydrogen gas released and mass losses. The concentrations of ionic corrosion products in the immersion solution were measured by the Inductive Coupled Plasma (ICP) technique. The changes of the pH of the corrosive solution during immersion were monitored using a micro pH meter (S220 SevenCompact, Mettler Toledo). After the immersion tests, the corrosion products were removed from the samples by using a chromic acid solution composed of CrO_3 (200 g/l) and $AgNO_3$ (10 g/l), according to ASTM G1-90.

3.2.4. Electrochemical tests

Specimens with a diameter of 13 mm were cut into slices and mounted in epoxy resin with only the top surface to be exposed to the electrolyte, followed by grinding with SiC sandpaper to 2400 grit. The exposed surface area was 1.33 cm^2. The slices were then made conductive by a copper wire with an isolation layer (also shielding the connection area). The three electrode configuration according to ASTM G 5-94

was adopted to perform polarization tests. A Saturated Calomel Electrode (SCE) was used as the reference electrode and a platinum mesh as the counter electrode. Open Circuit Potential (OCP) measurements during immersion up to 24 h were determined using a Solartron 1250/1255 potentiostat. Potentiodynamic polarization (PDP) tests were performed immediately after the OCP measurements at an initial potential of − 0.2 V *versus* OCP increasing to + 0.5 V *versus* OCP at a scan rate of 1 mV/s.

3.2.5. In vitro responses of rat bone marrow stromal cells

3.2.5.1. Cell attachment assay

Rat bone marrow stromal cells (rBMSCs) were used to assess cell attachment to the materials. In brief, cells were resuspended in the cell culture medium and then seeded on to the surfaces of pure Mg and Mg-20% bredigite composite samples with a seeding density of 2×10^4 cells per well in 24-well tissue culture plates. After an incubation period of 6 h, specimens were collected from the cell culture plates and rinsed with phosphate-buffered saline (PBS), which allowed the removal of non-adherent cells. The adherent cells were then fixed using 4% paraformaldehyde solution for 30 min. Subsequently, the specimens were treated with 0.1% Triton X-100 in PBS and blocked with 1% bovine serum albumin (BSA) for 20 min. The actin cytoskeletons of the cells were labelled in red by incubating with Phalloidin TRITC (Sigma, USA) for 30 min and in contrast the cell nuclei were labelled in blue by 40,6-diamidino-2-phenylindole dihydrochloride (DAPI, Sigma, USA) [91]. The cell morphology was then observed by using a confocal laser scanning microscope (CLSM, Leica, Germany).

3.2.5.2. Cytotoxicity tests

Monolithic and composite extracts were prepared with a method established in previous studies [92]. Briefly, magnesium and Mg-40% bredigite discs with a diameter of 13 mm and a thickness of 2 mm were soaked in Dulbecco's Modified Eagle's Medium (DMEM, GIBCO) with a surface area to volume ratio of 1 ml/cm^2 and incubated in a humidified incubator at 37 °C and 5% CO_2 for 24 h. The supernatant fluid was withdrawn and centrifuged at 1200 × *g* for 5 min at room temperature. To obtain desired concentrations of the extracts, the extracts were diluted with DMEM + 10% FBS (Fetal Bovine Serum) (HyClone) + 1% P/S (penicillin/streptomycin)

at ratios of 1/2, 1/4, 1/8 and 1/16, and they were then sterilized through a filter (Millipore, 0.22 m) and stored at 4 °C (ISO10993-1).

rBMSCs were adopted to evaluate the cytotoxicity of the materials. Cells were isolated, expanded using an established method with minimum modifications [93] and cultured in DMEM, 10% Fetal Bovine Serum (FBS), 100 U/ml penicillin and 100 mg/ml streptomycin at 37 °C in a humidified atmosphere of 5% CO_2. Cytotoxicity tests were carried out by indirect contact and the control groups involved the use of DMEM as the negative control. Cells were incubated in 96-well cell culture plates at 2×10^3 cells/100 µl medium in each well and incubated for 24 h to allow attachment. The medium was then replaced with 100 µl of extracts prepared as aforementioned. The number of viable cells was quantitatively assessed by the MTT test [94]. MTT (Sigma) [3-(4,5-dimethylthiazol-2-yl)-2,5-diphenyl tetrazolium bromide] is a yellow tetrazolium salt that can be enzymatically converted by a living cell to a purple formazan product. The intensity of the color produced is therefore directly proportional to the number of viable cells in culture and thus to their proliferation *in vitro*. The absorbance of the color can be measured at 590 nm (A590). In the present tests, after incubating at 37 °C and in an atmosphere with 5% CO_2 for 1, 3 and 6 days, 100 µl of the 0.5 mg/ml MTT solution was added to the well plate and incubated at 37 °C for 4 h. Then, 100 µl of dimethyl sulfoxide was added to each well and the plate was shaken for 5 min. The optical density (OD) at 590 nm was measured with an enzyme-linked immunoadsorbent assay plate reader (ELX800, Bio-TEK). The results were compared in OD units.

3.2.5.3. Alkaline phosphate activity assay

The original extracts and those diluted at ratios of 1/4 and 1/16 were selected for the assessment of alkaline phosphate (ALP) activity. rBMSCs were cultured for 7 days under the same culture conditions as described above. ALP activity was quantitatively determined by an assay based on the hydrolysis of *p*-nitrophenyl phosphate to *p*-nitrophenol using the method of Lowry et al. [95]. Cells were extracted from the extracts and permeabilized with the use of 0.1% Triton X-100 solution (Sigma). Cell lysate from each sample was then used for alkaline phosphatase assays. The absorbance was measured at 405 nm using a spectrophotometer (UV–vis 8500, Shanghai, China) and ALP activity was calculated from a standard curve after normalizing to the total protein content. The results were expressed as nanomoles of *p*-nitrophenol produced per minute per microgram of protein. ALP activity of cells cultured in the medium supplemented with 10% FCS without any addition of extracts served as the control. Data were expressed as

mean ± standard deviation (SD). Three independent experiments were carried out and at least five samples per each test were taken for statistical analysis.

A one-way analysis of variance (ANOVA) with Tukey's *post hoc* test was used for statistical analysis of multiple comparisons. Significant difference was considered when $p < 0.05$.

3.3. Results and discussion

3.3.1. Microstructure and mechanical properties of the composites

To achieve reduced biodegradation rates and extended mechanical functionality of magnesium-matrix composites, it is a prerequisite to prepare the composites with minimum microstructural defects, mainly pores, and a homogeneous distribution of bioceramic particles, especially when the volume fraction exceeds 20%. A fabrication technique should be carefully chosen and process conditions must be optimally set, which is challenging, given the pyrophoric nature of magnesium powders with a high affinity to oxygen [96]. We chose a solid-state powder metallurgy route instead of a liquid-state processing route, thereby limiting the reactivity of magnesium during processing and minimizing bulk porosity that would inevitably be introduced by applying casting techniques [96]. Fig. 1 shows the SEM micrographs of the monolithic magnesium, Mg-20% bredigite composite (by volume) and Mg-40% bredigite composite after processing by means of Pressure Assisted Sintering (PAS). The gray dark color and white color in the SEM micrographs correspond to the magnesium matrix and bredigite particles, respectively. These micrographs show highly densified, integrated microstructures and, in general, homogeneous dispersion of bredigite particles even at an unusually high volume fraction of 40%. It should be noted that achieving such densified microstructures would not be possible by processing at room temperature because of limited ductility of magnesium having an insufficient number of operable slip systems [97]. However, when magnesium is heated above 225 °C, more slip systems become operative, leading to a steep decrease in tensile strength to < 10 MPa at 350 °C [98]. This suggests that at the pressing temperature used in this study, *i.e.*, 350 °C, the magnesium matrix was considerably ductile, capable of fusing into pores and cavities to fill vacant spots in the microstructure (Fig. 1b and c). With the aid of PAS, the composites with a high volume fraction of bioceramic particles (40 vol.%) could be successfully processed with a minimum amount of porosity. The microstructures of the composites in this research were morphologically different from those of the composites that were prepared by using the extrusion technique. The extruded magnesium-matrix composites were shown to have anisotropic microstructures

with ceramic particles being aligned in the extrusion direction [23, 26]. The microstructures of the present composites, however, did not show any dependency on the compaction direction, but were isotropic with spherical Mg powder particles surrounded by homogenously dispersed small bredigite particles (Fig. 1).

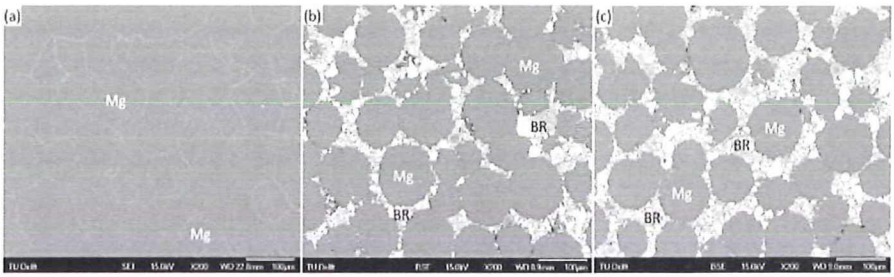

Fig. 1. Microstructures of the composites containing (a) 0, (b) 20 and (c) 40 vol% bredigite particles.

In addition, with the extrusion technique, shear forces, being applied to powder particles during processing, would be much larger than those in PAS and they would introduce additional pores to the microstructure, particularly at metal-ceramic interfaces [26] due to possible microstructure inhomogeneity, such as clustering of ceramic particles [23], mismatch at interface [94]and different deformation mechanisms of metals and ceramics [99]. Thus, the PAS technique would be more appropriate for fabricating Mg-matrix composites with high volume fractions of bioceramic particles (20–40 vol%, being at least 20% more than most of the Mg-matrix composites previously developed with the extrusion technique [23, 43, 100, 101]). Adding a large volume fraction of (> 20 vol%) of bioactive ceramic particles into the Mg matrix would be highly desirable, because it could significantly reduce the degradation rate of Mg and increase its bioactivity at the same time. The only concern would be the negative influence of ceramic particles on the mechanical behavior of the composites.

Table 1 compares the mechanical properties of the monolithic magnesium and composites with those of the human bone. Adding 20 vol.% bredigite particles to Mg increased the micro-hardness and ultimate compressive strength (UCS) of Mg by 68 and 67%, respectively. The compressive strengths of the composites were comparable to those of the human bone (Table 1). The superior mechanical strengths of the composite could be explained by the homogenous dispersion of hard bredigite particles throughout the Mg matrix, immobilizing dislocations and

thus causing enhanced resistance to deformation [102-105]. In addition, irregular bredigite particles with multiple sharp edges established stronger interfaces with magnesium by disrupting the pre-existing oxide layer on magnesium powder particles [106, 107] when they were compressed against the matrix during PAS, which contributed to the improved strength and hardness of the composite (Table 1). However, a further increase in the volume fraction of bredigite from 20 to 40 vol.% not only did not contribute much to a further improvement of the strength of the Mg-20 vol.% bredigite composite but also deteriorated the ductility (Table 1) as a consequence of the clustering of ceramic particles (bredigite), causing pores and weak bonding among brittle ceramic particles within the clusters and/or between the matrix and clustered particles [108, 109]. The large standard deviations of the mechanical property data of the Mg-40 vol.% composite suggested the relative inhomogeneity in its microstructure, causing its mechanical properties to deviate much more than those of the composite with a smaller volume fraction of bioceramic particles.

Table 1. Mechanical properties of the monolithic magnesium and composites in comparison with the strengths of human's tibia and femur.

Material	Compressive strength (MPa)	Ultimate compressive strength (MPa)	Micro-hardness ($HV_{1.0}$)	Elongation to fracture (%)
Mg	90 ± 3.8	114.27 ± 2.4	38.2 ± 0.1	6.1 ± 0.9
Mg-20% bredigite	135.0 ± 6.2	190 ± 6.0	64.05 ± 5.8	13.9 ± 1.8
Mg-40% bredigite	140.0 ± 7.8	192.6 ± 12.2	72.8 ± 9.7	9.8 ± 3.1
Cortical bone [110, 111]	130–180	–	–	–
Femur [112]	167	–	–	–
Tibia [112]	159	–	–	–

The overall porosity of the specimens, being fully densified at the core and semi-porous at the edges, was not larger than 5% for the Mg-40 vol.% bredigite composite (Table 2). Some micro-pores and cracks were observed mostly along the side wall and close to the bottom of cylindrical specimens that were in direct contact with the die during single-action uniaxial hot pressing. During compaction, mixed particles in the bulk under pressure could easily flow, while those at the interface would be locked by a large friction force at the die-material interface. During subsequent ejection, a large friction force at the die-material interface tended to cause the contacting layer of the specimen to be disintegrated from the bulk. The observed inhomogeneity in microstructure from the core to the surface negatively affected the biodegradation behavior, which will be discussed in the following sections.

Table 2. Porosity values of the materials PASed at 350 °C.

Material	Bulk porosity (%)
Mg	0
Mg-20% bredigite	3
Mg-40% bredigite	5

3.3.2. Degradation rates of the composites

Fig. 2 shows the degradation profiles of the composites and the accompanied pH changes during immersion in DMEM over different times up to 12 days, in comparison with those of the monolithic magnesium also prepared from the powder. It should be noted that the mass loss values of all the samples before 24 h of immersion were converted from the measurements of hydrogen evolution because the mass loss measurements were inaccurate at low degradation rates in the first phase of immersion. The other data points were directly taken from mass loss measurements. From Fig. 2, it is clear that all the samples degraded very slowly during the first 24 h and then degradation accelerated until day 6 and decelerated from day 6 to day 12. Despite the similar trends of degradation between the monolithic magnesium and the composites, the former was completely corroded by day 12, causing intense alkalization of the solution to reach a pH value of 9.8, despite the presence of HEPES as a pH buffer (see the black dashed line in Fig. 2). The average degradation rate of the monolithic magnesium (Table 3), *i.e.*, 31.41 mg/cm^2/day determined by measuring the mass loss after 12-day immersion per 1.33 cm^2 of the exposed area, was in good agreement with that determined in previous studies on cast magnesium specimens (19–44 mg/cm^2/day) [21]. By contrast, the Mg-20% bredigite and Mg-40% bredigite composites had markedly reduced average degradation rates of 1.26 and 2.65 mg/cm^2/day, respectively. Thus, a substantial reduction in degradation rate by up to a factor of 24 was achieved by adding bredigite particles to magnesium.

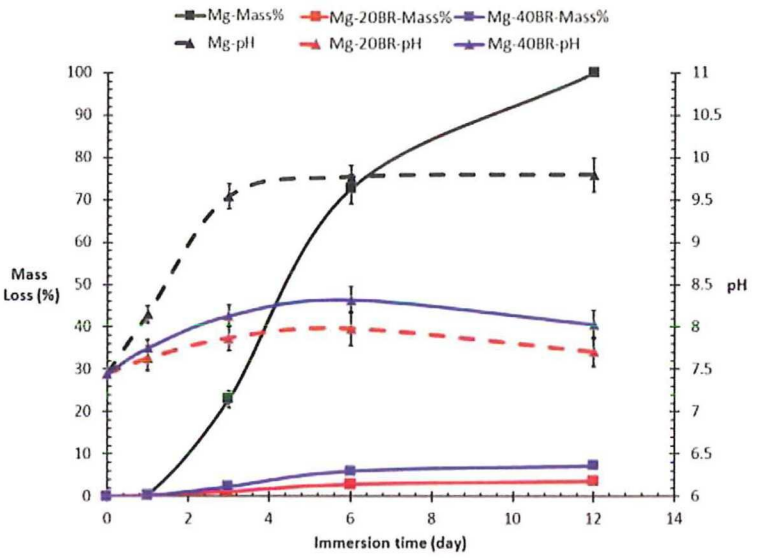

Fig. 2. Mass losses of samples and pH changes during immersion in DMEM for 12 days.

Table 3. Calculated average degradation rates of the materials after 12 days of immersion in HEPES-buffered DMEM.

Material	Degradation rate (mg/cm^2/day)
Mg	31.41
Mg-20% bredigite	1.26
Mg-40% bredigite	2.65

The degradation of the composites was slower than that of cast ZE41 and AZ91 alloys at average dissolution rates of 7.71 and 6.95 mg/cm^2/day in buffered Hank's solution, respectively [113]. According to the literature, the amount of Mg^{2+} released from the bredigite-containing magnesium-matrix composites is tolerable for the body (19–44 mg/cm^2/day, as long as the total surface area of a

magnesium implant is < 9 cm^2) although the amount of the equivalent hydrogen evolution for such a mass loss is still not tolerable for the body (tolerable level: 0.01 $ml/cm^2/day$) [21]. A distinct advantage of the magnesium-matrix composite with a large volume fraction of bredigite particles lies in a reduced amount of liberated hydrogen, which is not equivalent to the total mass loss anymore, because partial dissolution of bredigite particles also contributes to the total mass loss. In other words, because partial dissolution of bredigite particles does not produce additional hydrogen, the overall gas evolution of the composite would be less than monolithic Mg, having the same exposed area. For example, the Mg-20% bredigite composite that loses weight at a rate of 1.26 $mg/cm^2/day$ theoretically liberates hydrogen gas at a rate of 1.01 $ml/cm^2/day$, which is 0.25 $ml/cm^2/day$ less than the monolithic magnesium having the same weight at the start of immersion.

3.3.3. Electrochemical degradation of the composites

3.3.3.1. Open circuit degradation of the composites

When magnesium is exposed to water, it quickly oxidizes to form magnesium cations (Mg^{2+}) by giving up two valence electrons (Eq. 1). Water on the other hand takes up free electrons at cathodic sites and chemically reduces to hydroxyl anions and hydrogen gas (Eq. 2). With the accumulation of Mg^{2+} ions in the solution, there will be more cations reacting with OH^- groups to form $Mg(OH)_2$ that has a low solubility (12 mg/l) in water and precipitates out in the medium eventually [52, 114].

$Mg_{(s)} \rightarrow Mg^{2+}_{(aq)} + 2e^-$ Eq. 1 Anodic reaction

$H_2O_{(l)} + 2e^- \rightarrow OH^-_{(aq)} + H_{2(g)}$ Eq. 2 Cathodic reaction

$Mg^{2+}_{(aq)} + 2OH^-_{(aq)} \rightarrow Mg(OH)_{2(s)}$ Eq. 3 Product formation

A $Mg(OH)_2$ layer formed on the magnesium surface (Eq. 3) may be thought to act as a barrier against further dissolution by preventing mass diffusion between the magnesium substrate and the solution [55]. In electrochemistry, the formation of this layer shifts the Open Circuit Potential (OCP) of magnesium to more positive values [115]. OCP value evolutions of the monolithic magnesium and the composites over 24 h are presented in Fig. 3. The slopes of the OCP curves, indicative of the rates, at which the surface layer formed over time, were similar during the first hour of immersion. However, the differences became larger as degradation proceeded from 1 to 24 h. Fig. 3 shows that in the case of the monolithic magnesium a surface layer was rapidly formed. Solution alkalization, which occurs along with magnesium dissolution, encourages the formation of a

partially protective hydroxide layer (Eq. 3). In the case of the composites, however, the rate of the surface layer formation became lower with increasing volume fraction of bredigite particles (Fig. 3). Considering the fact that bredigite particles were present in the composites at the expense of the magnesium matrix on the whole surface, the delayed and incomplete development of a hydroxide surface layer on composite samples could be due to their low ability to reach a certain degree of solution alkalinity (Fig. 2 - dashed lines). It also indicated that within 24 h bredigite particles did not positively contribute to surface passivation.

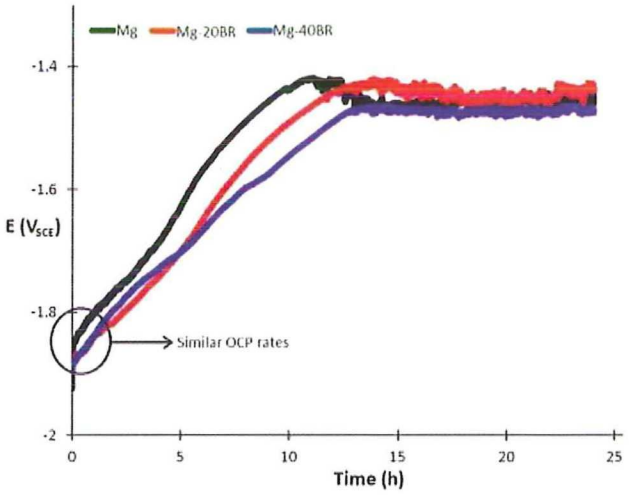

Fig. 3. Open Circuit Potential (OCP) curves of the materials immersed in HEPES-buffered DMEM for 24 h.

The question as to if bredigite really participated in the degradation process during the first 24 h could be answered by detecting silicon in the solution and in the surface layer, because only bredigite contains this element. EDS point scans could not identify the presence of silicon in the surface layer of corroded samples. Furthermore, ICP analysis (Fig. 4) showed very limited amounts of silicon, *i.e.*, < 3 ppm in the solution after one day of immersion, meaning that bredigite stayed almost inert during the first day of immersion, thus not contributing to the chemistry of the surface layer by dissolving. It confirmed that the partially protective surface layer was mainly formed during the first 24 h due to the chemical interaction between the magnesium matrix and DMEM. Thus, monolithic magnesium samples, having a larger exposed magnesium surface area as compared to composite

samples, could form a homogenous, complete surface layer more quickly than the composites (Table 4) as a result of a greater extent of interaction between magnesium and DMEM.

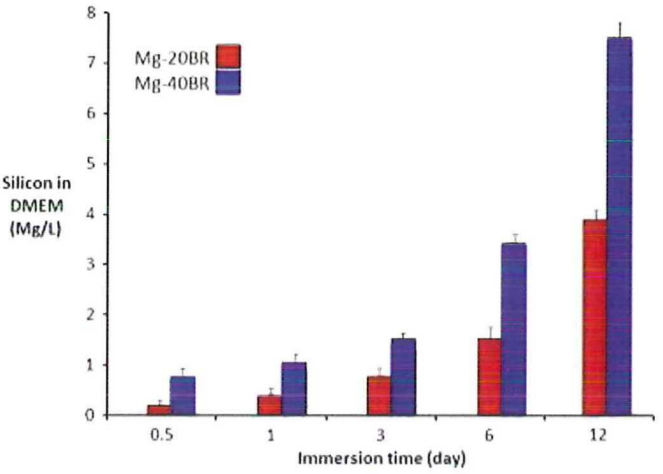

Fig. 4. Concentrations of silicon released from the composites to DMEM as a function of immersion time.

Table 4. Surface stabilization potentials and elapsed times for the materials immersed in HEPES-buffered DMEM.

Material	Stabilization potential E_s (V_{SCE})	Elapsed time till stabilization T_s (h)
Mg	− 1.43	10.56
Mg-20% bredigite	− 1.44	12.48
Mg-40% bredigite	− 1.47	13.01

3.3.3.2. Degradation under forced polarization conditions

Potentiodynamic polarization (PDP) curves of the composites at 1 and 24 h of immersion (Fig. 5a–d) showed an almost 230 mV increase in corrosion potential E (V_{SCE}) (visible by comparing the corrosion potentials in Fig. 5a to the ones in Fig. 5c) as a result of the gradual formation of a partially protective surface layer along with immersion time. The gradual formation of the surface layer caused the cathodic activity of all the samples to decline within 24 h (Fig. 5b and d, from 0 to 250 s). This suggested that the formation of a surface layer inhibited water reduction on the magnesium surface. On the other hand, the anodic activity of samples remained almost unchanged, despite the presence of the surface layer (Fig. 5b and d, from 250 s onwards), meaning that the formation of the surface layer exerted a smaller impact on the anodic activity than on the cathodic activity. This could be because anodic currents were derived from several highly intense anodic regions, occupying a relatively small proportion of the scanned area, while cathodic values were obtained from a much larger fraction of the working area [116]. In addition, the number and intensity of the local anodes were shown to increase with time in proportion to the area of the exposed local cathode [61]. In other words, localized corrosion in composite samples progressed under cathodic control. Thus, pH, affected by the cathodic reaction, must have had a significant effect on the magnitude of the corrosion current. It was found earlier by the present authors that in buffered solutions the cathodic and anodic current densities in the PDP tests were higher than those in DMEM without the buffer and the OCP values were more negative than those in DMEM without the buffer due to the pH maintenance effect of the buffer [79].

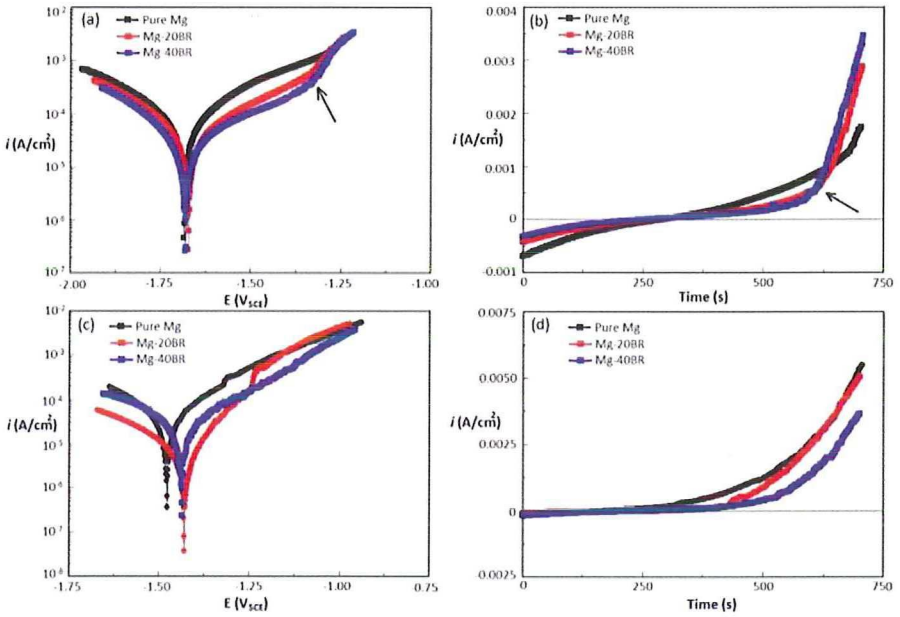

Fig. 5. Potentiodynamic polarization (PDP) curves at 1 h (a and b) and 24 h (c and d) of immersion. Note that during the PDP tests the OCP changed with exposure time from 1 to 24 h (panels a and c); the same potential range of 0.7 V from − 0.2 V_{OCP} to 0.5 V_{OCP} was applied at both exposure times.

At anodic over-potentials, both the monolithic magnesium and the composites went through surface breakdowns, which is visible from a sudden increase in corrosion current (Fig. 5a and b - indicated by arrows), meaning that pitting corrosion took place as one of the corrosion mechanisms involved.

3.3.4. Degradation mechanisms of the composites

3.3.4.1. Homogenous volumetric degradation

SEM micrographs of corroded samples (Fig. 6a–f, corresponding to an immersion time of 0.5 day) showed that the dissolution of monolithic magnesium samples and that of the magnesium matrix in composite samples mostly proceeded through pathways along grain and prior powder particle boundaries. Grain boundaries are known as the distorted areas with high internal energy, as compared to the grain

interior, and can be regarded as an area of defects in the crystal structure with a configuration of dislocations and crystal lattice mismatch. It is well known that anodic metal dissolution will be accelerated in the vicinity of dislocations [117]. In our previous study on magnesium made from powder, it was observed that grain and prior power particle boundary dissolution occurred quickly after 15 s immersion, causing nano-cracks, < 100 nm long, to appear on the surface [79]. These nano-cracks grew fast in size, up to 500 times larger than the initial length within 1 h. The further development of the surface crack-like features created an interconnected network of surface cavities, propagating transversely (Fig. 7) over the surface and longitudinally into the surface, which brought the electrolyte (DMEM) in contact with the fresh surface, causing further dissolution. Because the surface crack-like features, or in other words, grain and prior powder particle boundaries were distributed evenly on the surface, it resulted in homogenous dissolution of the magnesium matrix, as shown in Fig. 7a. The cross-section micrograph of the Mg-20% bredigite composite after six days of immersion in DMEM revealed a homogenous inward development of the dissolution front, as the magnesium matrix was transformed into the hydroxide form [117]. The inward development of the corrosion layer was confirmed by the presence of trapped, undissolved bredigite particles within the transformed layer after six days of immersion. Therefore, grain and prior powder particle boundary corrosion that initiated immediately after immersion provided a homogenous slow pattern of degradation through the volume. Given that the thickness of the transformed layer was approximately homogenous (Fig. 7a), the general degradation rate, mainly determined by grain and prior powder particle boundary dissolution, excluding pitting corrosion, could be calculated by measuring the average thickness of the surface layer at a given time of immersion, which resulted in an average degradation rate of 0.43 mg/cm^2/day for the Mg-20% bredigite composite. A similar degradation rate was calculated for magnesium samples, tested in DMEM and in McCoy's 5A-5% Fetal Bovine Serum (FBS) medium [118, 119]. This calculated degradation rate is considerably lower than the average degradation rate determined from the mass loss (Fig. 2), suggesting that another corrosion mechanism must have played a more decisive role. In other words, grain and prior powder particle boundary dissolution was only one of the active degradation mechanisms and due to its slow rate, it could not be responsible for the total disintegration of magnesium samples with a mass of 3 g in twelve days (Figs. 2 and 6).

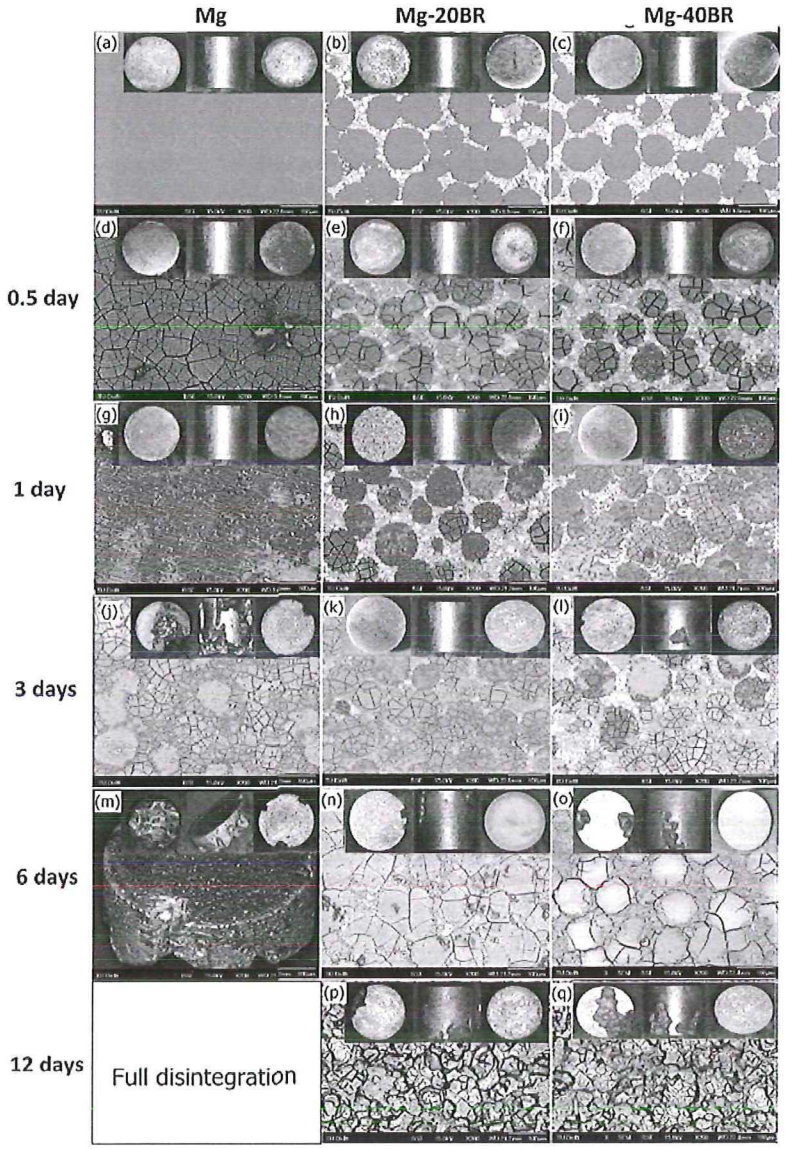

Fig. 6. SEM back-scattered micrographs of the materials containing 0 (the first column), 20 (the second column) and 40 vol.% (the third column) bredigite particles, showing different responses of these materials to DMEM during immersion through a period of 12 days. The insets represent bottom, side, and top of the samples from left to right.

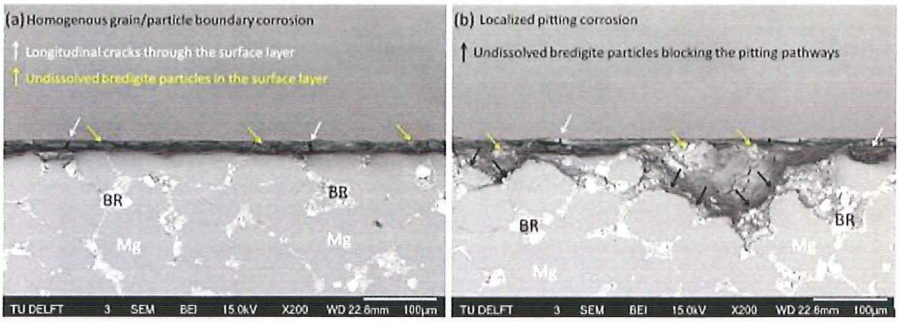

Fig. 7. SEM back-scattered images of the cross section of Mg-20% bredigite composite samples after 6 days of immersion. (a) shows the homogenous development of the corrosion layer. (b) shows the bredigite particles blocking pitting pathways across the magnesium matrix.

3.3.4.2. Localized pitting corrosion

Pitting was another phenomenon observed in corroded samples (Fig. 6g–n - the insets). In the preceding subsection on the electrochemical tests, the sudden increases in corrosion current density, mostly at anodic overpotential (Fig. 5b, indicated by the arrow), indicated the formation of early pits. These pits appeared within the first three days of immersion and grew into large corrosion cavities, appearing mostly on the side walls and bottom of samples, while the top surface of these samples remained intact (Fig. 6g–n - the insets). This could be due to the presence of structural disintegrity and cracks at the edges of samples formed during ejection subsequent to PAS, as discussed earlier. When samples were immersed in DMEM, the bulk matrix became undermined as pits (or cracks) provided feeding pathways for the corrosive medium to move forward through the anodic dissolution of crack tips [19]. Earlier studies on magnesium parts processed through the powder metallurgy route also indicated higher dissolution of samples mostly at the edges, because of the presence of disintegrity introduced during the material processing [118]. Pitting corrosion caused the degradation rates of all the samples to exceed the degradation rate due to grain and prior powder particle boundary corrosion (*i.e.* 0.43 mg/cm^2/day) by a factor of 73, 2.93 and 6 for the monolithic magnesium, Mg-20% bredigite and Mg-40% bredigite composites, respectively. It is thus clear that pitting corrosion, once initiated, plays a more important role than the grain and powder particle boundary degradation mechanism and dominates the degradation process. In addition to the edge effect, the presence of impurities beyond their tolerance limits may have contributed to pitting corrosion as well. XRF analysis of the magnesium powder used, having a purity of 99.86%, revealed 320

and 160 ppm of iron and nickel, respectively, which were higher than their tolerance limits (170 and 5 ppm, respectively) [120]. These impurities have very low solubility limits in the magnesium solid solution, leading to precipitation after solidification or PAS mostly along the grain boundaries. The precipitates generate strong micro-galvanic coupling with magnesium, causing intensive anodic dissolution of the magnesium solid solution in the vicinity of the precipitates.

When pitting occurs, the degradation rate is expected to decline after a while, since the dissolution process produces an alkaline environment that will stabilize magnesium hydroxide as a protective surface layer. However, in monolithic magnesium samples, pitting corrosion occurred at the beginning of immersion and even accelerated in alkaline environments (pH between 8 and 8.9, Fig. 2). It suggested that once early pits were initiated, they could autonomously grow, showing no sign of passivation. The PDP curves also indicated that surface passivation did not effectively take place after the surface breakdown as the corrosion currents in all the samples increased with time (Fig. 5b - arrow). Pitting is basically an intensive anodic dissolution process, leading to the accumulation of magnesium cations in the solution next to the corroding surface. In this manner, hydrolysis of magnesium cations with water will be possible [17, 72, 79], resulting in the formation of hydrogen protons, acidifying the anodic regions (Eq. 4).

$$4Mg^{2+}_{(aq)} + 4H_2O_{(l)} \rightarrow Mg_4OH_4{}^{4+}_{(aq)} + 4H^+_{(aq)} \qquad \text{Eq. 4}$$

The formation of hydrogen protons is catastrophic to the degradation of the magnesium matrix, because it can directly attack the hydroxide layer, producing water and magnesium cations, as expressed in Eq. 5.

$$Mg(OH)_{2(s)} + 2H^+_{(aq)} \rightarrow 2H_2O_{(l)} + Mg^{2+}_{(aq)} \qquad \text{Eq. 5}$$

The products of hydrogen attack (Eq. 5) can be consumed in the hydrolysis reaction (Eq. 4), acidifying the region again. In addition, hydrogen protons together with magnesium cations electrostatically attract chloride ions to the region, producing hydrochloric acid attacking the substrate, producing highly soluble $MgCl_2$ and hydrogen gas (Eqs. 6 and 7).

$$Mg_{(s)} + 2HCl_{(aq)} \rightarrow MgCl_{2(aq)} + H_{2(g)} \qquad \text{Eq. 6}$$

$$Mg(OH)_{2(s)} + 2Cl^-_{(aq)} \rightarrow MgCl_{2(s)} + 2OH^-_{(aq)} \qquad \text{Eq. 7}$$

The abovementioned reactions indicate that once pits get initiated, the magnesium matrix cannot re-establish a protective layer, leading to self-driven intense pit development, and finally to the total disintegration of cylindrical magnesium samples by day 12 despite the high level of alkalinity (Fig. 2). In the case of the

composites, a second phase with more resistance to H^+- and Cl^--driven attacks, such as bredigite, can limit the intense pit propagation by blocking pitting pathways, giving time to the matrix to re-establish a surface layer. The cross section of corroded composite samples after 6 days of immersion in DMEM indeed showed the blocking of pitting pathways by bredigite particles, once the inwardly developed pit front reached these particles (Fig. 7b). The remainders of bredigite particles within the body of the surface layer appeared to be partially dissolved ones, meaning that they degraded at a slower rate than the magnesium matrix.

3.3.4.3. Surface morphology and chemistry of corroded composite samples

The initial hydroxide layer showed an island-like feature because of the longitudinal and transversal surface cracks that separated the islands (Fig. 6d–f). Fig. 8 shows the co-existence of phosphorus (from DMEM) along with calcium and silicon on the corroding surfaces of the composites. Bioactive behavior initiates when these ions react with each other and/or react with other ions, originating from DMEM, such as calcium and phosphate ions, producing insoluble inorganic compounds precipitated on the surfaces (Figs. 8 and 9).

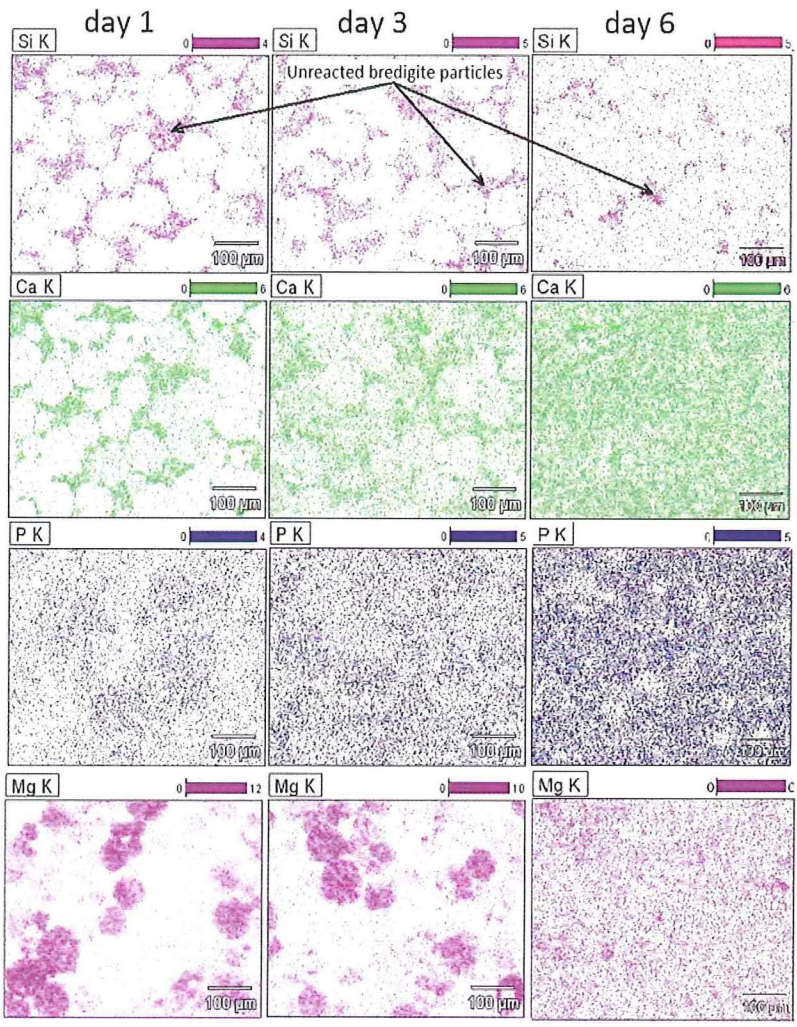

Fig. 8. EDX elemental mapping of the composite containing 40 vol% bredigite particles, showing the gradual precipitation of Si, Ca and P on the surface as a function of immersion time.

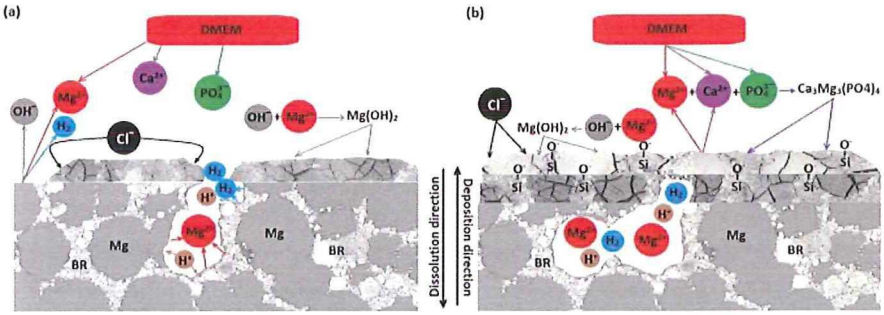

Fig. 9. Schematic of the biodegradation process of the composites after 1 day (a) and 6 days (b) of immersion in DMEM.

Phosphate ions preferentially bond with Ca^{2+} and Mg^{2+} [30] to form white compounds of magnesium-containing apatite on the corroding surfaces (Figs. 7d–i and 9). The involvement of magnesium in calcium phosphates as a corrosion layer decreases the degree of crystallinity and enhances the degradation rate of calcium- and phosphate-containing compounds, which, as compared to HA, brings about better bioactivity [121]. Mg-CaP is essential for exhibiting good biocompatibility and bioactivity because proteins, such as fibronectin and vitronectin that act as cell attachment–promoting proteins, can be better adsorbed in the presence of Ca-Mg-P precipitates [122]. The initial Mg-CaP-containing layer, appearing as the white spots embedded in the gray-colored hydroxide layer (until day 3 - Fig. 6g–l) gradually expanded over the whole surface until it fully covered the surface, thus appearing as a white Mg-CaP-containing layer (6th day-Figs. 6n and 9). The relative amount of phosphorus deposition was observed to be larger on the magnesium matrix (~ 11 at.%) than on bredigite particles (2.61 at.%) by day 3 of immersion (Fig. 8). This is mainly because the magnesium matrix dissolves faster than bredigite particles and the local pH value will be raised near the corroding magnesium surface, possibly well above 10 [79], thereby encouraging the precipitation of Ca- and P-containing phases [117].

Element mapping on composite sample surfaces showed negligible deposition of silicon by day 3 (Fig. 8). However, its involvement in the surface layer, yet below 1 at.%, was identified by day 6 and 12 of immersion. One reason for relatively low silicon deposition is that calcium ions from bredigite are released preferentially to silicon ions by ion exchange with H^+ [123]. Thus, most of silicon in bredigite would stay within the unreacted part, forming a negatively charged surface with the functional group ($\equiv Si\_\_O^-$) [123], which electrostatically attracts magnesium and calcium cations (Figs. 8 and 9). Some colonies of silicon visible on the surface after

6 days of immersion (Figs. 8 and 9) were actually the un-reacted parts of the ceramic retained within the body of the corrosion layer. Thus, by day 12, the simple hydroxide surface layer was transformed into a compact mixture of unreacted bredigite particles embedded within a layer of Mg, Ca, P and Si-containing compounds (Fig. 9).

With the addition of the HEPES buffer to DMEM, the local pH close to the magnesium surface could be largely maintained, which would result in slower formation of a surface hydroxide layer as well as faster progression and more intensive micro galvanic activities [116]. In addition, the tendency of calcium phosphates to precipitate from the HEPES-buffered DMEM solution would be significantly reduced, as the local pH of the solution was maintained at a relatively low level by the buffer [68, 79]. In other words, degradation rates derived from this research would have been lower and calcium phosphate precipitation would have been more intensive if the buffering agent had not been added to DMEM.

3.3.5. Mechanical properties of the composites in relation to biodegradation

Degradation of the composites in DMEM affected their mechanical behavior, causing the UCS to decrease gradually from 190 MPa to about 130 MPa in 12 days. Fig. 11 shows that mechanical cracks were preferably initiated at the corrosion pits during compression tests, deteriorating the mechanical strength as well as the ductility of the composites. On the other hand, there were no significant differences between the micro-hardness values, before and after immersion in DMEM (Fig. 10b). In the previous section we showed that pitting corrosion, as the dominant mechanism of degradation, mostly initiated at the edges of the sample and its penetration towards the core was limited by the blocking effect of bredigite particles. Thus, the core of the samples would still remain intact and thus showed the same values of micro-harness as before the immersion tests. The gradual loss of the compressive strength was also related to preventing the pitting corrosion from reaching the core of the samples.

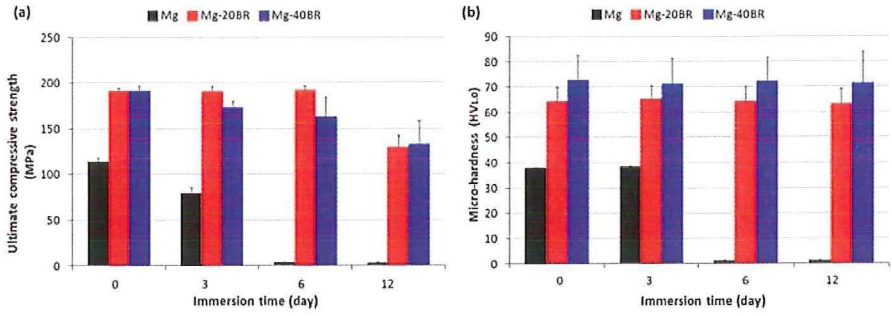

Fig. 10. Ultimate compressive strength (a) and micro-hardness (b) of the composites as a function of immersion time in DMEM.

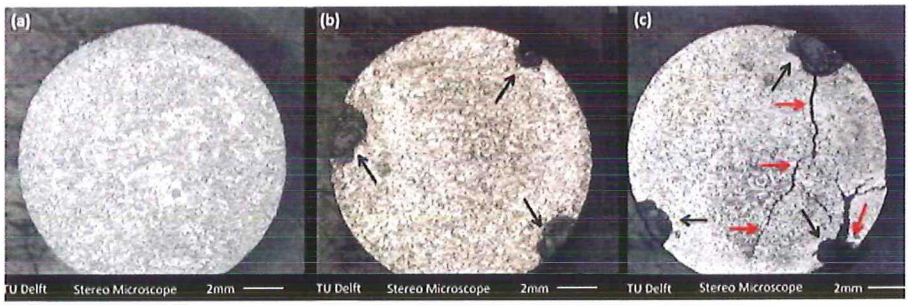

Fig. 11. Morphologies of the Mg-20% bredigite composites before immersion (a), after immersion for 12 days (b) and after the compression tests (c), showing corrosion pits (black arrows) and mechanical cracks initiating at the pits (red arrows).

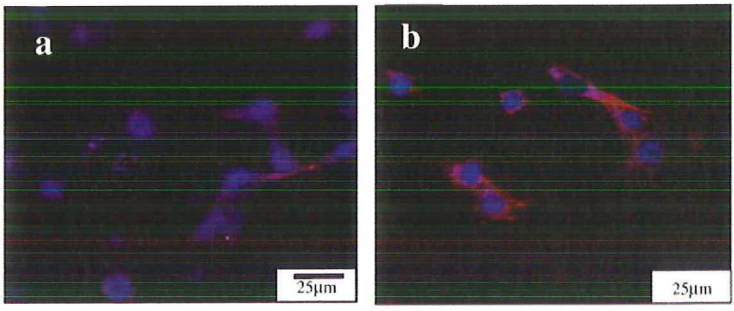

Fig. 12. Confocal microscopy images of the surfaces of pure Mg (a) and Mg-20% bredigite composite (b) samples after cell seeding for 6 h.

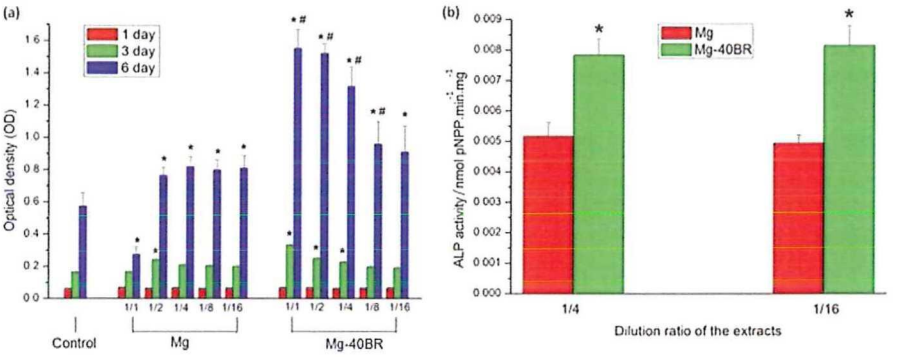

Fig. 13. (a) MTT assay of rBMSCs cultured in monolithic magnesium and Mg-40%bredigite extracts at different dilution ratios. The ratio of 1/1 stands for the original extract without diluting. The symbols * and # represent significant difference ($p < 0.05$) as compared with the control and with the magnesium extract, respectively. (b) ALP activity of rBMSCs in the presence of monolithic magnesium and Mg-40% bredigite composite extracts at the dilution ratios of 1/4 and 1/16. The asterisk (*) indicates that the ALP activity of the Mg-40% bredigite group was significantly higher than that of the magnesium group ($p < 0.05$).

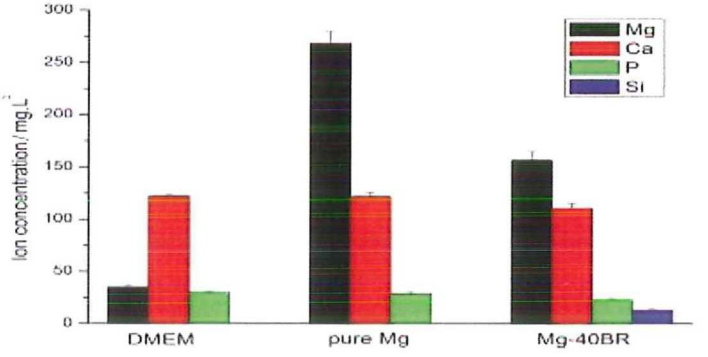

Fig. 14. Concentrations of ionic products in composite extracts after 24 h of immersion.

The mechanical properties of the composites after 12 days of immersion in DMEM were still in the range of those of femur and tibia (Table 1), confirming the mechanical functionality of the composites within the first two weeks of implantation. Our positive results on the short-term mechanical tests warrant further investigations on the degradation behavior and mechanical properties of the composites in the *in vivo* situations.

3.3.6. Biocompatibility and bioactivity of the composites in relation to biodegradation

3.3.6.1. Cell attachment

The morphologies of rBMSCs seeded on pure Mg and Mg-20% bredigite composite samples after incubation for 6 h are presented in Fig. 12. It is clear that the cell morphology on the Mg-20% bredigite composite (Fig. 12b) differed from that on pure Mg (Fig. 12a). The filopodia of the cells attached on pure Mg were hardly discernible. By contrast, the Mg-20% bredigite composite showed an enhanced ability of early cell attachment, as evidenced by the appearance of cytoplasmic extensions.

It is widely accepted that cell attachment is a desirable cellular response at the cell-material interface, as it promotes the cellular response to the implant surface [124]. However, pure Mg possesses a poor ability to support cell attachment due to extensive evolution of H_2 bubbles and rapid elevation of pH at its surface, which results in a hostile surface microenvironment, thereby inhibiting the attachment of cells [125]. In the present study, it was clear that the presence of bredigite in the composite led to improved cell attachment as compared with pure Mg. On the one hand, the enhanced cell attachment could be related to the fact that the degradation of the composite was significantly lower than that of pure Mg, which would result in much less H_2 evolution and lessened surface pH increase, thus presenting a more favorable surface condition for cellular response. On the other hand, the fast Ca-P deposition induced by the presence of bredigite (although not as a compact layer) [31], might have helped improve the initial cell attachment, as demonstrated in previous studies [125, 126]. The exact mechanism, however, is still unclear and worth further investigating in our follow-up studies. Nevertheless, it is reasonable to assume that, with an enhanced ability to support cell attachment, the Mg-20% bredigite composite would exhibit superior performance as compared with pure Mg, especially at the early stage right after implantation.

3.3.6.2. Cell proliferation and differentiation in the presence of the ionic products from the materials

A high degradation rate of magnesium causes the accumulation of ionic products in the vicinity of the corroding surface. In *in vitro* situations, the proliferation of cells is closely related to the ionic environment of the culture medium [127]. For Mg-based materials designed for biomedical applications, the extracts of the samples after a certain time of immersion in a corrosive solution are collected and then stored at 4 °C prior to the cytotoxicity test, which is known as the indirect cytotoxicity test [26, 128-134]. The extraction procedure is often conducted in the DMEM solution [132-135], which closely mimics the chemical composition of the blood plasma [136]. Our results from the indirect cytotoxicity tests on monolithic Mg samples confirmed that cell proliferation was significantly inhibited by the original (undiluted) magnesium extracts, whereas diluting the extracts led to enhanced proliferation of cells (Fig. 13a).

In contrast to the monolithic magnesium group, the extracts of the Mg-40% bredigite composite exhibited much higher abilities to stimulate the proliferation of rBMSCs. Considering the fact that magnesium ion concentrations in the extracts of the Mg-40% bredigite composite and those after dilution were lower than those in the magnesium group (Fig. 14), the stimulatory effect could only be attributable to the presence of silicon ions that were released from the bredigite component inside the composite material. Previous studies showed that silicon-containing ionic products from the degradation of silicate-based ceramics stimulated cell proliferation [127, 137]. It should be noted that for the Mg-40% bredigite composite, there might be a synergistic effect of silicon and magnesium ions on the proliferation of cells, as indicated by the previous studies on Ca-Mg-Si bioceramics including bredigite [33]. This inference needs to be confirmed in further investigation. Nevertheless, it is clear that the incorporation of bredigite into the magnesium matrix could lead to stimulated cell proliferation and thus enhanced bone regeneration, which is highly desirable for the clinical application of biodegradable implants [138].

The osteogenic differentiation of rBMSCs was investigated using an ALP assay on magnesium and Mg-40% bredigite extracts at dilutions of 1/4 and 1/16, and the results are presented in Fig. 13b. A quantitative study showed that Mg-40% bredigite composite extracts induced a higher ALP activity than the magnesium group. Further comparison between Mg-40% bredigite extracts with different diluting ratios, namely 1/4 and 1/16, revealed that the differences between the ALP activities of cells in these groups were not statistically significant ($p > 0.05$).

Osteogenic differentiation of BMSCs is one of the key steps to determining the success in bone regeneration and ALP is one of the widely recognized markers of osteogenic differentiation, which regulates phosphate metabolism [139]. Previous research showed that magnesium and silicon ion release during the degradation of silicate-based bioceramics, *e.g.*, bredigite, played an important role in raising ALP expression in BMSCs by providing a favorable ionic situation [89] and recent studies have demonstrated that silicon or magnesium ions alone at a certain concentration enhance the ALP expression of BMSCs [140]. In our study, it was difficult to make an assertive conclusion as to whether it was one kind of ions alone or their combination that was responsible for the enhanced ALP expression of the Mg-40% bredigite composite, as compared with that of the monolithic magnesium. Nevertheless, it was clear from our results that the presence of silicon ions in the Mg-40% bredigite composite, with even a minor portion in the extract, contributed to a significantly enhanced ability to induce osteogenic differentiation and thus to an improved rate, quality and progression of bone healing, as has been demonstrated in the *in vivo* studies on Si-substituted materials [141].

3.4. Conclusions

1. Magnesium-matrix composites containing up to 40 vol.% bredigite particles and possessing strengths in the strength range of cortical bone could be successfully produced by using the PAS technique.

2. The addition of bredigite to magnesium could significantly slow down the biodegradation rate of magnesium by up to 24 times, due to the blocking effect of bredigite particles in the pitting pathways of the magnesium matrix and the embedding of slowly degrading bredigite in a surface layer of Mg, Ca, P and Si-containing compounds.

3. The mechanical functionality of magnesium could be extended from 3 days to > 12 days. The strengths of the composites could be retained at a strength level of cortical bone after 12 days of immersion.

4. Bredigite-containing magnesium-matrix composites could improve the viability and proliferation of rat bone marrow stromal cells, while monolithic magnesium extracts without dilution were cytotoxic.

5. The magnesium-bredigite composites developed could have a great potential as a new generation of biodegradable and bioactive materials for orthopedic applications. The achieved simultaneous improvements in degradation behavior,

mechanical properties, biocompatibility and bioactivity prompted further *in vitro* and *in vivo* investigations.

CHAPTER 4

Fabrication of novel magnesium-matrix composites and their mechanical properties prior to and during in vitro degradation

This chapter is published as:

NaddafDezfuli, S., Leeflang, S., Huan, Z., Chang, J., Zhou, J., 2017. Fabrication of novel magnesium-matrix composites and their mechanical properties prior to and during in vitro degradation. Journal of the Mechanical Behavior of Biomedical Materials 67, 74-86.

Abstract

In our previous study, we developed Mg-matrix composites with bredigite as the reinforcing phase and achieved improved degradation resistance in comparison with Mg. However, the effects of materials processing method and process parameters on the mechanical behavior of the composites before and during degradation were still unknown. This research was aimed at determining the mechanical properties of Mg-bredigite composites prior to and during degradation. It was found that by optimizing the process parameters of Pressure Assisted Sintering (PAS), low-porosity Mg-bredigite composites with strong interfaces between homogeneously distributed bredigite particles and the Mg matrix could be fabricated. By reinforcing Mg with 20 vol% bredigite particles, the ultimate compressive strength and ductility of Mg increased by 67% and 111%, respectively. The in vitro degradation rate of the Mg-20% bredigite composite in a cell culture medium was 24 times lower than that of monolithic Mg. As a result of retarded degradation, the mechanical properties of the composite after 12 days of immersion in the cell culture medium were comparable to those of cortical bone. The encouraging results of this research warrant further investigations on the in vivo degradation behavior and mechanical properties of the composites.

4.1. Introduction

Magnesium is a light-weight metallic material with a density of 1.74 g/cm^3 and its mechanical properties are similar to those of the human bone [142]. The combination of excellent biomechanical compatibility and proven biodegradability in physiological environments has encouraged biomaterials scientists to make great efforts to gain a clear understanding of biodegradable Mg-based materials [17, 23, 79] for potential clinical applications, particularly for orthopaedic applications.

In the light of previous researches [23], Mg-matrix composites were introduced as a new generation of orthopaedic biomaterials, challenging the existing medical grade Mg alloys, mainly to avoid any known or uncertain clinical side effect that often comes with common alloying elements associated with magnesium e.g. zirconium [21]. The Mg-matrix composites studied have shown the possibilities of adjusting degradation properties and enhancing bioactivity [23, 43], although the issues related to their mechanical behavior along with degradation have not been addressed.

Degradation in a physiological solution will disrupt the structural integrity of Mg-matrix composites, especially when pitting corrosion is involved, which is often the dominant mechanism of the degradation of Mg and Mg-based alloys even without a ceramic phase [17]. Pitting corrosion, penetrating from the surface into the core, affects the mechanical behavior of Mg-matrix composites to a much greater extent than homogenous layer-by-layer corrosion, even at similar degradation rates. As a result of pitting corrosion, it is difficult to maintain the mechanical integrity over a certain period of time needed for orthopedic implants to bear a specific amount of load in a highly corrosive environment within the body [143]. Despite the strong need for experimental data, only a few studies on the mechanical properties of Mg alloys along with degradation have been conducted [43, 144] and, to the best of our knowledge, none on bioceramic-containing Mg-matrix composites.

From a biomedical point of view, incorporating a large volume fraction of bioactive reinforcing particles into the Mg matrix is highly desirable, considering the contributions of these particles to enhancing the bioactivity. Although, it may negatively affect the mechanical properties by increasing the chance of particle agglomeration in the Mg matrix and poor bonding at the interfaces, resulting in excessive embrittlement and premature failure [43, 145]. In the previous studies on P/M processed Mg-bioglass, Mg-calcium and Mg-hydroxyapatite (HA) composites, the volume fractions of reinforcing particles were limited to 10–20 wt.% (20 wt.% of HA with a density of 3.16 g/cm^3 being equal to 12 vol.%) so as to avoid excessive porosity [23, 43, 101].

We selected bredigite bioceramic particles in the $CaO.MgO.SiO_2$ family as a reinforcing phase added to magnesium, in large volume fractions, namely 20 and 40 vol.% (i.e., 28 and 57 wt.%, respectively). Bredigite has been proven to be cytocompatible [32] and bioactive by showing rapid hydroxyapatite (HA) mineralization and a strong stimulating effect on osteoblast proliferation [31]. The incorporation of silicon into Ca-P bioceramics together with their relatively high degradation rates has accounted for their superior bioactivity to HA ceramics [28, 87, 88]. The mechanical properties of bredigite are close to those of cortical bone [31, 33], enabling bredigite to bear mechanical load over a sustained period of time after implantation, which makes bredigite a more suitable option than the typically used calcium-phosphate-based compounds such as HA and tricalcium phosphate (TCP) in Mg-matrix composites.

The mechanisms of the degradation of the Mg-bredigite composites were proposed in our previous work. However, another critically important issue, i.e., their mechanical properties in relation to degradation behavior was not addressed. The present research was first aimed at developing a viable fabrication method for structurally integrated bioceramic-containing Mg-matrix composites, with a large extension in the range of the volume fractions of incorporated reinforcing particles to 40 vol.%.

Secondly, their mechanical properties in the as-fabricated state and during degradation in a cell culture medium over a period of 12 days were evaluated. It was expected that an understanding of the degradation mechanisms and degradation rate in relation to the gradual losses of the mechanical properties of the Mg-bredigite composites would improve the control of the degradation-related mechanical properties of the Mg-matrix composites, which would be of critical importance for the clinical applications of these advanced biomaterials.

4.2. Materials and methods

4.2.1. Materials and composite fabrication

Magnesium (with a purity of 99.86%, 320 ppm Fe and 160 ppm Ni and a mean particle size of 90 μm, provided by the Shanghai Institute of Ceramics) and bredigite ($Ca_7MgSi_4O_{16}$, BR, provided by the Shanghai Institute of Ceramics) powders were chosen as the starting materials. The as-fabricated irregular bredigite powder was sieved with mean particle size of 10 μm.

To evaluate the effect of the fabrication method on the integrity of composite structure and porosity, specimens were fabricated using two techniques, namely (i) Pressure Assisted Sintering (PAS) and (ii) cold compaction followed by high-temperature sintering. With the PAS technique, the powder mixtures with 20 and 40 vol.% bredigite particles in a cylindrical die with an inner diameter of 13 mm were first heated under a pre-pressure of 100 MPa and then uniaxially compacted at 500 MPa. A sintering step at 150, 250 or 350 °C for 1, 2 or 4 h under the compaction pressure of 500 MPa was taken to search for an optimum processing condition, leading to high densification. After sintering, specimens were air-cooled to room temperature. An illustration of the PAS technique is presented in Fig. 1. With the cold compaction and sintering technique, the mixed powders were first compacted at 500 MPa and at room temperature and then sintered at 500 or 600 °C for 2 h in a tube furnace under a protective atmosphere (high-purity argon). The value of bulk density was determined using Archimedes' principle according to ASTM B962 – 15, 2015.

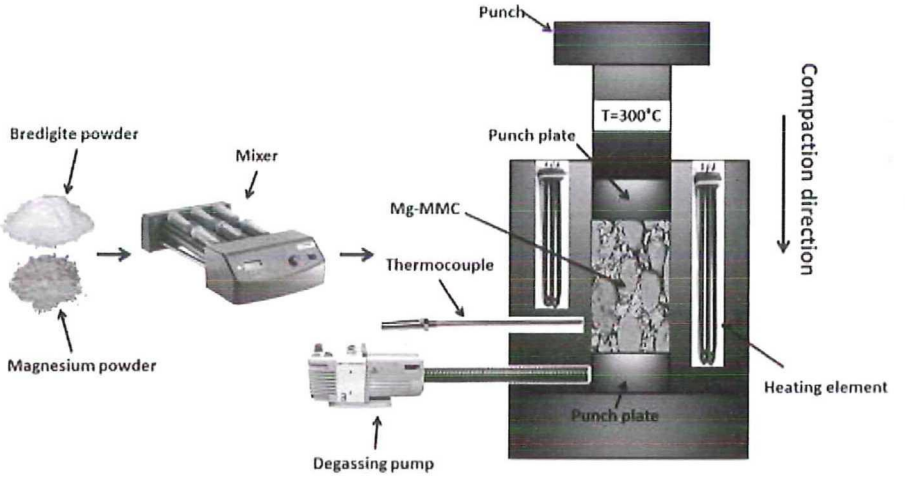

Fig. 1. Schematic illustration of the processing steps for the Mg-matrix composites developed in this research.

Samples for microstructure examination were sectioned and mounted in epoxy resin. Their cross sections were ground by using 2400 and 4000 grit sandpapers and then polished to attain a smooth surface.

4.2.2. Thermal properties

STA is a combination of Differential Scanning Calorimetric analysis (DSC) and Thermogravimteric analysis (TGA). During STA, the events that lead to the exchange of thermal energy with the surroundings and the changes in sample mass could be registered.

The thermal response of the monolithic Mg or the composites was monitored by heating a 60 mg of each sample in a Simultaneous Thermal Analyser (Netzsch STA 409). The samples were heated at a rate of 20 °C/min to the melting temperature of magnesium (i.e., 650 °C) under argon gas flow at a rate of 20 ml/min.

4.2.3. Microstructure and chemical analysis

The microstructures of the monolithic Mg and composite specimens were characterized by using a KEYENCE VHX-5000 Series-Digital Stereo Microscope (DSM) and a JEOL JSM-6500F Scanning Electron Microscope (SEM) working at an accelerating voltage of 15 kV.

Phase identification of the magnesium powder before and after sintering at 600 °C for 2 h was performed by using a Bruker D8 Advance X-ray diffractometer with monochromatic Cu radiation (Kα1 λ=0.154056 nm) over a 2θ-angle range between 10° and 130° and a step size of 0.020 degree. Data analysis was carried out with the Bruker program EVA. The chemical compositions of the surfaces of the composites subsequent to immersion tests in Dulbecco's Modified Eagle's medium (Sigma - DMEM) were obtained by elemental X-ray mapping using an Energy Dispersive X-ray Spectroscope (EDS) in a JEOL JSM-6500F Scanning Electron Microscope.

4.2.4. Mechanical properties prior to degradation tests

The microhardness (Vickers hardness) values of the monolithic Mg and composites were obtained by microindentation with a square-based pyramidal-shaped diamond indenter having an angle of 136° and at a dwelling time of 12 s, according to the standard test method ASTM E384-99, 1999 using a Vickers diamond micro-indenter (Leica VMHT). To evaluate the effect of indentation load and diagonal (i.e., a measure of the area covered by the indenter) on the hardness values of the materials, monolithic Mg samples were indented at 0.01, 0.49 and 9.8 N, while composite samples were indented at 0.49, 1.96, 2.94 and 9.8 N. Bredigite powder particles embedded in the Mg matrix were indented at 0.10 N. Indentation was

repeated at a minimum of 15 times to ensure a reliable mean value. After indentation, the affected area was observed by using DSM.

The bulk mechanical properties of the as-fabricated monolithic Mg and composites were determined by performing compression tests at a crosshead speed of 0.5 mm/min in an INSTRON universal testing machine using a 50 kN load cell. The height to diameter ratio of the samples were one, according to ASTM E9-09, 2009. The tests were stopped when a significant drop of compression load (>20% load) occurred.

To understand the effect of the structural imperfections at the edges of the as-fabricated specimens on the mechanical properties of the materials, a surface layer with a thickness of 1 mm that was in direct contact with the compaction die during fabrication was machined off from the PAS specimens containing 20% bredigite. Then, the machined specimens were subjected to the compression tests under the same condition.

4.2.5. Degradation tests

Degradation tests were conducted in a corrosion cell operating at 37 °C using DMEM as a corrosive environment. A HEPES (4-(2-hydroxyethyl)-1-piperazineethanesulfonic acid - 391338, Calbiochem) buffer was added to DMEM (25 mM) to maintain the solution pH during the tests. An anti-bacterial and anti-fungus agent (A5955, Sigma-Aldrich) was added to DMEM by 1% to prevent bacterial and fungi from growth. The ratio of solution volume to sample surface area (SV/SA) was 30 ml/cm^2 according to ASTM G31-72, 2004. The samples meant for the hydrogen liberation test were mounted in an epoxy resin with the top surface exposing. The exposing surface was then ground by using 2400 grit SiC sand paper, washed in an ultrasonic acetone bath for 3 min and dried by a hot air blower. After grounding, the samples were placed in a water jacketed beaker running at 37 °C filled with DMEM for a day. The liberated hydrogen was collected by a long-stem funnel inside a graduated burette, which was placed over the exposing surface of the specimens. The amount of hydrogen liberation then could be calculated by measuring the difference between the levels of the graduated burette as the degradation proceeds.

For the mass loss tests (long term tests), specimens were not mounted in epoxy to emphasize the effect of geometry on the degradation behavior of the specimens. Therefore, all the exposed surfaces were ground and washed with acetone. Subsequently, specimens were transferred to beakers filled with DMEM

(30 ml/cm^2), which were placed within a thermostatic water bath to maintain the temperature at 37 °C for 1, 3, 6 and 12 days. After the immersion tests, samples were dried at room temperature for two days inside an atmosphere-controlled glove box.

4.2.6. Mechanical properties along with degradation

After immersion in the DMEM solution for 1, 3, 6 and 12 days, magnesium and composite samples were subjected to compression tests under the same condition as described earlier (subsection 2.4).

4.3. Results and discussion

4.3.1. Processing of the Mg-bredigite composites

Fig. 2 shows the SEM micrographs of cold-compacted monolithic Mg specimens, sintered at 600 °C for 2 h. It is clear that densification during sintering did not effectively take place, as evidenced by a large number of micropores remaining in the microstructure after sintering. From the figure it appeared that inter-particle diffusion between powder particles was hindered, preventing densification from taking place. This could be attributed to the presence of a thermodynamically stable oxide layer on the surfaces of Mg powder particles [19, 146], disrupting the direct contact between neighboring Mg particles [147, 148]. When a magnesium powder is exposed to air with a high relative humidity, an amorphous hydroxide surface layer, i.e., $Mg(OH)_2$, will be formed instead of MgO [149].

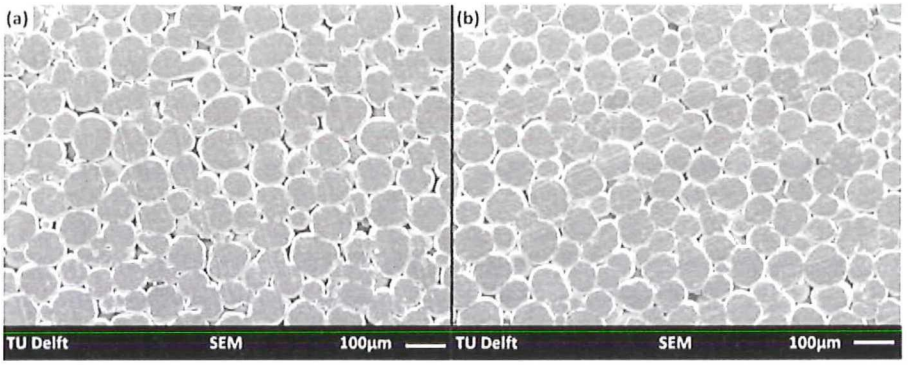

Fig. 2. SEM micrographs of Mg specimens cold-compacted at 500 MPa before (a) and after (b) sintering at 600 °C for 2 h.

Fig. 3a–b shows the XRD spectra of the monolithic Mg before and after sintering at 600 °C for 2 h, respectively. As indicated in Fig. 3a, only diffraction patterns of Mg (PDF 00-035-0821 - red dots) were visible before sintering. The absence of the diffraction patterns of hydroxide was due to the amorphous nature of the atmosphere-induced surface layer on Mg powder particles, as found by Nordlien et al. (1997) using TEM [149].

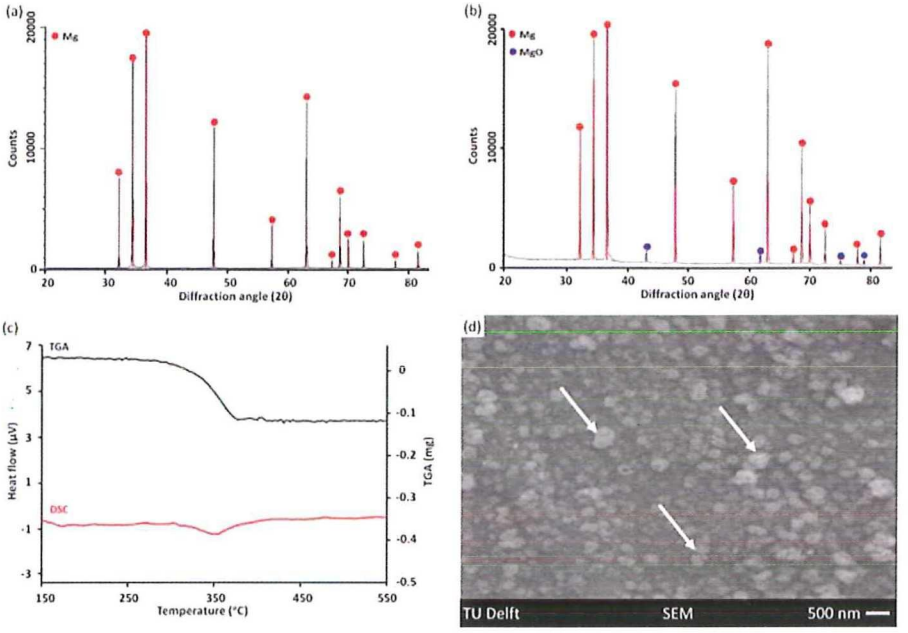

Fig. 3. X-ray diffraction spectra of Mg before (a) and after sintering at 600 °C for 2 h (b). Thermal profile of the magnesium powder obtained from STA (c). Morphology of the surface of Mg sample after sintering at 600 °C for 2 h (d), showing the thermally-formed oxide layer (white arrows). (For interpretation of the references to color in this figure, the reader is referred to the web version of this article.)

In the case of Mg-bredigite composite, the formation of magnesium oxide was not the only thermal event that took place during heating. When a cold-compacted Mg-bredigite composite was heated to 600 °C, a highly exothermic peak initiated around 550 °C and reached a peak at 592 °C, which was associated with a sudden mass loss, as shown in the TGA curve (Fig. 4a). The corresponding DSM micrograph of the Mg-20% bredigite composite suggested that the sudden mass loss in the TGA curve might be related to the evaporation of the local Mg matrix at the Mg-bredigite interface, as a result of the intense exothermic reaction between Mg and bredigite particles, producing cavities at the metal-ceramic interface (Fig. 4b – local cavities are indicated by white arrows). It indicated that a solid-state fabrication process, operating at temperatures higher than 550 °C, such as sintering at 600 °C, or any liquid-phase processing, would not be applicable to the Mg-bredigite composites. Thus, we decreased the sintering temperature from 600 to 500 °C so as to avoid the exothermic reaction between Mg and bredigite.

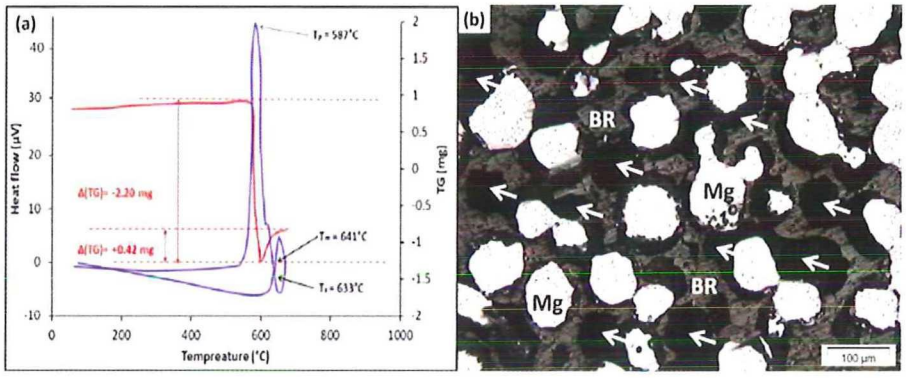

Fig. 4. STA curves of the Mg-20% bredigite composite, showing its thermal response from room temperature to the melting temperature of Mg (650 °C) (a). Microstructure of the Mg-20% bredigite composite after sintering at 600 °C for 2 h (b), indicating local evaporation of the Mg matrix (white arrows).

Adding ceramic particles to the Mg powder may have a double-sided effect on the porosity and structural integrity of the composites. On the one hand, adding bredigite particles to Mg may develop additional pores in the microstructure due to structure inhomogeneity, mismatch at the interface and different deformation responses of the metal and the ceramic [96]. On the other hand, pressing sharp and irregular ceramic particles against Mg powder particles during compaction can break up the oxide layer on the surfaces of Mg powder particles, which will facilitate surface diffusion during the sintering process. The values of bulk porosity as a function of the volume fraction of bredigite particles after sintering are given in Fig. 5. It was found that the bulk porosity of the cold-compacted and then sintered composites dramatically increased from 6% for pure Mg to 35% for the Mg-40 vol% bredigite composite and, once again, sintering at 500 °C could not annihilate the excessive porosity in the microstructure. It suggested that mechanical pressure should be applied during the sintering of the Mg-bredigite composites, such as PAS, in order to achieve higher bulk densities. Fig. 5 shows the density values of the PASed materials. These are indeed much higher than those of the cold-compacted and sintered ones.

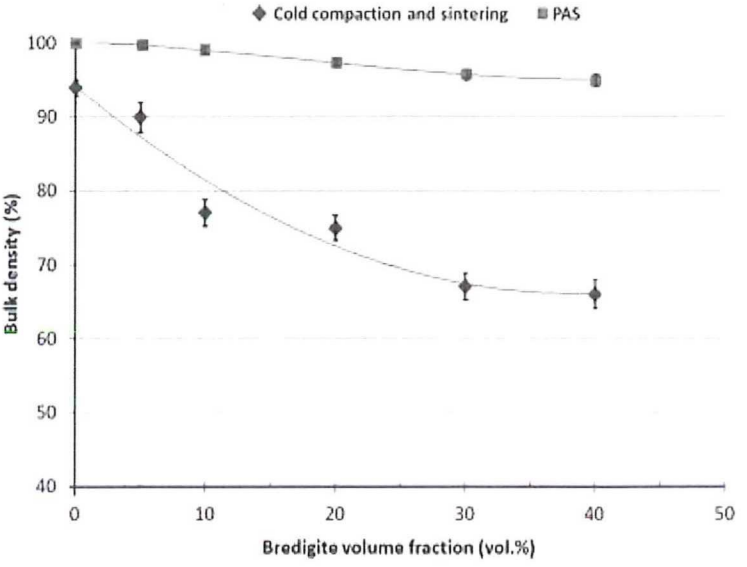

Fig. 5. Bulk density of cold compacted and then sintered composites at 500 °C, and PASed composites as a function of bredigite volume fraction.

The oxide layer can be disrupted during PAS (at 350 °C) because Mg becomes considerably ductile, when heated above 225 °C [98], and the enhanced plasticity of Mg powder particles would aid in breaking up the surface oxide layer due to its limited deformability, thereby allowing surface diffusion to take place during subsequent sintering.

The microstructures of the monolithic Mg specimens PASed at 150, 250 and 350 °C for 1, 2 and 4 h are shown in Fig. 6. The microstructures of the Mg specimens PASed at 150 °C (Fig. 6 – the first column) were quite similar to the microstructure of the cold-compacted and sintered specimen (Fig. 2b), containing a large number of micropores. When the PAS temperature was increased from 150 to 250 °C (Fig. 6 – the second column) and further to 350 °C (Fig. 6 – the third column), the number and sizes of pores (white arrows in Fig. 6) in the microstructure decreased to a point that full densification was achieved for the Mg specimens PASed at 350 °C. It is well known that surface diffusion is a time-dependent process. Thus, increasing sintering time under a mechanical pressure will positively contribute to the densification of the specimens. Fig. 6 also shows the effect of sintering time on the microstructures of the PASed Mg specimens (1 h – the first row, 2 h – the second row and 4 h – the third row). It was concluded that densification needed two hours and holding the

Mg specimens at 350 °C for a longer period of time (e.g., 4 h) did not have a strong effect on reducing the porosity level further.

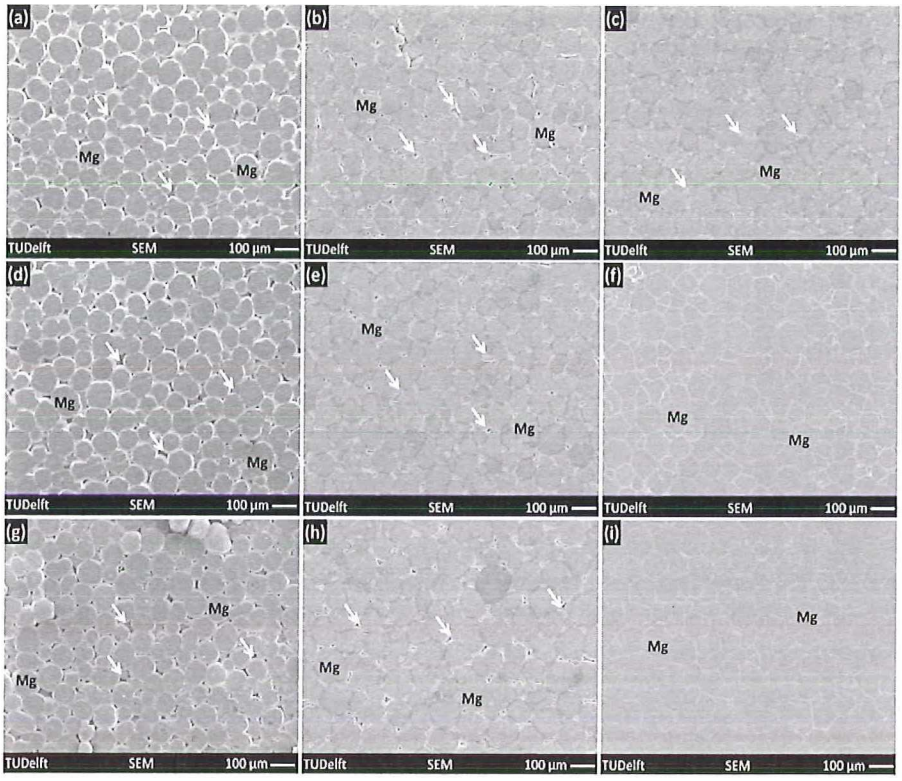

Fig. 6. SEM micrographs of monolithic Mg specimens PASed at 150 (the first column), 250 (the second column) and 350 °C (the third column) for 1 (the first row), 2 (the second row) and 4 h (the third row).

The microstructures of the Mg-20 vol% composites PASed at 150, 250 and 350 °C for 2 h are shown in Fig. 7a–c. Similar to the monolithic Mg specimens, increasing the PAS temperature from 150 to 350 °C resulted in a better integrated microstructure. The effect of sintering time on the porosity of the PASed composites (at 350 °C) is shown in Fig. 8. Once again, optimum densification for the composite was achieved after two hours and a longer sintering period (4 h) did not significantly influence the porosity level. Under an optimum PAS condition (at 350 °C for 2 h), the highly ductile Mg matrix was able to fuse into pores and fill vacant spots in the

microstructure, yielding well-integrated composites with unusually large amounts of bredigite (e.g., 40 vol.% - Fig. 7d–f).

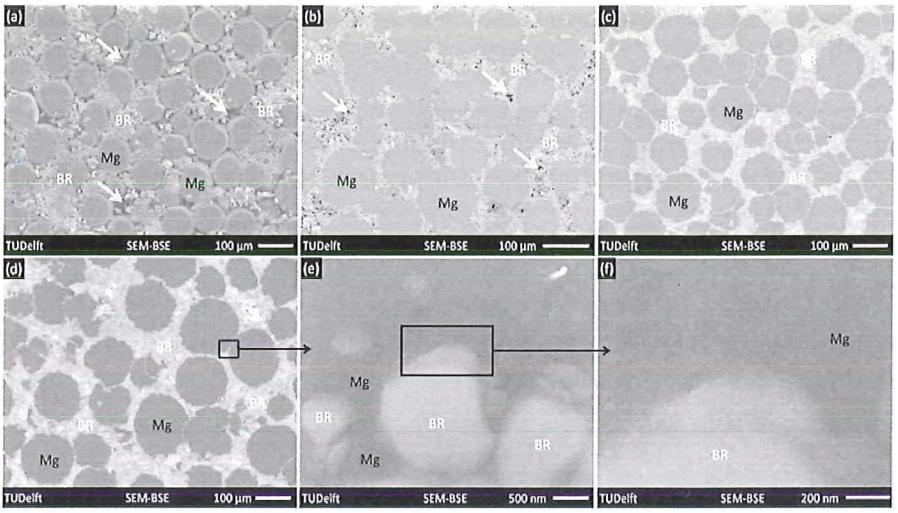

Fig. 7. Microstructures of the Mg-20% bredigite composite PASed at 150 (a), 250 (b) and 350 °C (c), and microstructure of the PASed Mg-40 vol.% bredigite at 350 °C (d). (e) and (f) illustrate the microstructure of the Mg-40 vol.% bredigite composite at higher magnifications.

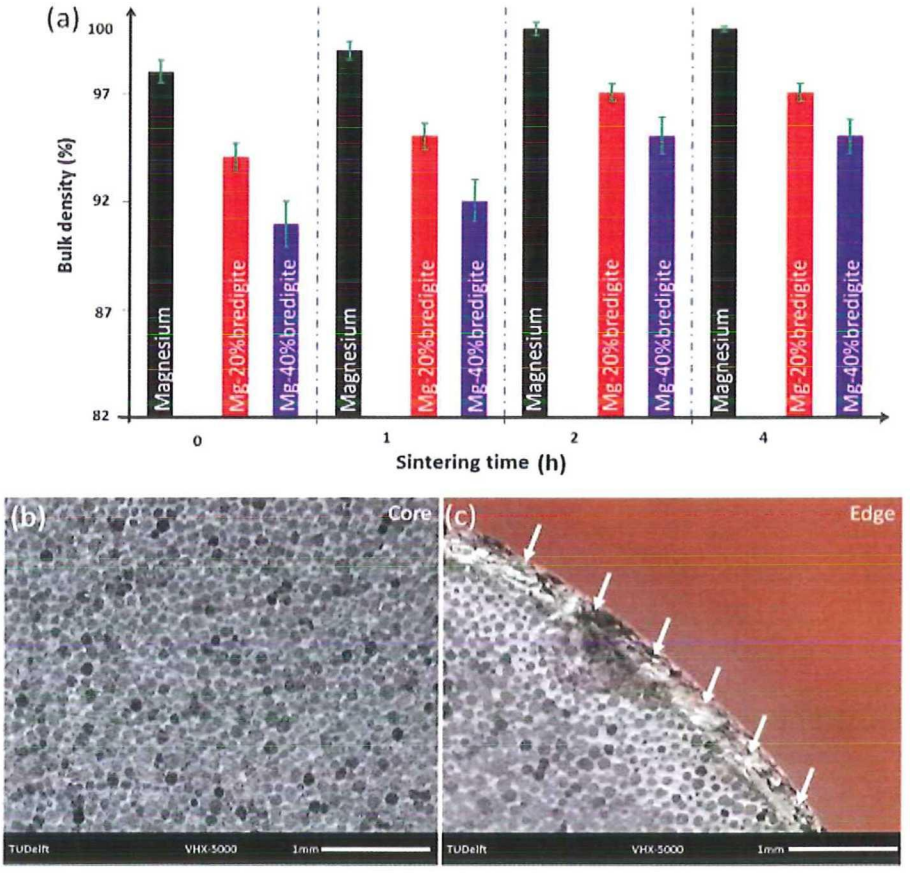

Fig. 8. Bulk density of the PASed Mg-bredigite composites (at 350 °C) as a function of sintering time and cross-sectional optical micrographs of the core (b) and edges (c) of Mg-20 vol.% bredigite composite specimen.

Under the optimum PAS condition, the porosity level significantly decreased from 25% to 3% and from 35% to 5% for Mg-20% bredigite and Mg-40% bredigite composites, respectively, in comparison with the values of cold compacted and then sintered composites (Fig. 5). The remaining pores were mostly located at the edges of the specimens (Fig. 8b–c), which were in direct contact with the compaction die and thus experienced the highest friction. Although most of the P/M techniques, including PAS and extrusion, come with a disadvantage of having localized porosity close to the edges of composite specimens, also known as the edge effect, it has an advantage over the casting techniques that are notorious for introducing pores throughout the bulk, e.g., gas cavities, which cannot be removed by machining off

the outer layer. The PAS technique developed in this research for the Mg-bredigite composites with high volume fractions of bioceramic particles (20–40 vol.%) showed another advantage, when compared to the extrusion technique that led to anisotropic microstructures aligned in the extrusion direction [23]. Moreover, it allowed the addition of larger volume fractions of bredigite particles to Mg as compared with the extrusion technique [23, 43, 100, 101]. It is of critical importance, because a larger volume fraction of bioactive particles contributes more to the enhancement of the bioactivity of magnesium, needed for bone regeneration.

4.3.2. Mechanical properties

4.3.2.1. Mechanical properties of monolithic magnesium

It is known that the mechanical properties of metallic materials processed by the (P/M) route are affected by the state of the surfaces of initial powder particles, which are often covered by an oxide layer [106, 107, 147, 148](Chang and Zhao, 2013; Esen, 2011; Krishnamurthy et al., 1991; Muhammad et al., 2011). As mentioned earlier, the oxide layer disrupts the direct contact between neighboring Mg particles [147] and hinders the diffusion between Mg powder particles during PAS [148], thus resulting in poor inter-particle bonding and pre-mature inter-particle fracture under loading [107]. The effect of the surface oxide layer on the mechanical behavior of monolithic Mg can be revealed by indentation at different loads and thus different indentation diagonal sizes. Table 1 presents the microhardness values of monolithic Mg samples using indentation loads of 0.10, 0.49 and 9.8 N. With increasing indentation load, microhardness decreased by almost 9%, indicating that the microhardness of monolithic magnesium was higher when no prior powder particle boundaries were involved in indentation. Fig. 9a shows that the indentation zone related to the 9.8 N load, covering a number of original powder particles and their boundaries because the diagonal of the indentation zone (220 μm) was larger than the mean particle size of Mg powder particles, i.e., 90 μm.

Table 1. Effect of indentation load on the microhardness of monolithic Mg samples.

Indentation load (N)	Indentation diagonal (μm)	Microhardness (HV)
9.8	220.42±0.36	38.2±0.14
0.49	47.05±0.97	41.3±1.05
0.10	22.06±0.76	41.9±0.57

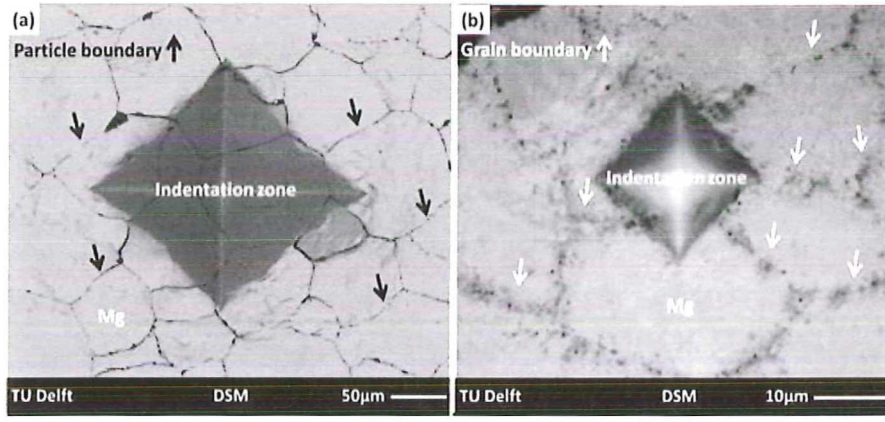

Fig. 9. Microstructures of PASed Mg specimens after indentation at 9.8 (a) and 0.10 N (b).

On the other hand, 0.49 and 0.10 N indentation loads resulted in smaller diagonals of 47.05 and 22 μm (Table 1), respectively, allowing the measurement of microhardness in the interior of one single Mg powder particle, containing grain boundaries but no prior powder particle boundaries. Fig. 9b shows the indentation zone resulting from the 0.10 N indentation load, covering only the interior of a Mg powder particle.

Fig. 10 shows the stress-strain curve of a monolithic Mg sample and Fig. 11 illustrates the phenomenon of inter-particle fracture in monolithic magnesium samples under a compressive load, separating neighboring powder particles. The

plastic region in the stress-stress curve of the monolithic magnesium sample appeared to be flat, showing a negligible strain-hardening effect. Despite the plateau region, monolithic Mg did not exhibit a high ductility (Table 2) but failed at a low strain because of the early inter-particle fracture and surface delamination, which caused pre-mature failure (Fig. 11a–b).

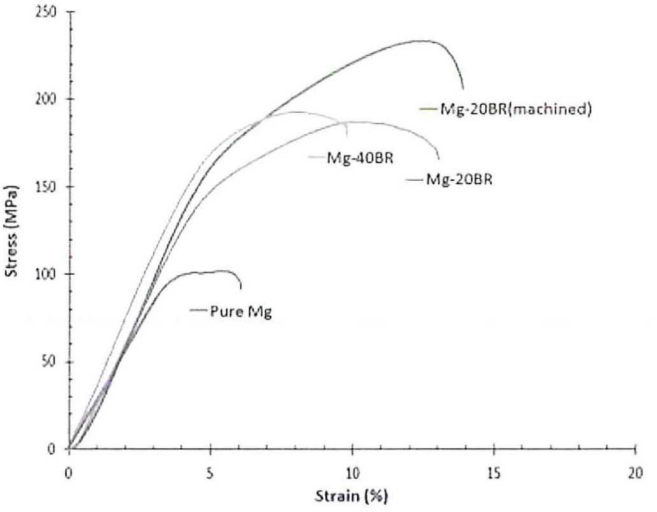

Fig. 10. Stress-strain curves of the pure Mg and Mg-bredigite (BR) composites obtained from compression tests.

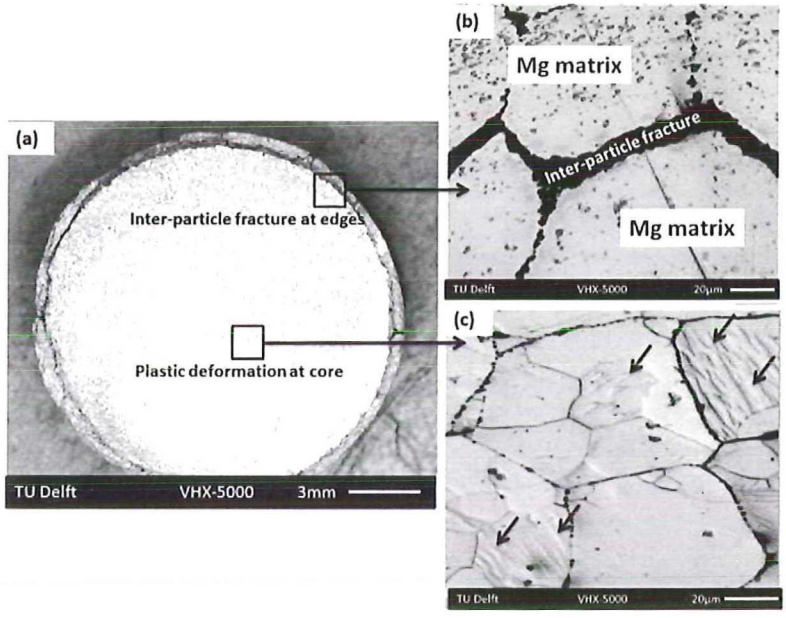

Fig. 11. Monolithic Mg samples subjected to compression tests, showing delamination close to the edges (a). While the edges went through inter-particle fracture (b), the core went through plastic deformation by forming twin bands (c – black arrows).

Table 2. Yield Compressive Strength (YCS) and Ultimate Compressive Strength (UCS), Microhardness (MV) at 9.8 N and Strain at Fracture (εf) of pure Mg and the Mg-matrix composites with different volume fractions of bredigite particles.

Material	Compressive strength (MPa)	Ultimate compressive strength (MPa)	Micro-hardness (HV)	Elongation till fracture (%)
Cortical bone	130–240 [42, 110, 111]	–	28–59 [150]	1.07–2.10 [42]
Cancellous bone	2–12 [110, 111]	1.7–10.44 [151, 152]	32.9±6.6 [153]	1.11±0.63 [154]
Mg	90±13.8	114.27±21.4	38.2±0.1	6.1±0.9
Mg-20 vol.% bredigite (28 wt.%)	135.0±7.8	190. ±12.2	64.05±5.8	13.9±1.8
Mg-20 vol.% bredigite^{m} (28 wt.%)	145.0±4.4	240.5±5.3	64.05±5.8	14.9±0.7
Mg-40 vol.% bredigite (57 wt.%)	140.0±6.2	192.6±6.0	72.8±9.7	9.8±2.1

m – a surface layer of the specimen was machined off.

Inter-particle fracture occurring during compressive tests was dominant at the edges of the sample (Fig. 11a–b), which resulted in surface delamination and produced shells with poor bonding to the core of the sample. The delamination was related to the high friction between the compaction die and powder particles at the hot pressing step of PAS, which resulted in poor densification close to the edges of the specimens, while the core went through plastic deformation as evidenced by extensive twinning in the cross-section microstructure of Mg samples (Fig. 11c). In polycrystalline Mg, the constraints applied by neighboring grains produce strain

incompatibility at grain boundaries, introducing additional stresses to maintain strain compatibility at these areas [155]. At room temperature, these compatibility stresses may activate non-basal dislocations (e.g. <c+a>) as well as twins [155]. When the amount of stress incompatibility is relatively low, twinning has the privilege to initiate since the critical resolved shear stress (CRSS) for the <c+a> slip (40 MPa) [156] is much higher than that for twining (2–3 MPa) [157]. Thus, the plateau plastic region of monolithic Mg in the stress-strain curve (Fig. 10) can be explained by the formation of twin bands that are capable of freely re-orienting the interior of grains to accommodate plastic strains with almost zero strain hardening [158]. There are two main twining systems, i.e., 101-2 and 101-1 that are often associated with the plastic deformation of polycrystalline magnesium [98]. 101-2} twins have a privilege to form, as compared to 101-1 twins, because the former can be formed without any relation to the direction of the applied load [55]. Moreover, the CRSS for 01-2} twining is only 2–3 MPa [157], while that for 101-1} twins requires 114 MPa [159]. Further detailed analysis of twining occurring in the Mg matrix of the composites during compression tests and the relation of twins to the direction and quantity of the applied load requires a separate systematic study by means of Electron Backscatter Diffraction (EBSD).

4.3.2.2. Mechanical properties of the magnesium-bredigite composites

From the results of the compression and hardness tests (Table 2), it could be stated that hard bredigite particles, being homogenously dispersed throughout the Mg matrix (Fig. 7c–d), were most probably responsible for the higher strengths of the composites by the following mechanisms. Firstly, the higher hardness of bredigite (365±17 $HV_{0.01}$ measured in this research would increase the overall hardness of the composites through dispersion hardening according to the rule of mixtures [104]. Secondly, as described in previous studies [106, 107], irregular bredigite particles with multiple edges could disrupt the pre-existing oxide layer on magnesium powder particle surfaces by being pressed against the matrix during PAS. This strengthened the interface with the Mg matrix so that the composites were more resistant to fracture under load. Thirdly, bredigite particles acted as obstacles to the free movement of dislocations within the Mg matrix (Fig. 12), causing larger resistance to deformation, which resulted in the enhancements of the compressive yield and ultimate strengths of the composites. It is well-known that plastic deformation is a result of active dislocation motion on a crystallographic plane. According to the Hall-Petch theory, grain boundaries act as the obstacles to dislocation motion, which results in the piling up of lattice dislocations at grain

boundaries along with plastic deformation [160], as shown in Fig. 12a (black arrows). Subsequently, hard bredigite particles pin the colliding dislocation lines along with plastic deformation (Fig. 12b) and this enhances the resistance to deformation, resulting in significant enhancements of the overall mechanical properties of the composites.

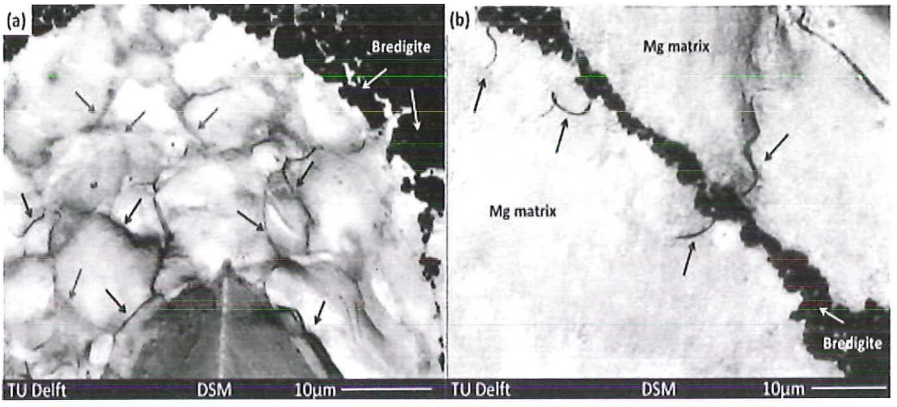

Fig. 12. Surface morphology of the plastic zone close to the indentation area, showing dense dislocation lines (black arrows) located at grain boundaries (blue arrows – a). b shows dislocation lines pinned by bredigite particles. (For interpretation of the references to color in this figure legend, the reader is referred to the web version of this article.)

The role of bredigite particles in enhancing the deformation resistance of the composites could be better observed in Fig. 13. It illustrates the indentation zones of an individual magnesium powder particle (grey in color) surrounded by bredigite particles (black in color) under three different indentation loads. As the indentation diagonal became larger at a greater load, the distance between the plastic zone and hard bredigite particles became shorter (see the distance between the sharp edges of the indentation zone and the black bredigite particles), corresponding to higher microhardness, confirming that the deformation of the Mg matrix close to bredigite particles was indeed more restricted.

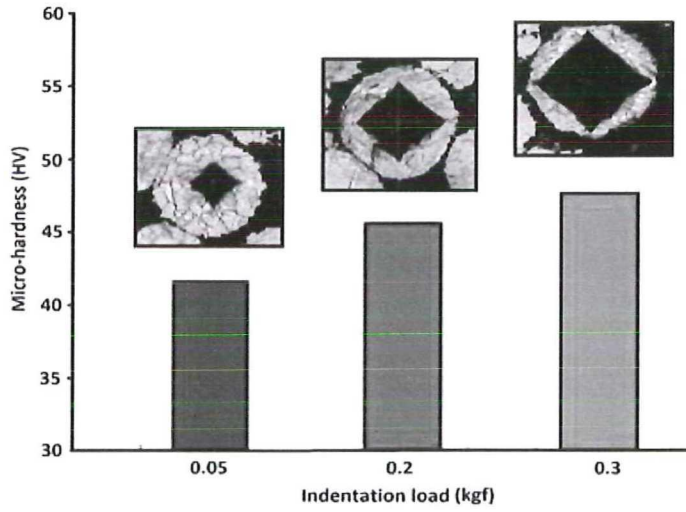

Fig. 13. Microhardness of an individual Mg powder particle surrounded by bredigite particles in the microstructure of the Mg-20 vol% bredigite composite as a function of indentation load.

The characteristics of the failure of the composites during the compression tests are shown in Fig. 14. Longitudinal cracks were observed along the side walls of specimens, which propagated in the same direction as the applied force. Subsequently, similar to monolithic Mg specimens, local instability and crack growth led to the global instability of composite specimens, producing delaminated shells under compression, as found in other composites [155, 161, 162]. Microscopic images of the delaminated region (Fig. 14b–c) confirmed that surface cracks propagated along both the Mg-Mg and Mg-bredigite interfaces.

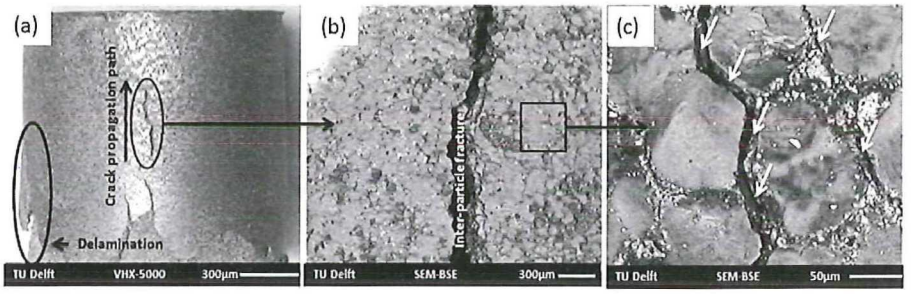

Fig. 14. Crack propagation and delamination of the Mg-20 vol% bredigite composite under compressive load (a). Inter-particle fracture was the dominant mechanism of failure (b), which occurred at both Mg-Mg and Mg-bredigite interfaces (c – white arrows).

Surface delamination is typical of P/M materials, especially P/M composites [163], most probably due to weaker bonding between the constituents close to the edges of the compaction die (Fig. 8c, indicated by white arrows) where high friction occurs at the die-material interface [164, 165]. To confirm this explanation, we performed the same compressive tests of the composite samples with an outer layer machined off. Indeed, the surface delamination delayed, which resulted in a higher ultimate compressive strength (Fig. 10). Thus, to achieve better mechanical properties, the outer layer of the P/M processed Mg-based composites should be machined off to remove the disintegrity remaining in the microstructure close to the edges.

In the case of the composites, inter-particle fracture was delayed to higher strains, allowing the Mg matrix to go through larger plastic deformation before the final failure occurred by inter-particle fracture and resulting in the higher ductility values of the composites up to 111% (Table 2). The interesting phenomenon of the increased ductility values of Mg-matrix composites with hard ceramic reinforcements has recently been documented [100, 102, 104, 105]. Ceramic reinforcements were held responsible to activate non-basal dislocations during the plastic deformation of the magnesium matrix, leading to higher ductility of the composites [105]. Hard bredigite particles introduce additional stresses to the adjacent Mg matrix, generating more strain incompatibility at grain boundaries close to reinforcing particles [102]. Subsequently, non-basal dislocations, necessary for the ductile behavior of the Mg matrix [166], can be activated in the area close to ceramic particles, which brings about better ductility at room temperature [155]. Fig. 12b shows activated dislocation lines close to bredigite particles. As can be seen in the microstructure, the dislocation lines were curvy, which was a morphological characteristic of non-basal dislocations [103]. When the non-basal <c+a> dislocations face an obstacle, such as a hard reinforcing particle, they tend to

split into sessile <c> and glissile <a> components and the immobile <c> component will cause a strain-hardening effect, while the mobile <a> component will introduce additional strain [156]. This can produce both higher ductility and a stronger strain-hardening effect at the same time, as seen in the Mg-bredigite composites (Fig. 10 and Table 2).

An increase in the volume fraction of bredigite particles from 20 to 40 vol.% did not contribute much to a further improvement of the strength but deteriorated the ductility (Table 2 and Fig. 10). Munitz et al. reported the same phenomenon in the case of TiC-reinforced Mg-matrix composites when the volume fraction of TiC particles increased from 20 to 30 vol.% [108]. It could be a consequence of the clustering of ceramic particles at a larger volume fraction, causing pores and weak bonding between brittle ceramic particles within the clusters and/or between the matrix and clustered particles. This resulted in a lack of load transfer from the matrix to ceramic clusters and thus the yielding behavior of the composites followed that of the matrix that contained the defects [109].

4.3.3. Mechanical properties as a function of degradation time

Fig. 15 shows the degradation profiles of the Mg-bredigite composites as a function of immersion time for 12 days in DMEM (solid lines). Monolithic Mg samples were completely corroded over 12 days at an average degradation rate of 31.41 mg/cm^2/day, being consistent with the in vitro degradation rates of cast Mg determined in previous studies (19–44 mg/cm^2/day) [21]. The Mg-20% bredigite and Mg-40% bredigite composites degraded at significantly reduced degradation rates of 1.26 mg/cm^2/day and 2.65 mg/cm^2/day, respectively. The morphologies of corroded samples are illustrated in Fig. 16a. Pitting corrosion as the dominating mechanism initiated at the side walls and bottom of samples (Fig. 16a), progressing towards the core, which caused total disintegration of monolithic Mg samples in 12 days. Bredigite particles contributed to slowing down the degradation mainly by blocking the pitting pathways of the matrix by dissolving at a lower rate and by establishing a protective surface layer, limiting the corrosive solution (DMEM) from reaching the fresh surface of magnesium. Fig. 16b–c shows the SEM micrographs taken on the cross section of a Mg-20% bredigite composite sample after 6 days of immersion in DMEM, showing a progressive corrosion pit in the Mg matrix, being arrested when it reached the bredigite particles (dark arrows). Some of the unreacted bredigite particles (white arrows in Fig. 16c) being entrapped in the corrosion layer could still be observed after 6 days of immersion, confirming the lower degradation rate of bredigite relative to the Mg matrix. The X-ray elemental mappings of the surface of Mg-20% bredigite composite sample after 6 days of

immersion are illustrated in Fig. 6dg. The presence of Ca and particularly P, originating from DMEM, in the chemistry of the surface layer confirmed the ability of the composites to encourage the formation and subsequent adsorption of bioactive CaP-containing salts such as Hydroxyapatite (HA). The silicon-rich regions in the x-ray chemical mapping (Fig. 16d) was due to the presence of unreacted bredigite particles in the corrosion layer, as illustrated in Fig. 16b–c. During the dissolution of bredigite particles, Ca ions are released preferentially to silicon ions by ion exchange with H^+. Thus, most of silicon in bredigite will stay within the unreacted part, forming a negatively charged surface with the functional group (≡Si–O^-), which electrostatically attracts magnesium and calcium cations (Fig. 16d–g). Thus, when Mg is present in the microenvironment close to the corroding surface (Fig. 16g), it will be attracted by the negatively charged (≡Si–O^-) functional group and then penetrate through the HA lattice by ionic exchange with Ca cations. Then, a calcium-deficient, Si- and Mg-containing HA is formed (Fig. 16d–g), which is more bioactive than the stoichiometric HA [123].

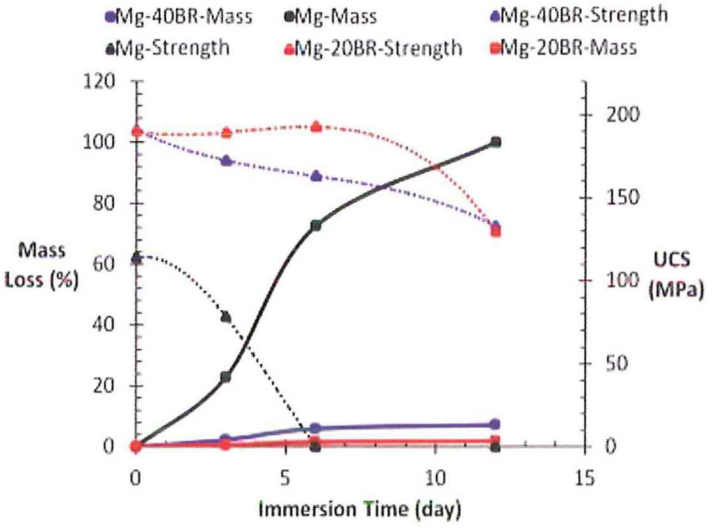

Fig. 15. Ultimate compressive strengths (UCS) and mass losses of the composites as a function of immersion time.

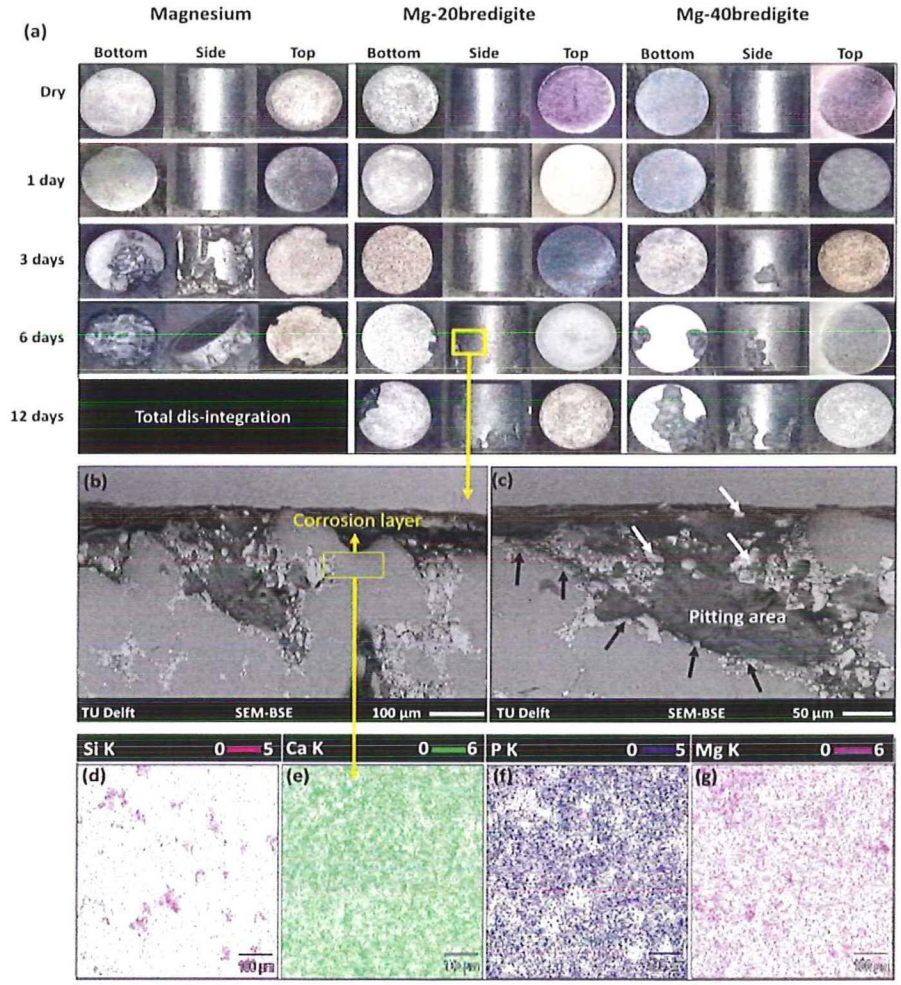

Fig. 16. Morphologies of corroded composite samples as a function of immersion time (a). SEM cross-section micrograph of the Mg-20% bredigite after degradation in DMEM for 6 days (b), showing unreacted bredigite particles blocking the pitting pathways of the matrix (c, black arrows) and remaining in the corrosion layer (c, white arrows). (d–g) illustrate the X-ray chemical mappings of the corrosion layer after 6 days of immersion.

Fig. 15 (dashed lines) shows the influence of degradation on the strength of the composites over a period of 12 days in DMEM. Monolithic Mg sample lost its mechanical integrity within 6 days due to a high degradation rate. However, the Mg-bredigite composites showed gradual losses of mechanical properties by dissolving

at slower rates. After 12 days, their strengths fell into the strength range of cortical bone (130–180 MPa [167, 168]). The morphologies of degraded composites subjected to immersion tests in DMEM and then compression tests showed that mechanical cracks nucleated at large corrosion pits (Fig. 17). Thus, pitting corrosion was mainly responsible for the gradual loss of the mechanical strengths of the composites. Thus, if mechanical cracks appear first, they will encourage the initiation and further growth of corrosion pits. However, if corrosion pits appear first, they will act as nucleation sites for the further development of mechanical cracks.

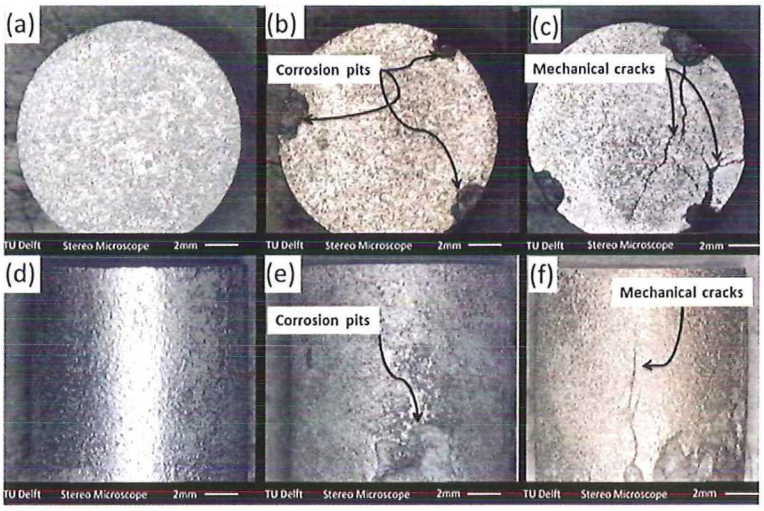

Fig. 17. Stereo-microscope micrographs of Mg and the Mg-20 vol% bredigite composite before (a and d, respectively) and after immersion testing (b and e, respectively) for 12 days. Mechanical cracks initiated at corrosion pits (c) and (f) in Mg and the Mg-20% bredigite composite, respectively.

Despite the differences in degradation rate between the Mg-20% bredigite and Mg-40% bredigite composites, they showed similar UCS values after 12 days (Fig. 15), because corrosion pits were limited to the edge of the samples (Fig. 16a). Different degradation rates but similar mechanical strengths of the Mg-20% bredigite and Mg-40% bredigite composites allowed us to adjust the degradation rate by changing the volume fraction of bredigite according to the requirements of the implantation site where a low or a high degradation rate would be needed with similar mechanical strengths (Table 2).

The mechanical properties of the Mg-bredigite composites, being close to those of cortical bone (Table 2) suggest adequate biomechanical compatibility. However, long-term in-vitro degradation tests, e.g., longer than 3 months, are still needed to determine the long-term degradation behavior of these composites. In addition, the biodegradability of the composites could be further improved by inhibiting inter-particle fracture at weak spots in the structure, as explained above. This would positively affect the mechanical and degradation properties of the composites at the same time.

Further improvement of the structural integrity of the composition is a new challenge. High temperature sintering of the composites under a compaction load could be an appropriate approach to eliminating the disintegrity in the microstructure of the PASed composites through enhanced inter-particle diffusion. As mentioned earlier, the major obstacle to the sintering of the Mg-bredigite composites would be the maximum temperature at which the composites could be heat-treated because heating the composites close to a desired sintering temperature of Mg (i.e., around 600 °C) would result in an exothermic reaction between the constituents and local evaporation of the adjacent matrix. If the exothermic reaction could be suppressed, then a proper heat treatment of the Mg-bredigite composites, preferably under mechanical load, could enhance surface diffusion across prior powder particle boundaries, resulting in a better integrated microstructure.

4.4. Conclusions

Our work demonstrated the critical importance of the processing method and process parameters for the mechanical properties and degradation behavior for the fabricated Mg-matrix composites. PAS at 350 °C for 2 h under a pressure of 500 MPa was found to be an optimum condition for the processing of the Mg-matrix composites with high volume fractions of bredigite particles. The PASed Mg-bredigite composites were shown to be promising biomaterials for load–bearing orthopedic applications. The presence of bredigite particles improved the mechanical strengths of Mg both before and after degradation. The reduced degradation rates of the Mg-bredigite composites led to the slower losses of the mechanical properties into the strength range of cortical bone after 12 days of immersion in DMEM. High-temperature sintering of the composites under an isostatic mechanical pressure could be useful to annihilate the weak spots in the microstructure. Further in vivo studies are necessary to evaluate the behavior of these newly developed composites in a real biological environment in order to establish a clear correlation between the in vitro and in vivo results.

CHAPTER 5

Biodegradation and mechanical behavior of an advanced bioceramic-containing Mg matrix composite synthesized through in-situ solid-state oxidation

This chapter is published as:

NaddafDezfuli, S., Brouwer, J.C., Mol, J.M.C., van der Helm, F.C.T., Zhou, J., 2018. Biodegradation and mechanical behavior of an advanced bioceramic-containing Mg matrix composite synthesized through in-situ solid-state oxidation. Journal of the mechanical behavior of biomedical materials 80, 209-221.

Abstract

Recent studies have shown great potential of Mg matrix composites for biodegradable orthopedic devices. However, the poor structural integrity of these composites, which results in excessive localized corrosion and premature mechanical failure, has hindered their widespread applications. In this research, an in-situ Powder Metallurgy (PM) method was used to fabricate a novel biodegradable Mg-bredigite composite and to achieve enhanced chemical interfacial locking between the constituents by triggering a solid-state thermochemical reaction between Mg and bredigite particles. The reaction resulted in a highly densified and integrated microstructure, which prevented corrosion pits from propagating when the composite was immersed in a physiological solution. In addition, chemical interlocking between the constituents prohibited interparticle fracture and subsequent surface delamination during compression testing, enabling the composite to withstand larger plastic deformation before mechanical failure. Furthermore, the composite was proven to be biocompatible and capable of maintaining its ultimate compressive strength in the strength range of cortical bone after 25-day immersion in DMEM. The research provided the necessary information to guide further research towards the development of a next generation of biodegradable Mg matrix composites with enhanced chemical interlocking.

5.1. Introduction

Magnesium, being among the lightest structural materials, is considered one of the biggest investment opportunities of this century [169]. Magnesium is 75 % lighter than steel, 50 % lighter than titanium, and 33 % lighter than aluminum [170, 171]. In the biomedical field, particularly in orthopedics, Mg stands out of the rest of the metals in the periodic table due to its biodegradable nature, high strength-to-density ratio and mechanical properties comparable to those of human bone [172].

However, Mg actively dissolves in physiological solutions at an undesirably high rate [79], leading to premature structure disintegration and subsequent loss of mechanical properties before the damaged bone is fully recovered. Lowering the degradation rate of Mg has been one of the most studied subjects in pursuit of clinically applicable Mg-based materials [173].

Most of the previous attempts to slow down the biodegradation of Mg were focused on adding alloying elements such as aluminum and zirconium to Mg [174-176], and quite a few, on developing Mg-matrix composites with bioactive particles embedded throughout the Mg matrix [23, 34, 101]. Mg matrix composites use monolithic Mg as the metallic matrix so as to avoid possible toxic complications caused by alloying elements [21]. In addition, the chemical and mechanical properties of Mg matrix composites are adjustable by controlling material parameters such as bioceramic type, particle shape, sizes and distribution as well as processing conditions [24].

In the previous research, Powder Metallurgy (PM) Mg matrix composites containing up to 40 vol.% of bredigite were developed and these composites had integrated and homogenous microstructures and mechanical properties similar to those of human bone [24, 177]. However, the Mg matrix composites still suffered from premature inter-particle fracture and surface delamination under compressive loading [24], causing the outer layer of specimen to be disintegrated from its core, which would be fatal in clinical cases. Inter-particle fracture and surface delamination were identified to be the two dominating failure mechanisms of the Mg matrix composites under mechanical loading, indicating that mechanical interlocking between Mg and bioceramic powder particles was not sufficiently strong to resist inter-particle fracture [24]. Inter-particle fracture became even more intense after the composites had been immersed in a physiological solution and suffered from localized corrosion at the edges of specimens. These localized corrosion sites in the Mg-matrix composites would provide nucleation sites for mechanical cracking, thereby reducing their durability if they were used for implants [18].

With the recognition of the weak spots in the composites developed earlier, there was a strong desire to improve the composites in terms of structural integrity, degradation behavior and mechanical properties. Improving the integrity of the Mg-bioceramic interface is a challenge because metals generally do not bond strongly with ceramics due to the differences in the nature of atomic bonding in metals and in ceramics [178]. Nevertheless, there is a possibility to strengthen the metal-ceramic interface in Mg matrix composites, if an interlayer is formed, which allows chemical interlocking between the constituents. One way to achieve this is to trigger a thermochemical reaction at the Mg-bioceramic interface, causing atoms from both sides to swap by diffusion and forming an intermediate layer as a product of the reaction. The first criterion to achieve this would be the ability of magnesium to reduce oxide phases in bioceramic (e.g., SiO_2) into their elemental constituents (e.g., Si) through a solid state reaction. The second criterion would be the diffusivity of bioceramic elemental constituents into Mg crystal to establish a chemically integrated interface.

With these two criteria in mind, in this research, micro-sized bredigite powder particles was used (bredigite being a biodegradable ceramic in the CaO-MgO-SiO_2 family and known as a bioactive material with mechanical properties close to those of cortical bone and a stimulatory effect on osteoclast proliferation [31, 32]), considering the fact that Mg is able to react with bredigite through a solid state oxidation reaction [24], and the possible elemental products of the reaction (such as Si and Ca) are able to diffuse into Mg crystal [34, 179].

The goal of this study was to fabricate biodegradable Mg-bredigite composites with chemical bonding between powder particles, as an additional bonding mechanism to mechanical interlocking to prolong their service life by avoiding premature inter-particle fracture and delamination. Microstructure, mechanical and degradation behavior, in-vitro cytotoxicity and bioactivity of the newly developed composite were evaluated.

5.2. Materials and Methods

5.2.1. In-situ synthesis of Mg matrix composite

A magnesium powder (containing 320 ppm Fe and 160 ppm Ni impurities - Shanghai Institute of Ceramics) with spherical particles and a mean particle size of 90 μm was mixed with a bredigite ($Ca_7MgSi_4O_{16}$ - Shanghai Institute of Ceramics) powder with a mean particle size of 10 μm and an irregular morphology by 20 vol.%. Mixing lasted 12 h using a rotary mixer to obtain a homogenous mixture.

70 mg of the powder mixture was heated from ambient temperature to 620 °C at 2, 5, 10, 15 and 20 °C·min^{-1} in a Simultaneous Thermal Analyzer (STA – Setaram SetsysEvo) to pinpoint the critical temperature, at which the thermochemical reaction between Mg and bredigite took place at its highest intensity (T_p), and possible mass change as a result of the exothermic reaction. The STA furnace was flushed with high purity argon gas for 4000 s. The STA tests were repeated three times for each heating rate.

Composite specimens were fabricated using a powder metallurgy method known as Pressure Assisted Sintering (PAS) [24]. In this method, the powder mixture was first heated to 350 °C in a 13 mm diameter die made from hot-work tool steel and then uniaxially compacted at 500 MPa. To ensure optimum densification of the PAS composite, the mixture was kept at 350 °C for 2 h under the compaction pressure. The PAS composite was then heated to 600 °C, which was close to the reaction peak temperature measured in the thermoanalytical tests. The thermal treatment was conducted in a tube furnace by heating the PAS composite to 500 °C at a heating rate of 5 °C.min^{-1} and then from 500 to 600 °C at 1 °C·min^{-1} to exercise more precise control over the heating process. An isothermal step of 1 h was followed, after the composite reached 600 °C, to allow diffusion to take place within and across Mg powder particles. The Thermally Treated (TT) composite was then cooled at 5 °C.min^{-1} to room temperature. The thermal treatment was conducted under a protective atmosphere (high-purity argon). An illustration of the processing steps is given in Fig. 1. The exposing surfaces of PAS and TT composite samples were ground by using 2400 grit SiC sandpaper, washed in an ultrasonic acetone bath for 3 min and then dried by an air blower.

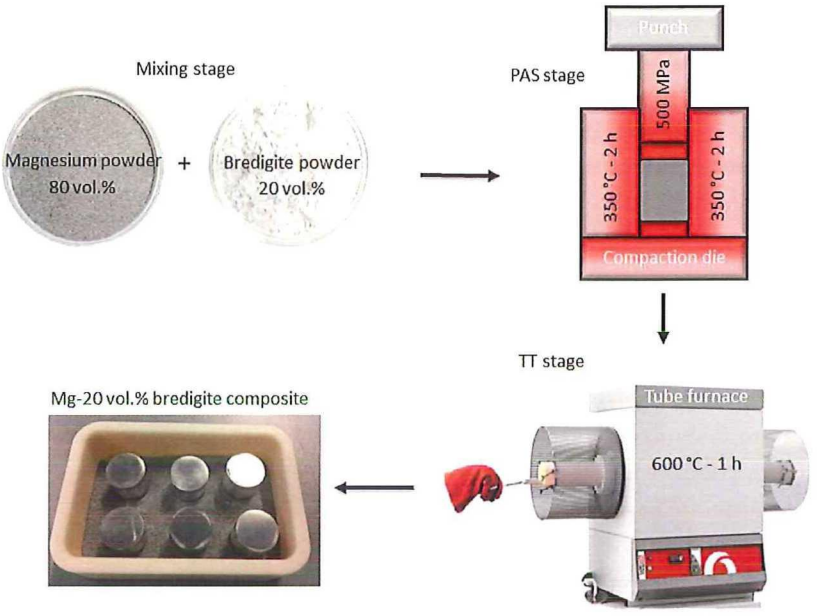

Fig. 1. Schematic illustration of the processing steps for the Mg–bredigite composite.

5.2.2. Microstructure and chemical composition

The value of bulk density was determined using Archimedes' principle according to (ASTM B962 – 15, 2015). Microstructures and surface morphologies of the composite before and after the thermal treatment were characterized by using a high-resolution Digital Stereo Microscope (DSM, KEYENCE VHX-5000) and a Scanning Electron Microscope (SEM, JEOL-JSM-6500F) working at an accelerating voltage of 15.0 kV, which was equipped with an Energy Dispersive X-ray Spectroscope (EDS).

Phase identification of the composite before and after the thermal treatment was carried out by using a Bruker D8 Advance X-ray diffractometer with monochromatic Cu radiation (Kα1 λ = 0.154056 nm) over a 2θ-angle range between 10 and 130° and a step size of 0.020 °. Semi-quantitative analysis was performed by scaling the intensities of the diffraction peaks from the sample to one diffraction peak intensity value of corundum (α-alumina). A Reference Intensity Ratio (RIR or I/Icor) was applied to each phase and the relative intensities compared to the I/Icor values were obtained from the ICDD-PDF4 database.

The chemical compositions of the surfaces of composite samples were determined by using a Fourier Transform Infrared Spectroscope (FTIR, Nicolet 6700 spectrometer, scan range 600 – 1300, three scans per sample) and an Energy Dispersive X-ray Spectroscope attached to the SEM microscope. Multiple point scanning and elemental mapping were carried out to determine the concentrations and distributions of elements in the surface layer.

5.2.3. Mechanical tests

The bulk mechanical properties of the composite were determined by performing compression tests at a crosshead speed of 0.5 mm/min in an INSTRON universal testing machine using a 50 kN load cell. The height-to-diameter ratio of specimens was one, according to (ASTM E9-09, 2009). The tests were stopped when the compressive load dropped by 20%.

The microhardness values of the composite before and after the thermal treatment were obtained from Vickers hardness test (Leica VMHT), using a square based pyramidal-shaped diamond indenter having an angle of 136° and at a dwelling time of 12 s, according to the standard test method (ASTM E384-99, 1999). Composite samples were indented at loads of 0.49, 1.96 and 9.8 N to evaluate the effect of indentation load on the mean value of microhardness. Indentation was repeated at least 15 times to ensure a reliable mean value. After indentation, the affected area was observed by using DSM.

5.2.4. In vitro degradation tests

5.2.4.1. Degradation in DMEM

Composite samples (13 mm diameter and height-to-diameter ratio of 1) were immersed in a HEPES buffered (25 mM) Dulbecco's modified Eagle's medium (DMEM - D1145, Sigma-Aldrich) at 37 °C for 1, 3, 6, 12, 24 and 30 days. An anti-bacterial and anti-fungus agent (A5955, Sigma-Aldrich) was added to DMEM by 1% to prevent bacterial and fungi from growth. The ratio of solution volume to surface area (SV/SA) was 30 ml/cm^2 according to ASTM G31-72. Degradation profiles of the composite before and after the thermal treatment were constructed by measuring the mass loss (%) of composite samples as a function of immersion time (day) in DMEM.

The composite specimens were washed in an ultrasonic acetone bath and then dried in air for 24 h after each immersion period. The chemical compositions of the surfaces of composite samples were determined using FTIR and EDAX according to section 2.2. The mechanical properties of the dried specimens were evaluated by subjecting the specimens to compression tests, as described in subsection 2.3.

5.2.4.2. Electrochemical degradation

To evaluate the electrochemical behavior of composite samples, a three-electrode configuration was adopted to perform potentiodynamic polarization tests. A Saturated Calomel Electrode (SCE) was used as the reference electrode and a platinum mesh as the counter electrode. Prior to the potentiodynamic tests, Open Circuit Potential (OCP) measurements were performed during immersion up to 20 h using a Solartron 1250/1255 potentiostat. Cathodic polarization tests were carried out at an initial potential of - 0.2 V versus OCP increasing to 0.0 V versus OCP. Anodic polarization tests were carried out separately at an initial potential of 0.0 V versus OCP increasing to +0.5 V versus OCP. Both cathodic and anodic polarization tests were conducted at a scan rate of 1 mV/s in HEPES-buffered DMEM at 37 °C.

5.2.5. Biocompatibility and bioactivity assessments

5.2.5.1. Preparation of biomaterial extracts

For extraction, monolithic Mg and TT Mg-20 vol. %bredigite samples with a diameter of 13 mm were cut into disks with a thickness of 2 mm and then the exposing surfaces were ground by 2400 grit SiC sandpaper. Subsequently, monolithic and composite disks were immersed in DMEM containing 10% fetal bovine serum with a surface area to volume ratio of 1.25 cm^2/ml and incubated in a humidified incubator at 37 °C and with 5% CO_2 for 24 and 72 h. The extracts were withdrawn and centrifuged at 1200 × g for 5 min at room temperature. The extracts were diluted with DMEM + 10% FBS + 1% penicillin/streptomycin at ratios of 1/4 and 1/16, and stored at 4 °C according to ISO 10993-12.

5.2.5.2. Indirect cell proliferation assay

MG-63 cells were adopted to evaluate the cytotoxicity of the composite [34]. The cell cytotoxicity of each extract sample was evaluated using 3-(4, 5-dimethylthiazol-

2-yl)-2, 5-diphenyltetrazolium-bromide (MTT) assay. MG-63 cells were incubated in 96-well cell culture plates at a density 1 x 10^4 cells per well and incubated for 24 h. After incubation, the medium was replaced by the extracted medium and incubated for further 1, 6 and 12 days. The proliferation rate of cultured cells on each sample was compared with the tissue culture polystyrene plate (TCPS) as a control. After incubation with the extracts, the culture medium of each well was removed and 0.1 mL MTT solution (0.5 mg/mL, Sigma) added, followed by incubation for 4 h at 37 °C. The purple formazan crystals were dissolved by adding 0.1 mL Isopropanol (Sigma) per well on a shaking incubator for 15 min prior to absorbance measurement. The solutions of each well were transferred to 96-well plate and the optical density (OD) was recorded on a microplate reader (STAT FAX 2100, USA) at 545 nm. This assay was repeated five times and the final ODs normalized to the control OD.

5.2.5.3. Indirect cell differentiation assay

The differentiation behavior of MG-63 cells was evaluated by measuring ALP activity. Cells were cultured at a density of 1 x 10^4 cells/well in a 24-well plate for 24 h. Then the medium was replaced with the 24 and 72 h extracted media and incubated for further 3, 6 and 12 days. Subsequently, the cells in each well were lysed in 0.1% Triton X-100 (Sigma) and the lysates were incubated with p-nitrophenyl phosphate (pNPP) (Sigma) for 60 min at 37 °C. The quantity of p-nitrophenol produced was measured at 405 nm and the total protein content was acquired with the aid of a BCA Protein Assay Kit (Sigma). The results were expressed as nanomoles of p-nitrophenol produced per minute per microgram of protein. ALP activity of cells cultured in the medium supplemented with 10% FBS without any addition of extracts served as the control. At least five samples per each test were taken for statistical analysis. The statistical significance was defined as a *p*-value of less than 0.05.

5.3. Results

5.3.1. Processing details and microstructure

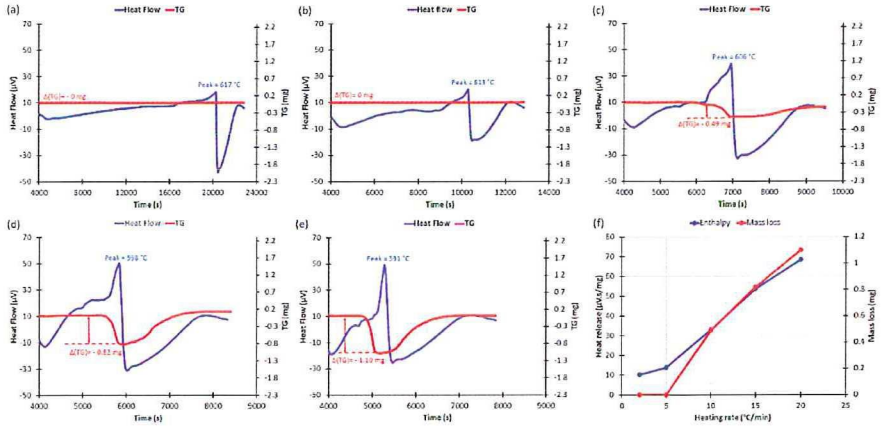

Fig. 2. Thermo-gravimetric profiles of Mg-20% bredigite samples heated to 620 °C at 2 (a), 5 (b), 10 (c), 15 (d) and 20 °C.min^{-1} (e). Exothermic heat flow and mass loss as a function of heating rate (f).

Fig. 2 shows the thermal and gravimetric profiles of the Mg-20 vol. % bredigite composite from room temperature to 620 °C, plotted by the data acquisition system of STA at 2, 5, 10, 15 and 20 °C·min^{-1}. The heat flow curves of the composite revealed an exothermic event at all the heating rates (Fig. 2a-e). Surprisingly, the peak temperature of the reaction decrased with increasing heating rate. The amount of the generated heat increased by almost seven times when the heating rate was increased from 2 to 20 °C·min^{-1} (Fig. 2f). Significant mass losses were observed in the TG curves when the composite was heated at relatively high heating rates (10, 15 and 20 °C).

Fig. 3 shows the optical microscopic images taken from the PAS composite after the thermal treatment (a-d), including SEM back-scattered micrographs and EDS elemental maps (e-h). The TT composite appeared to have a homogenous microstructure (Fig. 3a) with almost no pores or cracks throughout the material (Fig. 3b). A closer look at the microstructure of the etched TT composite (Fig. 3c with red arrows) revealed the grain structure of the Mg matrix with a mean grain size of approximately 10 μm.

After the thermal treatment, a newly formed interlayer at the Mg-bredigite interface was observed, appearing as a blue polygonal phase in the optical micrograph (Fig. 3d). This blue phase was also visible in the SEM-BSE image (Fig. 3e, indicated by blue arrows) having a strong contrast with the neighboring bredigite particles. EDS elemental mapping of the interface (Fig. 3f-h) showed the presence of Si and Ca in the interlayer between Mg and bredigite particles, indicating the diffusion of atoms from bredigite to this interlayer.

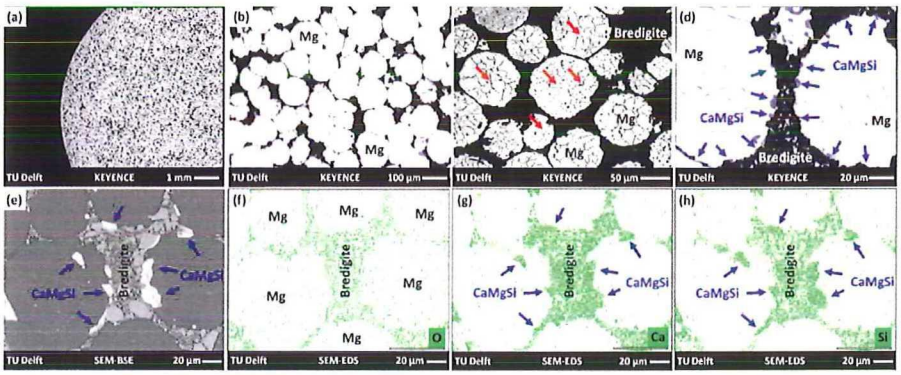

Fig. 3. Macroscopic and microscopic illustrations of the Mg-20% bredigite composite after the thermal treatment at 600 °C at different magnifications (a-d). Optical images of grain boundaries after etching (c – red arrows) and CaMgSi compound at the Mg-bredigite interface (d - blue arrows). SEM-BSE image of the TT composite (e) associated with EDS elemental distribution maps of oxygen (f), calcium (g) and silicon (h).

Fig. 4a and b shows the XRD spectra of composite samples before and after the thermal treatment. The X-ray reflections of the Mg matrix (red dots in Fig. 4) were assigned according to PDF 04-015-2580 and those of bredigite (blue dots in Fig. 4) were assigned according to PDF 00-036-0399. The crystal lattice of Mg was Hexagonal Close-Packed (HCP) and that of bredigite orthorhombic.

The XRD spectrum of the TT composite (Fig. 4b) contained the diffraction patterns of crystalline CaMgSi and MgO with relative amounts of 92 and 8 wt%, respectively. It confirmed that the blue-colored polygonal phase in light microscopy was in fact a CaMgSi intermetallic phase, present at the Mg-bredigite particle interface. The density of the PAS composite was increased by 2.1 % (from 96.6 % to 98.7 %) as a result of the thermal treatment (Table 1).

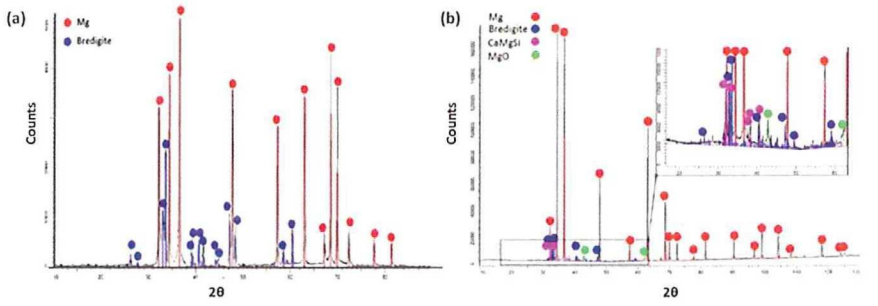

Fig. 4. XRD spectra of the Mg-20% bredigite composite before (a) and after (b) the thermal treatment at 600 °C.

Table 1. Bulk densities of monolithic Mg and Mg-20% bredigite composite before (PAS) and after the thermal treatment (TT) at 600 °C.

Material	**Bulk density (vol.%)**
Mg	99.8%±0.2
Mg-20%Bredigite (PAS)	96.6%±0.7
Mg-20%Bredigite (TT)	98.7%±0.4

5.3.2. Mechanical behavior

Fig. 5a illustrates the stress-strain curves of PAS and TT composite specimens in comparison with the curve of monolithic Mg. Superior mechanical behavior of the TT composite as compared to that of PAS and monolithic specimens was apparent. The Compressive Yield Strength (σ_{CYS}) of PAS specimens after the thermal treatment increased from 135.0 to 170.1 MPa, which represents a 26 % improvement. The Ultimate Compressive Strength (σ_{UCS}) of the TT composite improved by 18 % and 97 %, relative to the values of PAS and monolithic specimens, respectively. The values of strain to fracture (ε_f), which represents bulk ductility, were 17.1, 13.9 and 6.1 % for TT, PAS and monolithic specimens, respectively.

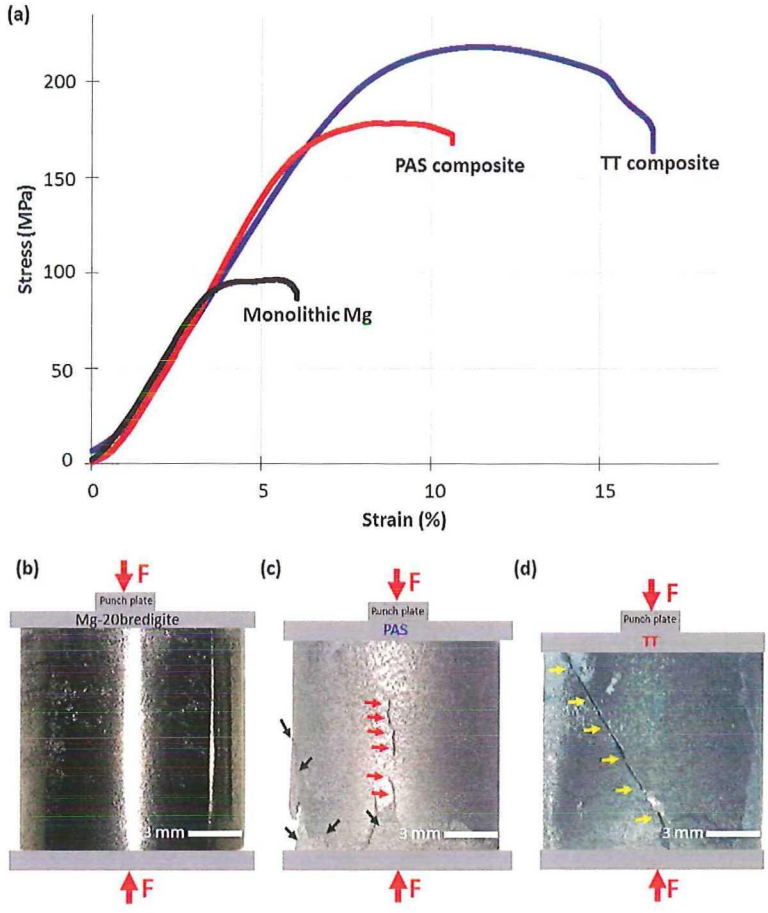

Fig. 5. Stress-strain curves of monolithic Mg, PAS and TT composite specimens (a). Bulk overview of Mg-20% bredigite composite specimen before the compression tests (b). Bulk overview of PAS (c) composite specimen after the compression tests, revealing longitudinal cracks (red arrows) and surface delamination (black arrows). Bulk overview of TT composite specimen after the compression test (d), revealing a 45 ° diagonal crack (yellow arrows).

The morphologies of specimens before the compression tests and after the failure are shown in Fig. 5b-d. Longitudinal cracks (Fig. 5c - red arrows) and surface delamination (Fig. 5c – black arrows) were the main characteristics of the PAS composite [24]. On TT specimens, however, no surface delamination was observed

and longitudinal cracks were replaced by a 45 ° diagonal crack (Fig. 5d – yellow arrows).

Fig. 6a illustrates an overview of a representative crack on the cross section. Higher magnification images of the crack are given in Fig. 6b and d. Owing to the stronger Mg-bredigite interface, cracks (Fig. 6b, d - black arrows) propagated through the original Mg powder particles (yellow circle) rather than through the Mg-bredigite interface. Hence, the interface remained intact and inter-particle fracture was prohibited (Fig. 6d – green arrows). The second column of Fig. 6 shows relatively smaller cracks propagating through bredigite particles (Fig. 6c, e - black arrows) and being arrested when these cracks reached the metal-ceramic interface.

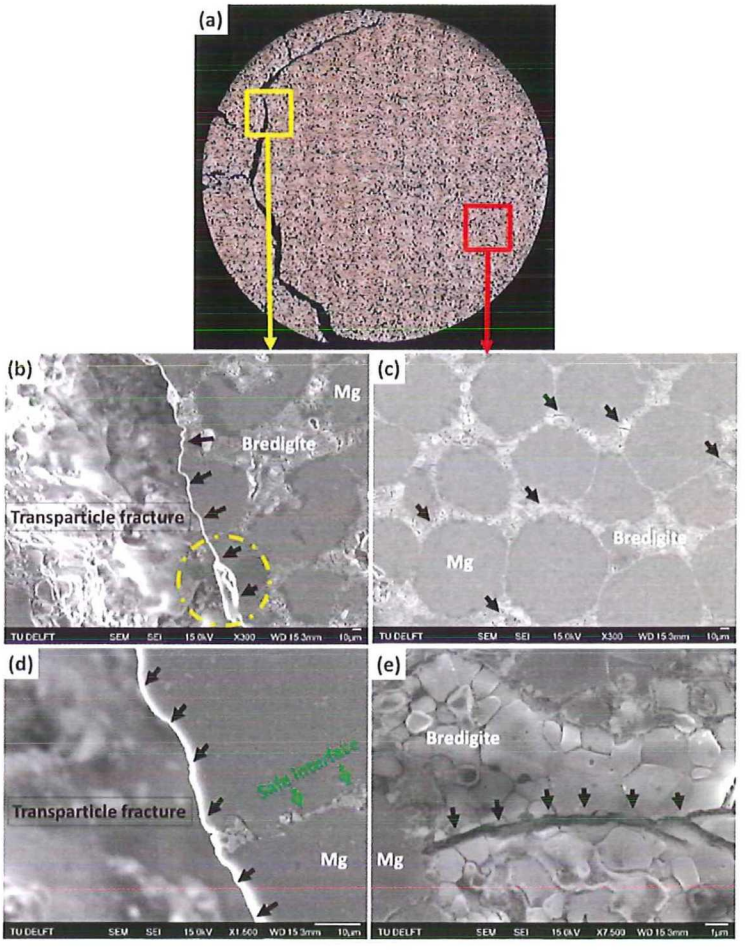

Fig. 6. Crack propagation pattern in a TT composite specimen (a) through Mg (first column) and bredigite (second column) original powder particles. Transparticle fracture through Mg (b, d – black arrows) and bredigite particles (c, e – black arrows) at different magnifications.

Fig. 7 shows the microstructure of the TT composite before and after indentation at different indentation loads. Increasing the indentation load from 0.49 to 9.80 N resulted in a larger value of microhardness, from 43.2 to 65.2 HV (Fig. 9a-d) and affected an increasing surface area of composite specimen (Fig. 7e-h), giving a better estimation of hardness on a larger scale. This is necessary since indenting specimens at different locations at the same load resulted in different values of microhardness (Fig. 7, second and third row). When the TT composite was indented at the Mg-

bredigite interface, it resulted in a higher microhardness value (62.2 HV) as compared to the value when the composite was indented on an Mg particle surrounded by bredigite particles (54.7 HV).

Upon a closer look at the microstructure, large twinning bands were observed in the affected plastic deformation region, and their number appeared to be directly related to the applied load (black arrows in Fig. 7e-h).

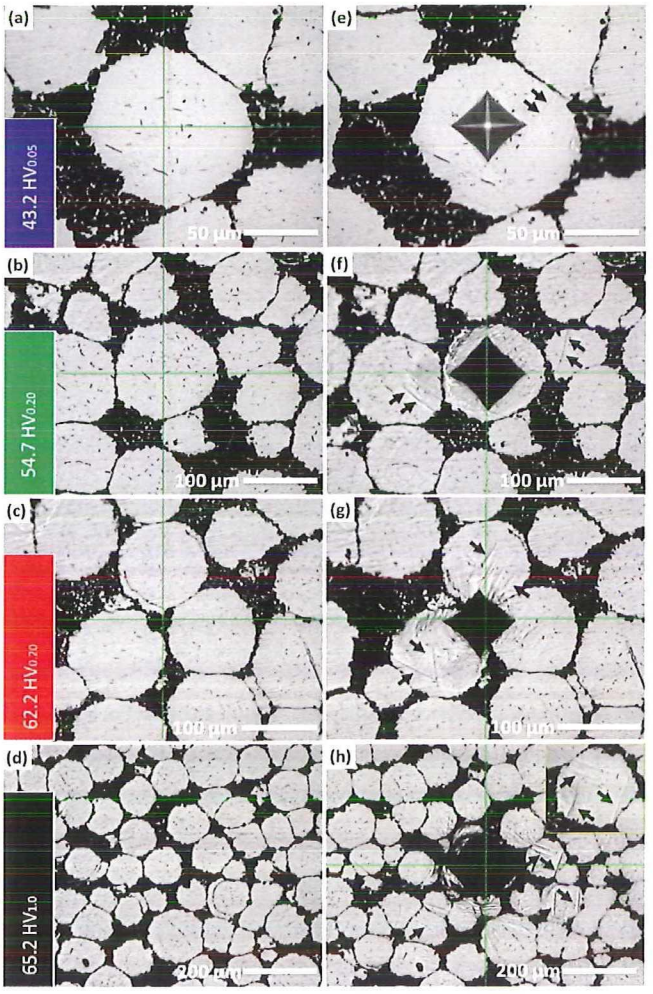

Fig. 7. Microstructures of the TT composite before (a-d) and after (e-h) indentation at $HV_{0.05}$ (a, e), $HV_{0.20}$ (b-c, f-g) and $HV_{1.0}$ (d, h), revealing large twin bands after the indentation (black arrows).

The mechanical properties of the specimens and comparison to those of human bone are summarized in Table 2.

The microhardness values of the composite specimens were close to those of Mg-hydroxyapatite composites reported in [27]. On the other hand, the yield and ultimate compressive strengths of the TT composite were significantly higher than AZ91, Mg-hydroxyapatite, Mg-ßTCP and Mg-fluorapatite composites [180].

Table 2. Mechanical properties of monolithic, PAS and TT specimens as compared to those of cortical and cancellous bone.

Material	σ_{CYS} (MPa)	σ_{UCS} (MPa)	Microhardness ($HV_{1.0}$)	ε_f (%)
Mg	90.5 ± 13.8	114.2 ± 21.4	38.2 ± 0.1	6.1 ± 0.9
PAS composite	135.0 ± 7.8	190.3±12.2	64.0±5.8	13.9 ± 1.8
TT composite	170.1 ± 6.4	225.5 ± 5.3	65.2 ± 6.8	17.1 ± 1.7
Cancellous bone	2-12 [110, 111]	1.7-12.0 [110, 111, 181]	32.9 ± 6.6 [182]	1.1 ± 0.6 [154]
Cortical bone	115.1 ± 16.4 [183]	153.6 ± 21.6 [183]	28–59 [150]	1.1-2.1 [42]

5.3.3. In vitro biodegradation

Fig. 8a shows the mass loss profiles of PAS and TT Mg-20% bredigite composite samples as compared to the profile of monolithic Mg sample as a function of immersion time in DMEM. Fig. 8b shows the ultimate compressive strengths of specimens as a function of immersion time. The monolithic Mg specimens did not pass the test period of one month and were totally dissolved after 12 days of immersion. The average degradation rate of monolithic magnesium , i.e., 31.41 $mg{\cdot}cm^{-2}{\cdot}day^{-1}$, was in good agreement with that determined in previous studies on cast magnesium specimens (19 - 44 $mg{\cdot}cm^{-2}{\cdot}day^{-1}$) [21]. However, the PAS and thermally treated (TT) Mg-20 %bredigite composites survived the test period of one month by dissolving at much slower rates than monolithic Mg. The thermal treatment considerably improved the degradation rate of the PAS composite (almost by 117 %). The calculated amounts of mass loss, after one month immersion in DMEM, were 100 %, 6.1 % and 2.8 %, equivalent to 31.41, 0.87, and 0.40 $mg/cm^2/day$ for Mg, PAS and TT Mg-20% bredigite, respectively. The average degradation rate of TT composite was slightly higher than that of WE43 in 3.5% NaCl solution (0.26 $mg.cm^{-2}.day^{-1}$), and much lower than that of cast ZE41 and AZ91 alloys at average dissolution rates of 7.71 and 6.95 $mg.cm^{-2}.day^{-1}$ in buffered Hank's solution, respectively [21, 113].

As a result of a lower degradation rate, the compressive yield strength of the TT composite remained within the strength range of cortical bone up to one month of immersion in DMEM (Fig. 8). On the other hand, the compressive yield strengths of monolithic and the PAS composite fell below the strength range of cortical bone within 12 days of immersion.

Localized corrosion was still the dominating degradation mechanism of the TT composite, initiating mostly from the bottom edges of the specimens (Fig. 8c-e yellow insets and black arrows). These localized corrosion features resulted in stress concentrations, facilitating the initiation of cracks when the material was under compressive loading, as shown in Fig. 8d and e (indicated by yellow arrows).

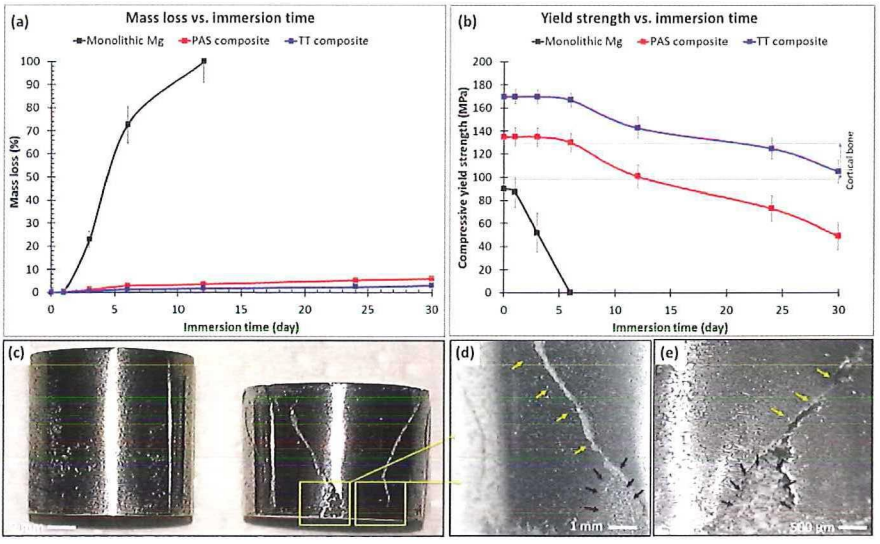

Fig. 8. Mass loss (a) and ultimate compressive strength (b) profiles of monolithic Mg and Mg-20% bredigite composite before (PAS) and after (TT) the thermal treatment as a function of immersion time. Optical micrographs of the TT composite subsequent to degradation tests and mechanical tests (c) with a magnified view (d, e) of localized corrosion (black arrows) and mechanical cracks (yellow arrows).

Fig. 9a shows the open circuit corrosion potentials (OCP) of monolithic Mg and Mg-20% bredigite composite before and after the heat treatment. The OCP potentials of samples first increased to more positive values and then gradually reached a steady state where the OCP potentials remained relatively constant. The TT composite showed a higher OCP value after 20 h immersion. In the PDP curves, the TT composite showed a mild shift towards higher cathodic activities with respect to the PAS specimen (Fig. 9b). It was difficult to judge the general anodic activity of the TT composite with respect to that of the PAS composite, because it was marginally shifting below and above that of the PAS composite during the polarization test (Fig. 9C).

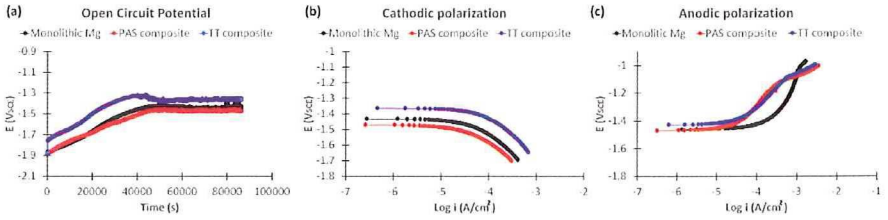

Fig. 9. OCP (a), cathodic (b) and anodic polarization (c) curves of the Mg-20% bredigite composite before (PAS composite) and after the heat treatment (TT composite).

5.3.4. Morphology and chemistry of the corrosion product layer

Fig. 10 shows the SEM micrographs taken from the TT composite after 1, 3, 6, 12, 24, and 30 days of immersion in DMEM. The surface layer after 1-day immersion revealed an integrated network of large cracks surrounding original Mg powder particles (Fig. 10a - black arrows). After three days, a second layer started to form on top of the first layer and the former contained smaller cracks, which posed a slightly lighter contrast with respect to the first layer under backscattered electron imaging (Fig. 10b-f – yellow arrows). Localized corrosion initiated during the first day of immersion, mostly at the bottom edges of specimens where the material was in direct contact with the die during processing, and further expanded over the edges as immersion time increased from 3 to 30 days (Fig. 10 - insets).

The SEM back-scattered micrographs at higher magnifications (Fig. 11a-d) showed that after one-day immersion, the surface layer was composed of submicron spherical agglomerates, being tightly bonded with each other and protecting the substrate from extensive dissolution. This initial compact layer also acted as a substrate for further heterogeneous nucleation of agglomerates. The sizes of spheres were about 500 nm and they precipitated on top of each other, forming larger agglomerates (Fig. 11b-d). The second layer of agglomerates was more porous and had less magnesium incorporated into its structure, which caused the Ca/P ratio of the surface layer to increase from 1.18 to 1.51 at day 12 (Fig. 11e-h).

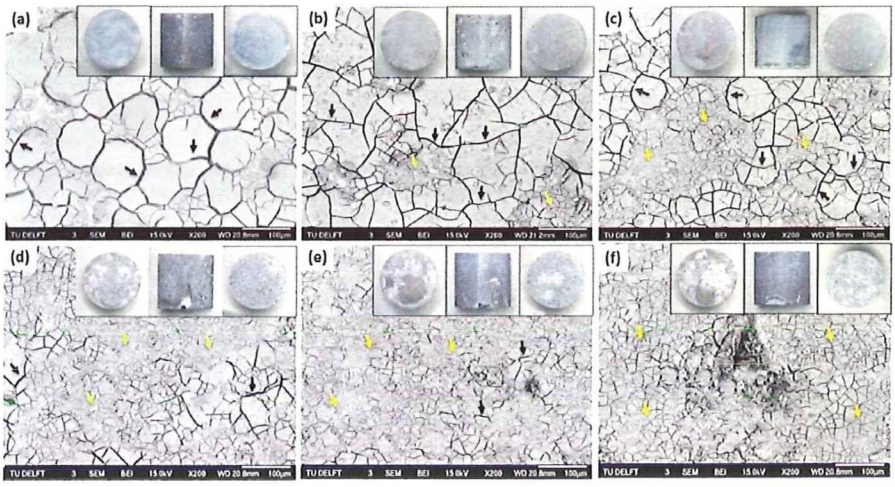

Fig. 10. SEM micrographs of the thermally treated Mg-20% bredigite composite after immersion in DMEM solution for 1 (a), 3 (b), 6 (c), 12 (d), 24 (e) and 30 (f) days, showing large cracks within the initial layer (black arrows) and relatively smaller cracks within the second layer (yellow arrows). The insets represent the bottom, front and top view of corroded samples, from left to right, respectively.

Our results show that after one-day immersion, the protective surface layer on the TT composite was mainly composed of O, C, Mg, Ca, and P (Fig. 11e-h). The Ca/P ratio of the surface layer (1.18) was lower than the stoichiometric value of hydroxyapatite (HA, 1.67), indicating that the surface layer was deficient in calcium. The FTIR spectra of the same surface (Fig. 11i-l) showed absorption bands of carbonate, phosphate and a low intensity band of HA hydroxyl ions [184], indicating the early formation of magnesium-containing hydroxyl-carbonate apatite precipitates. The absorption bands of silica appeared at day 6 and became more distinguishable from those of carbonate at day 12.

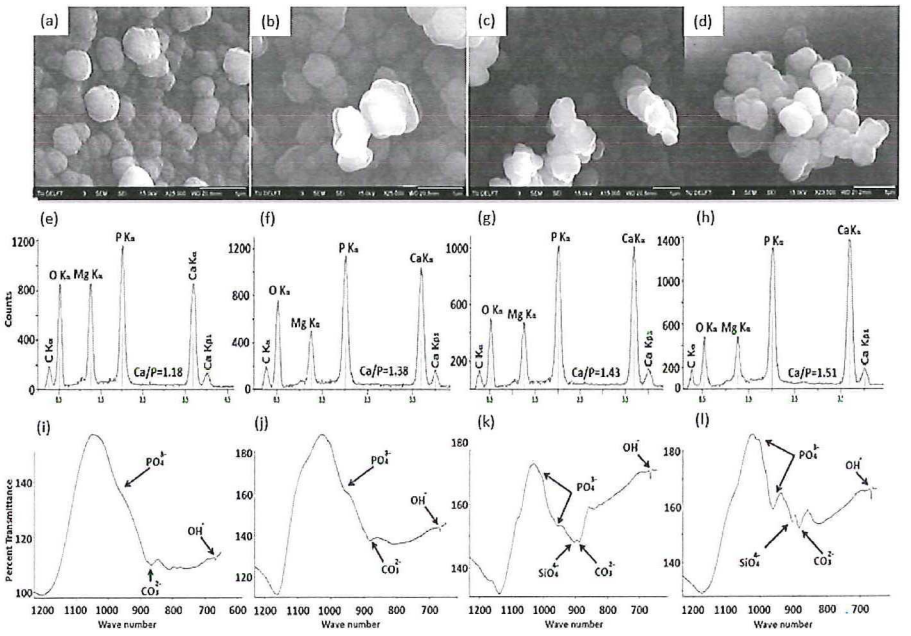

Fig. 11. Surface morphologies (a-d), EDS point scans (e-h) and FTIR spectra (i-l) of the thermally treated Mg-20% bredigite composite after 1 (1st column), 3 (2nd column), 6 (3rd column) and 12 (4th column) day immersion.

5.3.5. Cytotoxicity and bioactivity

Fig. 12a and b shows the elemental concentrations of Mg and Si in the original 1- and 3-day extracts of monolithic Mg and TT composite samples. The concentration of Mg in the original Mg extracts increased by 441 mg/L in 3-day extraction while that of Mg in the original TT composite extracts increased only by 40 mg/L. On the other hand, the amount of Si in the original TT extracts remained below 2 mg/L after 3-day extraction, revealing limited participation of Si in the original TT composite extracts.

The results of the MTT assay (Fig. 12c) revealed similar optical densities for the extracts of Mg and Mg-20% Bredigite TT composite after one day of immersion. After 6 and 12 days of incubation, the density of the MG-63 cells in the Mg original extract (concentration of Mg = 45 mg/L) was still slightly higher than that of cells in the TT composite extract (concentration of Mg = 14 mg/L), indicating that cells in the original 1-day Mg extracts were more viable. When the original 1-day extracts were diluted by 1/4 and 1/16, the cell viability values of the control, monolithic Mg

and the TT composite were almost the same with no statically significant differences, which means that the viability was dominated by the concentration of Mg ions in the extracts. The 3-day extraction period gave enough time to Mg and bredigite particles at the exposing surface to react with the solution, which resulted in higher concentrations of Mg and Si ions in DMEM. As a result, the 3-day Mg original extracts (concentration of Mg i = 486 mg/L) were cytotoxic from the beginning throughout the testing period (Fig. 12). At day 3, the viability of MG-63 cells and their density in the original extracts of the TT composite were higher than those in the Mg group and also the control group, indicating the stimulatory effect of the composite extracts on the proliferation of MG-63 cells (Fig. 12). The same as the 1-day extracts, 1/16 dilution of the original extracts resulted in similar viability levels for all the samples, showing once again that the viability of cells in contact with the extracts was closely related to the concentrations of ionic products, particularly Mg and Si ions in the DMEM solution.

The alkaline phosphatase activity of MG-63 cells in response to 1-day and 3-day extracts resembled the trend of viability assays (Fig. 12d, f). MG-63 cell differentiation in the 1-day original Mg extracts was higher than the control, although cell differentiation was obviously limited in 3-day Mg original extracts. On the other hand, the TT composite showed no sign of limited differentiation in its extracts. Similar to the MTT tests, diluting the extract by 1/16 overshadowed the effect of corrosion products on cell proliferation, resulting in a similar extent of cell proliferation for monolithic and TT composite samples.

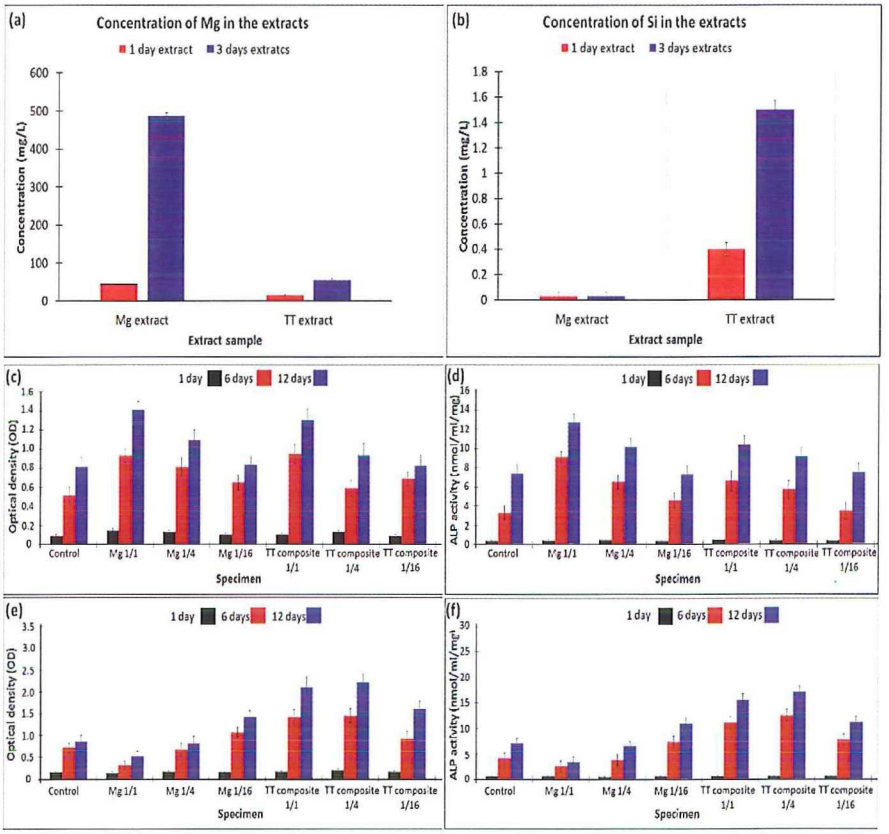

Fig. 12. Concentrations of Mg (a) and Si (b) ions in the original Mg and TT composite extracts after 1 and 3 days of extraction. MTT (a and c) and ALP assays (b and d) of MG-63 cells in 1-day (first row) and 3-day (second row) monolithic and TT composite extracts at different dilution ratios.

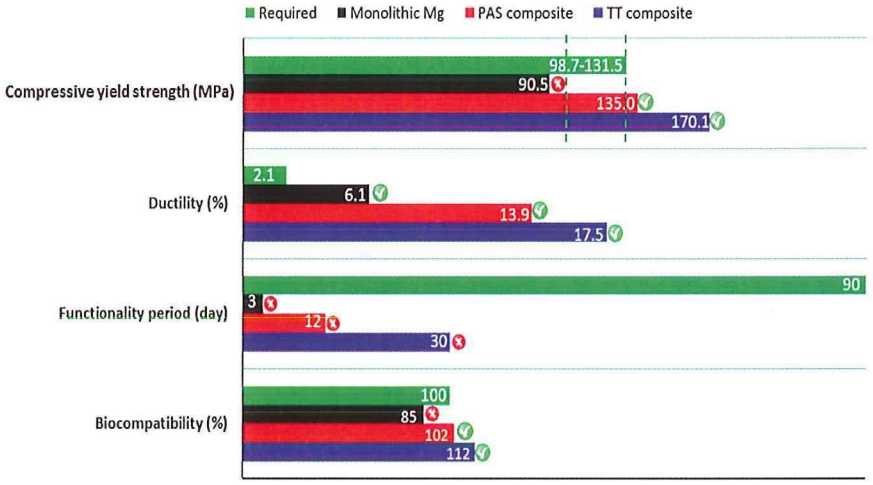

Fig. 13. Mechanical properties, degradation and biocompatibility of the PAS and TT Mg-bredigite composite compared to the minimum requirements for meaningful long-term in-vivo tests.

Fig. 13 illustrates the mechanical properties, mechanical functionality period and biocompatibility of the PAS and TT composite as compared to the minimum requirements for meaningful long-term in-vivo tests. It shows that to prepare the TT composite for meaningful long-term in-vivo tests, the period of the mechanical functionality in DMEM should be further extended to at least 3 months in order to allow full recovery of damaged bone before the composite loses its role as a mechanical support.

5.4. Discussion

The exothermic reaction between bredigite and Mg resembles the reaction between Mg and SiO_2 particles, because the atomic configuration of Si-O in bredigite is identical to that of the monolithic SiO_2 [185]. Both form tetrahedrons with Si atoms in the center, and oxygen atoms at the corner of the tetrahedrons. The only difference is that in SiO_2, bridging oxygen atoms at the corner of a tetrahedron are connected to another Si atom in the adjacent tetrahedron, while in the bioceramics the bridging O atoms could be connected to Mg and Ca atoms [186, 187]. The Mg-O bonds in the bioceramic form an octahedron structure with Mg atoms at the center and six bridging oxygen atoms at the corners of tetrahedrons [188]. Each

chain of tetrahedrons is connected to an adjacent octahedral layer (Mg octahedrons) by a bridging oxygen, producing a structure of alternating tetrahedral-octahedral-tetrahedral (T-O-T) layers. Calcium atoms connect the alternate T-O-T layers together with a coordination number of 8. Thus, three types of atomic bonding, namely Si-O-Si, Si-O-Mg and Si-O-Ca, co-exist in the crystal structure of bredigite. Practically, there are only two types of atomic bonds, namely Si-O-Si and Si-O-Ca that can be broken by Mg because magnesium cannot reduce its own oxide. Since dissociation of Si-O bonds during the solid-state exothermic reaction would release a larger amount of energy due to the higher bond dissociation energy of Si-O bonds, compared to that of Ca-O bonds [189, 190], its bonding energy will dominate the amount of energy that is released during the exothermic reaction (Fig. 2). The thermal dissociation of bredigite could be initiated through a reaction between Mg and Si-O-Si and Si-O-Ca bonds, in which Mg removes the bridging oxygen and oxidizes into MgO, exposing elemental Si and Ca to the interface and producing CaMgSi and MgO at the interface, which could be simplified as:

$16Mg + Ca_7MgSi_4O_{16} \rightarrow 16MgO + 4Si + 7Ca + Mg$ reaction 1

$Mg + Si + Ca \rightarrow CaMgSi$ reaction 2

Some intermediate products could also form during the thermal dissociation of bredigite, which would make reaction 1 and 2 more complex. This could be clarified by means of in-situ high temperature X-day diffraction. According to the ternary phase diagram of Ca-Mg-Si [191], if diffusion is allowed to take place, then the formation of CaMgSi above 400 °C would be possible when Ca atoms are added at the expense of Mg atoms in the structure of Mg_2Si to an equal atomic fraction of 33.33%. The structural similarity of bredigite to CaMgSi may also assist in the formation of the CaMgSi compound at the interface, because both have an orthorhombic crystal structure [186].

This CaMgSi layer allows diffusion through the Mg-bredigite interface (Fig. 3f-h), developing a much stronger and more integrated Mg-bredigite particle interface compared to that in the PAS composite (Fig. 5). The thermal treatment has a second benefit, i.e., the strengthening of Mg-Mg particle bonds through inter-particle diffusion. The PAS composite has a better chance to be sintered than original powder particles because the oxide layer on Mg powder particles is disrupted by large plastic deformation of Mg particles during PAS [24].

The in-situ fabrication of TT composites is a delicate process and thus requires careful control over the heating process. It was shown that when the composite was heated at a relatively fast heating rate (10, 15 and 20 $°C.min^{-1}$), the exothermic

reaction between Mg and bredigite particles took place at a much higher intensity, which generated a larger amount of heat at a short time (Fig. 2), resulting in significant mass loss which could cause the evaporation of Mg particles [24]. On the other hand, the TG curves at lower heating rates (<5°C·min^{-1}) revealed no evidence of possible mass loss during the exothermic reaction. In this research, the solid-state reaction between Mg and bredigite was successfully triggered while overcoming the issue of local evaporation of the Mg matrix [24] by heating the composites at 1 °C·min^{-1}. The reasons for the strong influence of heating rate on the reaction peak temperature and on the amount of heat released from the exothermic reaction are not clear and it requires a thorough thermoanalytical study which is out of the scope of this research.

A stronger particle interface in the TT composite resolved the issue of a lack of load transfer from the matrix to ceramic particles and cracks deviated from powder particle interfaces to the interior of Mg and bredigite particles, shifting the failure mode from *inter-particle* fracture to *trans-particle* fracture (Fig. 6) during compression testing. As a result, inter-particle fracture and surface delamination, which are often associated with metal matrix composites [24, 163], were prohibited, resulting in 26 and 18 % improvements in yield and ultimate compressive strengths, respectively (Table 2).

The difficulty of cross slip in HCP magnesium and the higher critical resolved shear stress (CRSS) required for the < c+a > slip (40 MPa) than for twining (2–3 MPa) [157, 192] reduce the ability of the material to deform by dislocation slip, and thus deformation twinning occurs (Fig. 7). However, the presence of micro-sized bredigite particles in the composite may activate non-basal dislocations necessary for the ductile behavior of the Mg matrix [24, 193]. This explains the enhanced strains of the composite obtained from the compression tests, in comparison with monolithic magnesium.

When TT composite specimens were immersed in the DMEM solution, surface cracks developed (Fig. 10) as a consequence of grain/powder particle boundary dissolution caused by high energy domains of dislocations at grain boundaries [61], which activated the anodic dissolution of the adjacent Mg matrix [79]. They provided pathways for fresh DMEM to reach the unreacted part of the substrate and thereby encouraging further dissolution of the matrix, leading to the accumulation of magnesium cations close to the corroding surface. Accumulation of Mg^{2+} cations close to the corroding surface encouraged the formation of a $Mg(OH)_2$ layer, with incorporation of Ca and P into this layer later (Fig. 11). The early submicron magnesium-containing hydroxyl-carbonate apatite precipitates, shown in Fig 11a-d, were deficient in calcium, resembling the biological HA, which is also

deficient in calcium [194]. The hydroxyl-carbonate apatite phase is chemically and structurally equivalent to the mineral phase in bone, which is responsible for the bonding of bone tissue with the implant [110, 195]. After 1-day immersion, more incorporation of Ca into HA crystals took place at the expense of Mg (Fig. 11e-h), owing to the better protection of the surface after one-day immersion and thus a smaller amount of Mg^{2+} became available around the corroding surface. Silicon from bredigite or CaMgSi was detected in the chemistry of the surface layer only after day 6 (Fig. 11k and l). One reason for relatively low silicon involvement is that calcium ions from bredigite were released preferentially to silicon ions by ion exchange with H^+ [123]. Thus, most of silicone in bredigite would stay within the unreacted part [196], forming a negatively charged surface with the functional group ($\equiv Si - O^-$) [123].

Localized corrosion of the Mg matrix eventually resulted in the accumulation of magnesium cations in the vicinity of the corroding surface, which could be hydrolyzed by water, producing H^+ and acidifying the microenvironment [79]. High concentration of H^+ discouraged the formation of a protective layer over the Mg matrix, which resulted in progressive local corrosion [17, 79]. The role of bredigite particles in blocking the progressive local corrosion sites in the Mg matrix was due to a relatively lower degradation rate of bredigite particles with respect to Mg [24] and more importantly, due to the consumption of an excess amount of H^+ ion inside a corrosion pit [197] through ion exchange by either magnesium or calcium [110, 197]. The CaMgSi interlayer could also assist bredigite in blocking the corrosion pathways by consuming H^+ ions, similar to bredigite [198], although its role in balancing the pH might be negligible, considering its limited surface area with respect to bredigite particles. As a result of slower degradation, the mechanical properties of the TT composite remained within the strength range of cortical bone for nearly a month after immersion, which outperformed monolithic and PAS specimens (Fig. 8). The original extracts were proven to be stimulatory to the proliferation and differentiation of MG-63 cells (Fig. 12).

However, as Illustrated in Fig. 13, the period of the mechanical functionality in DMEM should be further extended to at least 3 months in order to prepare the TT composite for a meaningful long-term in-vivo test.

One effective way to gain more control over the localized corrosion at the edges of specimens would be to limit, or in an ideal case, totally prevent the development of friction between the outer layer of composite specimen and the die during compaction. In this way, the material close to the edges of the specimen could move freely during compaction, enhancing the integrity of the microstructure particularly

around the edges. Examples of possible useful fabrication methods would be Acoustic Levitation (AL) and Hot Isostatic Pressing (HIP) [199, 200].

5.5. Conclusions

The in-situ fabrication of the Mg-20%bredigite composite was proven to be a feasible method to achieve homogeneity and integration in microstructure, mechanical compatibility to human bone, controlled degradation rate, cytocompatibility and bioactivity at the same time. It was found that the mechanical properties of the Mg-20%bredigite composite were significantly affected by the bonding strength of the composite constituents. The bonding strength of the Mg-bredigite interface was improved by triggering a solid-state exothermic reaction between Mg and bredigite particles, developing a CaMgSi intermetallic compound at the interface and enabling chemical interlocking at particle interfaces through diffusion across the CaMgSi interlayer.

The mechanical properties of the composite after the thermal treatment were comparable with those of human bone, outperforming monolithic and PAS specimens in strength and ductility. It shows that further improving the mechanical properties of the TT composite for orthopedic applications would not be necessary, although it is still possible if needed.

On the other hand, the degradation rate of the TT composite, particularly due to the localized corrosion, should be limited further to preserve the mechanical functionality of the composite for a longer period of time. Further research should be directed towards improving the degradation behavior of the TT composite by either removing susceptible areas for degradation in the microstructure, or by protecting the surface with a compact biodegradable surface layer to delay the degradation of the substrate.

CHAPTER 6

General Conclusions and Discussion

6.1. General conclusions

- In this research, advanced magnesium matrix composites containing bredigite bioceramic particles were successfully fabricated and shown to be promising biomaterials for load–bearing orthopedic applications.
- Our work emphasized the critical importance of the processing method and parameters to obtain an integrated, and almost defect-free microstructure in order to achieve slowed degradation and retained mechanical strength.
- Pressure Assisted Sintering (PAS) at 350 °C for 2 h under a pressure of 500 MPa was found to be an optimum condition for the processing of the Mg-matrix composites with high volume fractions (20-40 vol.%) of bredigite particles.
- The process of biodegradation of magnesium made from powder in DMEM started with grain and prior particle boundary dissolution, slowly attacking the bulk in a homogenous manner, followed by localized corrosion within the first three days of immersion, which surpassed grain/particle boundary dissolution.
- Once localized corrosion got initiated, the magnesium matrix could not re-establish a protective layer despite the high level of alkalinity (pH>10), leading to self-driven intense pit development and finally to total disintegration.
- Bredigite played an important role in improving the degradation resistance of magnesium due to its resistance to H^+- and Cl^--driven attacks, limiting the intense pit propagation into the magnesium matrix.
- The mechanical properties and corrosion resistance of the PAS Mg-20%bredigite composite can be further improved by thermally treating the composite at a temperature close to the melting temperature of magnesium.
- Despite the significant improvements made in this project, the localized corrosion, initiating at the edges of specimens remained to be the dominant corrosion mechanism of the thermally treated composite, which limited the period of mechanical functionality to a month. Thus, to preserve the mechanical functionality of the composite for a longer period of time, further research should be directed towards limiting or prohibiting this mechanism, which results in localized corrosion at the edges.

6.2. Discussion

6.2.1. Degradation behavior of magnesium-bredigite composites

Improving the biodegradation behavior of magnesium-based materials requires a full understanding of the underlying mechanisms of biodegradation in a specified condition (i.e., type of electrolyte, temperature, etc.), which in turn requires an array of systematic evaluations in an environment closely mimicking the biological conditions of the human body so as to minimize the inconsistencies between in-vitro and in-vivo tests due to poorly chosen test conditions for in-vitro tests. Accordingly, we conducted all the degradation studies in a simplified bioreactor, which simulated some of the conditions of the body (buffered DMEM solution at 37 °C and pH 7.45 – Chapter 2).

However, to perform representative in vitro experiments that display the in vivo situation in order to establish a correlation between in vitro and in vivo observations, other factors have to be considered. For example, human body is a dynamic environment, where pH is actively regulated, and contains amino acids, proteins and cells, as well as inorganic compounds. The simplified bioreactor used in this research was only capable of providing a static condition with no ability to actively control the pH (by CO_2 and O_2 exchange, kidneys and other biochemicals in the body) nor to involve or sustain living cells while conducting the biodegradation test. Thus, to better mimic the situations in-vivo, new generation of bioreactors should be equipped with adequate pH control and a liquid circulation system and have the ability to culture living cells.

The PAS (pressure-assisted sintering) Mg-bredigite composites degraded up to 25 times more slowly than monolithic Mg made from powder due to the resistance of bredigite to H^+- and Cl^--driven attacks, limiting intense pit propagation into the magnesium matrix, particularly around the edges of the specimens, to a certain extent. Thus when it comes to the choice of a reinforcing phase for biodegradable magnesium-based composites, greater resistivity to H^+- and Cl^--driven attacks relative to the magnesium matrix should be taken into account, if slower degradation rates are desired. There are other criteria, such as cytocompatibilty, bioactivity, osteogenic potential and adequate mechanical properties, ideally being close to those of cortical bone that should be also taken into account. By that logic, bredigite is a more suitable choice than the typically used calcium-phosphate-based compounds such as hydroxyapatite (HA) and tricalcium phosphate (TCP) in Mg-matrix composites, due to its excellent bioactivity and mechanical properties close to those of cortical bone.

The surface of the Mg-bredigite composites after immersion in DMEM transformed into a compact mixture of unreacted bredigite particles embedded in a layer of Mg, Ca, P and Si-containing compounds, which enhanced the ability to induce osteogenic differentiation and thus proved the potential to improve the quality and progression of bone healing (Chapter 3). To prove this potential further, long-term effects of degrading magnesium-bredigite implants on bone tissue in animal models, using continuous in vivo micro-Computed Tomography and histological staining should be investigated.

6.2.2 Fabrication process and mechanical properties of Mg-bredigite composites

When it comes to the choice of a suitable processing method for the composites, the pyrophoric nature of magnesium and its hardly deformable HCP crystal at temperatures below 225 ^{0}C, together with the differences in the physical, chemical and mechanical properties of the composite constituents (magnesium and bredigite) are the most important issues that should be taken into account.

As far as the fabrication of magnesium-based composite materials is concerned, solid-state fabrication methods are preferred over the liquid-state ones, such as casting, to avoid the risks due to the extreme (and dangerous) reactivity of magnesium in the liquid state, especially in case no suitable shielding gas is applied. We have chosen a solid-state powder metallurgy method - Pressure Assisted Sintering (PAS) to fabricate the bioceramic-reinforced magnesium matrix composites. One of the main advantages of this method over the traditional powder extrusion method is that extruded composite materials are prone to develop an anisotropic microstructure, being aligned in the extrusion direction, while PASed materials do not show any dependency on the processing direction. Moreover, extruding metal and ceramic particles together generates large shear forces between the constituents and a large amount of friction between the constituents and the die bearing, generating pores and defects in the microstructure.

Bredigite bioceramic particles contributed to the strengthening mechanisms of the magnesium matrix by acting as obstacles to the free movement of dislocations and thus, causing larger resistance to deformation (Chapter 4). In addition, the bioceramic-reinforced composites developed in this research revealed an interesting behavior of improved ductility, with respect to the monolithic metal, which could be due to the activation of non-basal dislocations during plastic deformation, and to a stronger powder particle interface, thereby delaying interparticle fracture to higher strains. This phenomenon overcomes the well-

known disadvantage of poor ductility, which is associated with most of other particle-reinforced metal matrix composites, offering a great flexibility in design and fabrication of magnesium matrix composites. The effect of activating non-basal dislocations during plastic deformation could be validated by analyzing the microstructure and texture of deformed composites by means of X-ray diffraction (XRD) and electron backscatter diffraction (EBSD).

On the other hand, it was demonstrated that an increase in the volume fraction of bredigite particles from 20 to 40 vol.% would not contribute to a further improvement of the strength but deteriorate the ductility due to the clustering of ceramic particles. Thus, to achieve optimum corrosion and mechanical performance, it is highly recommended to limit the volume fraction of reinforcing particles (i.e. bredigite) to 20 %.

The remaining pores in the microstructure were mostly located at the edges of the specimens which were in direct contact with the compaction die and thus experienced the highest friction. The localized porosity, close to the edges of composite specimens, is a common disadvantage of the P/M techniques (including PAS and extrusion), which is possible to be removed by machining off the outer layer. Nevertheless, it has an advantage over the casting techniques that are notorious for introducing pores throughout the bulk, e.g., gas cavities, which cannot be removed by machining off the outer layer. Alternatives to PAS to achieve a better integrated microstructure are proposed in the "future research" section below.

6.2.3. Improving the degradation and mechanical behavior of Mg matrix composite through in-situ solid-state oxidation

In chapter 4, it was demonstrated that reducing the degradation rate of magnesium increased the period of mechanical functionality because corrosion pits acted as nucleation sites for the further development of mechanical cracks, and mechanical cracks encouraged the initiation and growth of corrosion pits. Further improvement of the mechanical and degradation properties of the composite would be possible by annihilating the remaining weak spots in the microstructure, which are responsible for premature mechanical failure through interparticle fracture as well as high degradation rates through localized corrosion.

To prevent interparticle fracture and postponing the initiation of mechanical cracks to higher stresses, the bonding strength of Mg-bredigite interface should be improved. It was achieved by triggering a solid-state exothermic reaction between Mg and bredigite particles by sintering the composite with 20% bredigite at a

temperature close to the melting temperature of magnesium, developing a CaMgSi intermetallic compound at the interface, and enabling chemical interlocking at particle interfaces through diffusion across the CaMgSi interlayer (Chapter 5). The reaction resulted in a highly densified and integrated microstructure, which limited corrosion pits from propagating into the magnesium matrix, when the Mg-20% bredigite composite was immersed in a physiological solution. In addition, chemical interlocking between the constituents prohibited early interparticle fracture and subsequent surface delamination during compression testing, enabling the composite to withstand larger plastic deformation before mechanical failure, outperforming the monolithic and PAS specimens in strength and ductility. The mechanical strength of the Thermally Treated (TT) composite was comparable to that of cortical bone after one month of immersion. It shows that further improving the mechanical properties of the TT composite for orthopedic applications would not be necessary, although it is still possible if needed. On the other hand, an ideal biodegradable orthopedic implant should be able to preserve its mechanical functionality over the whole healing period of defected bone (3–6 months). Thus, future research should be directed towards further improving the corrosion resistance of the composite to prevent the pre-mature loss of mechanical functionality due to localized corrosion.

6.2.4. Future research

As mentioned earlier, the period of mechanical functionality of Mg-bredigite composites was limited to a month due to the localized corrosion, initiating at the edges of specimens.

One effective way to gain better control over localized corrosion at the edges of the specimen would be to limit, or in an ideal case, totally prevent the development of friction between the outer layer of the composite specimen and the die during compaction. In this way, the material close to the edges of the specimen could move freely during compaction, enhancing the integrity of the microstructure, particularly around the edges. An example of possible useful fabrication method would be Hot Isostatic Pressing (HIP). HIP is an important tool in powder metallurgy, which has been used to convert powder particles to fully dense components, resulting in better mechanical properties than those achieved by traditional casting or pressing and sintering fabrication methods. Complex components often require a lot of machining, resulting in costly material preparation. HIP has the ability to produce components with more complex geometry to near-net shape, which reduces material loss due to machining. In addition, HIPed components are isotropic in their properties, while the materials produced by traditional methods have a certain

microstructure that gives rise to different mechanical values depending on the loading direction. However, there are some downsides of the HIP technology. Firstly, it is generally applicable in to small production quantities, typically less than 10,000 pieces annually. Secondly, it is a more costly method than other powder metallurgy processes due to its slow processing speed.

Another way to extend the period of mechanical functionality of the composites would be to delay the onset of the degradation of the substrate by covering the exposing surfaces of the composites with a biodegradable coating, which gradually dissolves during immersion in DMEM. Surface modification methods are relatively less costly compared to fabricating new alloys and composites. Surface coatings are able to play the role of protecting the substrate from severe corrosion, particularly at initial stages after implantation. Some coating methods, such as chemical conversion coatings and plasma electrolytic oxidation (PEO) coatings, involve the magnesium substrate in the process of coating formation, which forms a layer that adheres strongly to the substrate, reducing the danger of partial delamination after implantation. Among the coating methods that involve the substrate in the surface layer formation, PEO provides high adhesion strength to substrate. However, the long term corrosion resistance of PEO coatings is not satisfactory due to its porous structure. Thus, reducing the porosity level should be further investigated for practical applications. One disadvantage of the substrate-involving surface layers is the relatively poor bioactivity of magnesium-based compounds compared to other compounds that contain bioactive elements such as calcium and silicon.

By limiting the involvement of the substrate in the formation of the surface layer, more effective coatings can be made that are composed of materials with better corrosion resistance and proper bioactivity such as silicon-containing hydroxyapatite. Particular attention should be paid to the adhesion strength of these types of coatings as they may pose a potential risk of partial delamination after implantation. To effectively cover the magnesium substrate with a layer that has proper adhesion, corrosion resistance and bioactivity, further research should be directed towards designing and fabricating a compact composite layer that involves the substrate in the process of coating formation, providing adhesion and corrosion resistance, which also contains bioactive compounds, providing adequate bioactivity.

By determining the period of mechanical functionality of the substrate, the corrosion rate of the composite surface coating could be engineered in such a way that provides adequate protection to the underlying substrate until the whole system (substrate + coating) reaches a functionality period that is satisfactory (e.g., three months).

Finally, impurities in the magnesium substrate, especially iron-containing phases, act as cathodic sites in galvanic corrosion, which accelerates the degradation of the substrate. Thus, using high-purity magnesium powder with iron impurity less than 2 ppm would result in much slower and more homogenous corrosion, improving the biodegradation behavior of Mg-bredigite composites to a considerable extent.

References

1. Johnell, O. and J. Kanis, *An estimate of the worldwide prevalence and disability associated with osteoporotic fractures.* Osteoporosis international, 2006. **17**(12): p. 1726-1733.
2. Willson, T., et al., *The clinical epidemiology of male osteoporosis: a review of the recent literature.* Clinical Epidemiology, 2015. **7**: p. 65-76.
3. Wade, S.W., et al., *Estimating prevalence of osteoporosis: examples from industrialized countries.* Archives of Osteoporosis, 2014. **9**(1): p. 182.
4. Svedbom, A., et al., *Osteoporosis in the European Union: a compendium of country-specific reports.* Archives of Osteoporosis, 2013. **8**(1-2): p. 137.
5. Gullberg, B., O. Johnell, and J. Kanis, *World-wide projections for hip fracture.* Osteoporosis international, 1997. **7**(5): p. 407-413.
6. Svedbom, A., et al., *Osteoporosis in the European Union: a compendium of country-specific reports.* Archives of osteoporosis, 2013. **8**(1-2): p. 137.
7. Matassi, F., et al., *Porous metal for orthopedics implants.* Clinical Cases in Mineral and Bone Metabolism, 2013. **10**(2): p. 111.
8. Jovanovic, S.A., H. Spiekermann, and E.J. Richter, *Bone regeneration around titanium dental implants in dehisced defect sites: a clinical study.* International Journal of Oral & Maxillofacial Implants, 1992. **7**(2).
9. Li, G., et al., *In vitro and in vivo study of additive manufactured porous Ti6Al4V scaffolds for repairing bone defects.* Scientific Reports, 2016. **6**: p. 34072.
10. Schmidt, M., H. Weber, and R. Schön, *Cobalt Chromium Molybdenum Metal Combination for Modular Hip Prostheses.* Clinical Orthopaedics and Related Research, 1996. **329**: p. S35-S47.
11. Williams, D. and G. Meachim, *A combined metallurgical and histological study of tissue-prosthesis interactions in orthopedic patients.* Journal of Biomedical Materials Research Part A, 1974. **8**(3): p. 1-9.
12. Kop, A.M. and E. Swarts, *Corrosion of a Hip Stem With a Modular Neck Taper Junction: A Retrieval Study of 16 Cases.* The Journal of Arthroplasty, 2009. **24**(7): p. 1019-1023.
13. Collire, J.P., et al., *Corrosion at the Interface of Cobalt-Alloy Heads on Titanium-Alloy Stems.* Clinical Orthopaedics and Related Research, 1991. **271**: p. 305.
14. Lhotka, C., et al., *Four-year study of cobalt and chromium blood levels in patients managed with two different metal-on-metal total hip replacements.* Journal of Orthopaedic Research, 2003. **21**(2): p. 189-195.
15. Jacobs, J.J., et al., *Metal release in patients who have had a primary total hip arthroplasty. A prospective, controlled, longitudinal study.* JBJS, 1998. **80**(10): p. 1447-58.

16. Jacobs, J.J., et al., *Metal degradation products: a cause for concern in metal-metal bearings?* Clinical orthopaedics and related research, 2003. **417**: p. 139-147.
17. Song, G.L. and A. Atrens, *Corrosion Mechanisms of Magnesium Alloys.* Advanced Engineering Materials, 1999. **1**(1): p. 11 - 33.
18. Witte, F., et al., *In vivo corrosion of four magnesium alloys and the associated bone response.* Biomaterials, 2005. **26**(17): p. 3557-3563.
19. Song, G.-L., *Corrosion of magnesium alloys*. 2011: Elsevier.
20. Witte, F., et al., *In vivo corrosion of four magnesium alloys and the associated bone response.* Biomaterials, 2005. **26**(17): p. 3557-3563.
21. Song, G., *Control of biodegradation of biocompatable magnesium alloys.* Corrosion Science, 2007. **49**(4): p. 1696-1701.
22. El-Rahman, S.S.A., *Neuropathology of aluminum toxicity in rats (glutamate and GABA impairment).* Pharmacological Research, 2003. **47**(3): p. 189-194.
23. Witte, F., et al., *Biodegradable magnesium-hydroxyapatite metal matrix composites.* Biomaterials, 2007. **28**(13): p. 2163-74.
24. Dezfuli, S.N., et al., *Fabrication of novel magnesium-matrix composites and their mechanical properties prior to and during in vitro degradation.* Journal of the Mechanical Behavior of Biomedical Materials, 2017. **67**: p. 74-86.
25. Feng, A. and Y. Han, *Mechanical and in vitro degradation behavior of ultrafine calcium polyphosphate reinforced magnesium-alloy composites.* Materials & Design, 2011. **32**(5): p. 2813-2820.
26. Huan, Z., et al., *In vitro degradation behavior and bioactivity of magnesium-Bioglass((R)) composites for orthopedic applications.* J Biomed Mater Res B Appl Biomater, 2011. **100B**(2): p. 437-446.
27. Witte, F., et al., *Biodegradable magnesium–hydroxyapatite metal matrix composites.* Biomaterials, 2007. **28**(13): p. 2163-2174.
28. Mastrogiacomo, M., et al., *Tissue engineering of bone: search for a better scaffold.* Orthodontics & craniofacial research, 2005. **8**(4): p. 277-284.
29. Kovtun, A., et al., *In vivo performance of novel soybean/gelatin-based bioactive and injectable hydroxyapatite foams.* Acta Biomaterialia, 2015. **12**: p. 242-249.
30. Carlisle, E.M., *Silicon: a possible factor in bone calcification.* Science, 1970. **167**(3916): p. 279-280.
31. Wu, C. and J. Chang, *Synthesis and in vitro bioactivity of bredigite powders.* J Biomater Appl, 2007. **21**(3): p. 251-63.
32. Yi, D., et al., *Bioactive bredigite coating with improved bonding strength, rapid apatite mineralization and excellent cytocompatibility.* Journal of biomaterials applications, 2014. **28**(9): p. 1343-1353.
33. Wu, C., et al., *Preparation and characteristics of a calcium magnesium silicate (bredigite) bioactive ceramic.* Biomaterials, 2005. **26**(16): p. 2925-31.

34. Zheng, Y., et al., *In vitro degradation and cytotoxicity of Mg/Ca composites produced by powder metallurgy.* Acta Biomaterialia, 2010. **6**(5): p. 1783-1791.
35. Kaplan, H.I., J.N. Hryn, and B.B. Clow, *Magnesium Technology 2000*. 2013: John Wiley & Sons.
36. !!! INVALID CITATION !!! [19, 32].
37. Woodard, J.R., et al., *The mechanical properties and osteoconductivity of hydroxyapatite bone scaffolds with multi-scale porosity.* Biomaterials, 2007. **28**(1): p. 45-54.
38. Athanasiou, K.A., et al., *Orthopaedic applications for PLA-PGA biodegradable polymers.* Arthroscopy: The Journal of Arthroscopic & Related Surgery, 1998. **14**(7): p. 726-737.
39. Temenoff, J.S. and A.G. Mikos, *Injectable biodegradable materials for orthopedic tissue engineering.* Biomaterials, 2000. **21**(23): p. 2405-2412.
40. Zeng, R., et al., *Progress and Challenge for Magnesium Alloys as Biomaterials.* Advanced Engineering Materials, 2008. **10**(8): p. B3-B14.
41. Huan, Z., et al., *In vitro degradation behavior and cytocompatibility of Mg–Zn–Zr alloys.* Journal of Materials Science: Materials in Medicine, 2010. **21**(9): p. 2623-2635.
42. Witte, F., et al., *Degradable biomaterials based on magnesium corrosion.* Current Opinion in Solid State and Materials Science, 2008. **12**(5-6): p. 63-72.
43. Zheng, Y.F., et al., *In vitro degradation and cytotoxicity of Mg/Ca composites produced by powder metallurgy.* Acta Biomater, 2010. **6**(5): p. 1783-91.
44. Gu, X., et al., *In vitro corrosion and biocompatibility of binary magnesium alloys.* Biomaterials, 2009. **30**(4): p. 484-498.
45. Bowen, P.K., J. Drelich, and J. Goldman, *A new in vitro–in vivo correlation for bioabsorbable magnesium stents from mechanical behavior.* Materials Science and Engineering: C, 2013. **33**(8): p. 5064-5070.
46. Gu, X.N., Y.F. Zheng, and L.J. Chen, *Influence of artificial biological fluid composition on the biocorrosion of potential orthopedic Mg–Ca, AZ31, AZ91 alloys.* Biomedical Materials, 2009. **4**(6): p. 065011.
47. Kirkland, N., et al., *Buffer-regulated biocorrosion of pure magnesium.* Journal of Materials Science: Materials in Medicine, 2012. **23**(2): p. 283-291.
48. Tas, A.C., *The use of physiological solutions or media in calcium phosphate synthesis and processing.* Acta Biomaterialia, 2014. **10**(5): p. 1771-1792.
49. Gilbert, D.L., *Buffering of Blood Plasma.* The Yale journal of biology and medicine, 1960. **32**(5): p. 378.
50. Ellison, G., J.V. Straumfjord, and J. Hummel, *Buffer capacities of human blood and plasma.* Clinical Chemistry, 1958. **4**(6): p. 452-461.

51. Ng, W.F., K.Y. Chiu, and F.T. Cheng, *Effect of pH on the in vitro corrosion rate of magnesium degradable implant material.* Materials Science and Engineering: C, 2010. **30**(6): p. 898-903.
52. Willumeit, R., et al., *Chemical surface alteration of biodegradable magnesium exposed to corrosion media.* Acta biomaterialia, 2011. **7**(6): p. 2704-2715.
53. Darzynkiewicz, Z. and B. Jacobson, *HEPES-buffered media in lymphocyte cultures.* Experimental Biology and Medicine, 1971. **136**(2): p. 387-393.
54. Ferguson, W.J., et al., *Hydrogen ion buffers for biological research.* Analytical Biochemistry, 1980. **104**(2): p. 300-310.
55. Yamamoto, A. and S. Hiromoto, *Effect of inorganic salts, amino acids and proteins on the degradation of pure magnesium in vitro.* Materials Science and Engineering: C, 2009. **29**(5): p. 1559-1568.
56. Doepke, A., et al., *A system for characterizing Mg corrosion in aqueous solutions using electrochemical sensors and impedance spectroscopy.* Acta Biomaterialia, 2013. **9**(11): p. 9211-9219.
57. Yang, L. and E. Zhang, *Biocorrosion behavior of magnesium alloy in different simulated fluids for biomedical application.* Materials Science and Engineering: C, 2009. **29**(5): p. 1691-1696.
58. Kirkland, N.T., N. Birbilis, and M.P. Staiger, *Assessing the corrosion of biodegradable magnesium implants: A critical review of current methodologies and their limitations.* Acta Biomaterialia, 2012. **8**(3): p. 925-936.
59. Song, G.-L. and Z. Xu, *The surface, microstructure and corrosion of magnesium alloy AZ31 sheet.* Electrochimica Acta, 2010. **55**(13): p. 4148-4161.
60. Aung, N.N. and W. Zhou, *Effect of grain size and twins on corrosion behaviour of AZ31B magnesium alloy.* Corrosion Science, 2010. **52**(2): p. 589-594.
61. Andrei, M., et al., *DC and AC polarisation study on magnesium alloys Influence of the mechanical deformation.* Materials and Corrosion, 2002. **53**(7): p. 455-461.
62. Song, G. and S. Song, *A possible biodegradable magnesium implant material.* Advanced Engineering Materials, 2007. **9**(4): p. 298-302.
63. Posner, A.S. and F. Betts, *Synthetic amorphous calcium phosphate and its relation to bone mineral structure.* Accounts of Chemical Research, 1975. **8**(8): p. 273-281.
64. Kim, S.R., et al., *Synthesis of Si, Mg substituted hydroxyapatites and their sintering behaviors.* Biomaterials, 2003. **24**(8): p. 1389-1398.
65. Ng, W., K. Chiu, and F. Cheng, *Effect of pH on the< i> in vitro</i> corrosion rate of magnesium degradable implant material.* Materials Science and Engineering: C, 2010. **30**(6): p. 898-903.

66. Serro, A.P., et al., *In vitro mineralization of a glass-ceramic of the MgO-3CaO · P2O5-SiO2 system: Wettability studies.* Journal of Biomedical Materials Research, 2002. **61**(1): p. 99-108.
67. Platt, G.M., et al., *In Silico Experiments of Carbon Dioxide Atmosphere and Buffer Type Effects on the Biomimetic Coating with Simulated Body Fluids.* Advances in Materials Physics & Chemistry, 2012. **2**(4).
68. Marques, P.A.A.P., et al., *Mineralisation of two calcium phosphate ceramics in biological model fluids.* Journal of Materials Chemistry, 2003. **13**(6): p. 1484-1490.
69. Xin, Y. and P.K. Chu, *Influence of Tris in simulated body fluid on degradation behavior of pure magnesium.* Materials Chemistry and Physics, 2010. **124**(1): p. 33-35.
70. Baes, C.F. and R.E. Mesmer, *Hydrolysis of cations.* 1976.
71. Robinson, H. and P. George, *Effect of Alloying and Impurity Elements in Magnesium Alloy Cast Anodes.* Corrosion, 1954. **10**(6): p. 182-188.
72. Bender, S., et al., *A new theory for the negative difference effect in magnesium corrosion.* Materials and Corrosion, 2012. **63**(8): p. 707-712.
73. Frankel, G.S., A. Samaniego, and N. Birbilis, *Evolution of hydrogen at dissolving magnesium surfaces.* Corrosion Science, 2013. **70**(0): p. 104-111.
74. Maguire, M.E. and J.A. Cowan, *Magnesium chemistry and biochemistry.* Biometals, 2002. **15**(3): p. 203-210.
75. Marier, J., *Dietary magnesium and drinking water: Effects on human health status.* Metal ions in biological systems, 1990. **26**: p. 85-104.
76. Wen, C., et al., *Compressibility of porous magnesium foam: dependency on porosity and pore size.* Materials letters, 2004. **58**(3): p. 357-360.
77. Witte, F., et al., *Cartilage repair on magnesium scaffolds used as a subchondral bone replacement.* Materialwissenschaft und Werkstofftechnik, 2006. **37**(6): p. 504-508.
78. Xu, L., et al., *In vivo corrosion behavior of Mg-Mn-Zn alloy for bone implant application.* Journal of Biomedical Materials Research Part A, 2007. **83**(3): p. 703-711.
79. Naddaf Dezfuli, S., et al., *Influence of HEPES buffer on the local pH and formation of surface layer during in vitro degradation tests of magnesium in DMEM.* Progress in Natural Science: Materials International, 2014. **24**(5): p. 531-538.
80. Kirkland, N.T., et al., *A survey of bio-corrosion rates of magnesium alloys.* Corrosion Science, 2010. **52**(2): p. 287-291.
81. Atrens, A., M. Liu, and N.I. Zainal Abidin, *Corrosion mechanism applicable to biodegradable magnesium implants.* Materials Science and Engineering: B, 2011. **176**(20): p. 1609-1636.
82. Fenwick, S., et al., *In end-stage renal failure, does infection lead to elevated plasma aluminium and neurotoxicity? Implications for monitoring.* Annals of clinical biochemistry, 2005. **42**(2): p. 149-152.

83. Nassif, N. and I. Ghayad, *Corrosion Protection and Surface Treatment of Magnesium Alloys Used for Orthopedic Applications.* Advances in Materials Science and Engineering, 2013. **2013**: p. 10.
84. Staiger, M.P., et al., *Magnesium and its alloys as orthopedic biomaterials: a review.* Biomaterials, 2006. **27**(9): p. 1728-34.
85. Liu, D., et al., *Fabrication of biodegradable nano-sized β-TCP/Mg composite by a novel melt shearing technology.* Materials Science and Engineering: C, 2012. **32**(5): p. 1253-1258.
86. Wang, Y., et al., *Corrosion properties in a simulated body fluid of Mg/β-TCP composites prepared by powder metallurgy.* International Journal of Minerals, Metallurgy, and Materials, 2012. **19**(11): p. 1040-1044.
87. Vallet-Regí, M. and D. Arcos, *Silicon substituted hydroxyapatites. A method to upgrade calcium phosphate based implants.* Journal of Materials chemistry, 2005. **15**(15): p. 1509-1516.
88. Gibson, I., S. Best, and W. Bonfield, *Chemical characterization of silicon-substituted hydroxyapatite.* Journal of biomedical materials research, 1999. **44**(4): p. 422-428.
89. Zhai, W., et al., *Stimulatory effects of the ionic products from Ca–Mg–Si bioceramics on both osteogenesis and angiogenesis in vitro.* Acta Biomaterialia, 2013. **9**(8): p. 8004-8014.
90. Huang, Z. and S. Yu, *Microstructure characterization on the formation of in situ Mg2Si and MgO reinforcements in AZ91D/Flyash composites.* Journal of Alloys and Compounds, 2011. **509**(2): p. 311-315.
91. Xia, L., et al., *Enhanced osteogenesis through nano-structured surface design of macroporous hydroxyapatite bioceramic scaffolds via activation of ERK and p38 MAPK signaling pathways.* Journal of Materials Chemistry B, 2013. **1**(40): p. 5403-5416.
92. Huan, Z., et al., *In vitro degradation behavior and bioactivity of magnesium-Bioglass® composites for orthopedic applications.* Journal of Biomedical Materials Research Part B: Applied Biomaterials, 2012. **100B**(2): p. 437-446.
93. Mauney, J.R., et al., *In vitro and in vivo evaluation of differentially demineralized cancellous bone scaffolds combined with human bone marrow stromal cells for tissue engineering.* Biomaterials, 2005. **26**(16): p. 3173-3185.
94. Cory, A.H., et al., *Use of an aqueous soluble tetrazolium/formazan assay for cell growth assays in culture.* Cancer communications, 1991. **3**(7): p. 207-212.
95. Lowry, O.H., et al., *The quantitative histochemistry of brain II. Enzyme measurements.* Journal of Biological Chemistry, 1954. **207**(1): p. 19-38.
96. Han, B. and D. Dunand, *Microstructure and mechanical properties of magnesium containing high volume fractions of yttria dispersoids.* Materials Science and Engineering: A, 2000. **277**(1): p. 297-304.

97. Avedesian, M.M. and H. Baker, *ASM specialty handbook: magnesium and magnesium alloys*. 1999, Ohio: ASM International.
98. Emley, E.F., *Principles of magnesium technology*. first ed. 1966, New York: Pergamon Press.
99. Courtney, T.H., *Mechanical behavior of materials*. second ed. 2005, Long Grove: Waveland Press.
100. del Campo, R., et al., *Mechanical properties and corrosion behavior of Mg–HAP composites.* J. Mech. Behav. Biomed. Mater., 2014. **39**: p. 238-246.
101. Gu, X., et al., *Microstructure, mechanical property, bio-corrosion and cytotoxicity evaluations of Mg/HA composites.* Materials Science and Engineering: C, 2010. **30**(6): p. 827-832.
102. Mazahery, A. and M.O. Shabani, *Plasticity and microstructure of A356 matrix nano composites.* Journal of King Saud University - Engineering Sciences, 2013. **25**(1): p. 41-48.
103. Agnew, S.R. and Ö. Duygulu, *Plastic anisotropy and the role of non-basal slip in magnesium alloy AZ31B.* International Journal of Plasticity, 2005. **21**(6): p. 1161-1193.
104. E Wong, W.L. and M. Gupta, *Simultaneously Improving Strength and Ductility of Magnesium using Nano-size SiC Particulates and Microwaves.* Advanced Engineering Materials, 2006. **8**(8): p. 735-740.
105. Wong, W.L.E. and M. Gupta, *Improving Overall Mechanical Performance of Magnesium Using Nano-Alumina Reinforcement and Energy Efficient Microwave Assisted Processing Route.* Advanced Engineering Materials, 2007. **9**(10): p. 902-909.
106. Chang, I. and Y. Zhao, *Advances in powder metallurgy: Properties, processing and applications*. 2013, London: Elsevier.
107. Krishnamurthy, S., I. Weiss, and F. Froes, *Consolidation of Rapidly Solidified Magnesium Alloy Powder.* Key Engineering Materials, 1991. **29**: p. 135-146.
108. Munitz, A., et al., *Microstructural Characterization of Cast Mg-TiC MMC's.* Int. J. Mater. Sci., 2012. **2**: p. 5.
109. Tun, K.S., et al., *Tensile and compressive responses of ceramic and metallic nanoparticle reinforced Mg composites.* Materials, 2013. **6**(5): p. 1826-1839.
110. Hench, L.L., *Bioceramics: from concept to clinic.* Journal of the American Ceramic Society, 1991. **74**(7): p. 1487-1510.
111. Hench, L.L. and J. Wilson, *An introduction to bioceramics*. Vol. 1. 1993, London: World Scientific.
112. Katti, K.S., *Biomaterials in total joint replacement.* Colloids and Surfaces B: Biointerfaces, 2004. **39**(3): p. 133-142.
113. Taltavull, C., et al., *Influence of the chloride ion concentration on the corrosion of high-purity Mg, ZE41 and AZ91 in buffered Hank's solution.* Journal of Materials Science: Materials in Medicine, 2014. **25**(2): p. 329-345.

114. Lei, T., et al., *On the corrosion behaviour of newly developed biodegradable Mg-based metal matrix composites produced by in situ reaction.* Corrosion Science, 2012. **54**: p. 270-277.
115. Williams, G. and H.N. McMurray, *Localized corrosion of magnesium in chloride-containing electrolyte studied by a scanning vibrating electrode technique.* Journal of the electrochemical Society, 2008. **155**(7): p. C340-C349.
116. Williams, G., H. ap Llwyd Dafydd, and R. Grace, *The localised corrosion of Mg alloy AZ31 in chloride containing electrolyte studied by a scanning vibrating electrode technique.* Electrochimica Acta, 2013. **109**(0): p. 489-501.
117. Song, Y., et al., *Biodegradable behaviors of AZ31 magnesium alloy in simulated body fluid.* Materials Science and Engineering: C, 2009. **29**(3): p. 1039-1045.
118. Liu, H., *The effects of surface and biomolecules on magnesium degradation and mesenchymal stem cell adhesion.* Journal of Biomedical Materials Research Part A, 2011. **99A**(2): p. 249-260.
119. Yun, Y., et al., *Biodegradable Mg corrosion and osteoblast cell culture studies.* Materials Science and Engineering: C, 2009. **29**(6): p. 1814-1821.
120. Yang, L., et al., *Effect of traces of silicon on the formation of Fe-rich particles in pure magnesium and the corrosion susceptibility of magnesium.* Journal of Alloys and Compounds, 2015. **619**(0): p. 396-400.
121. Jia, J., et al., *Development of magnesium calcium phosphate biocement for bone regeneration.* J R Soc Interface, 2010. **7**(49): p. 1171-80.
122. Razavi, M., et al., *Controlling the degradation rate of bioactive magnesium implants by electrophoretic deposition of akermanite coating.* Ceramics International, 2014. **40**(3): p. 3865-3872.
123. Liu, X., C. Ding, and P.K. Chu, *Mechanism of apatite formation on wollastonite coatings in simulated body fluids.* Biomaterials, 2004. **25**(10): p. 1755-1761.
124. Faix, J., et al., *Filopodia: Complex models for simple rods.* International Journal of Biochemistry and Cell Biology, 2009. **41**(8-9): p. 1656-1664.
125. Dorozhkin, S.V., *Calcium orthophosphate coatings on magnesium and its biodegradable alloys.* Acta Biomaterialia, 2014. **10**(7): p. 2919-2934.
126. Waterman, J., et al., *Corrosion resistance of biomimetic calcium phosphate coatings on magnesium due to varying pretreatment time.* Materials Science and Engineering B: Solid-State Materials for Advanced Technology, 2011. **176**(20): p. 1756-1760.
127. Sun, Z.L., J.C. Wataha, and C.T. Hanks, *Effects of metal ions on osteoblast-like cell metabolism and differentiation.* J. Biomed. Mater. Res., 1997. **34**: p. 29-37.
128. Han, H.-S., et al., *The modification of microstructure to improve the biodegradation and mechanical properties of a biodegradable Mg alloy.*

Journal of the mechanical behavior of biomedical materials, 2013. **20**: p. 54-60.
129. Gu, X., et al., *In vitro corrosion and biocompatibility of binary magnesium alloys.* Biomaterials, 2009. **30**(4): p. 484-98.
130. Ye, C.-h., et al., *In vitro corrosion and biocompatibility of phosphating modified WE43 magnesium alloy.* Transactions of Nonferrous Metals Society of China, 2013. **23**(4): p. 996-1001.
131. Yang, L., et al., *Element distribution in the corrosion layer and cytotoxicity of alloy Mg–10Dy during in vitro biodegradation.* Acta biomaterialia, 2013. **9**(10): p. 8475-8487.
132. Gu, X., et al., *In vitro degradation performance and biological response of a Mg–Zn–Zr alloy.* Materials Science and Engineering: B, 2011. **176**(20): p. 1778-1784.
133. Zhang, B., et al., *Mechanical properties, degradation performance and cytotoxicity of Mg–Zn–Ca biomedical alloys with different compositions.* Materials Science and Engineering: C, 2011. **31**(8): p. 1667-1673.
134. Li, H., et al., *Microstructures, mechanical and cytocompatibility of degradable Mg–Zn based orthopedic biomaterials.* Materials & Design, 2014. **58**: p. 43-51.
135. Sun, Y., et al., *Preparation and characterization of a new biomedical Mg–Zn–Ca alloy.* Materials & Design, 2012. **34**: p. 58-64.
136. Gupta, M. and G.K. Meenashisundaram, *Insight into Designing Biocompatible Magnesium Alloys and Composites: Processing, Mechanical and Corrosion Characteristics*. 2015, New York: Springer.
137. Sun, H., et al., *Proliferation and osteoblastic differentiation of human bone marrow-derived stromal cells on akermanite-bioactive ceramics.* Biomaterials, 2006. **27**(33): p. 5651-5657.
138. Tan, L., et al., *Biodegradable materials for bone repairs: a review.* Journal of Materials Science & Technology, 2013. **29**(6): p. 503-513.
139. Marom, R., et al., *Characterization of adhesion and differentiation markers of osteogenic marrow stromal cells.* Journal of cellular physiology, 2005. **202**(1): p. 41-48.
140. Han, P., C. Wu, and Y. Xiao, *The effect of silicate ions on proliferation, osteogenic differentiation and cell signalling pathways (WNT and SHH) of bone marrow stromal cells.* Biomater. Sci., 2013. **1**(4): p. 379-392.
141. Hing, K.A., et al., *Effect of silicon level on rate, quality and progression of bone healing within silicate-substituted porous hydroxyapatite scaffolds.* Biomaterials, 2006. **27**(29): p. 5014-5026.
142. Bureau, M.N., J.G. Legoux, and J. Denault, *Implantable biomimetic prosthetic bone*. 2009, Google Patents.
143. Hansen, D.C., *Metal corrosion in the human body: the ultimate bio-corrosion scenario.* The Electrochemical Society Interface, 2008. **17**(2): p. 31.

144. Kannan, M.B. and R.K.S. Raman, *In vitro degradation and mechanical integrity of calcium-containing magnesium alloys in modified-simulated body fluid.* Biomaterials, 2008. **29**(15): p. 2306-2314.
145. Chua, B., L. Lu, and M. Lai, *Influence of SiC particles on mechanical properties of Mg based composite.* Composite Structures, 1999. **47**(1): p. 595-601.
146. Nie, H., M. Schoenitz, and E.L. Dreizin, *Oxidation of Magnesium: Implication for Aging and Ignition.* The Journal of Physical Chemistry C, 2016. **120**(2): p. 974-983.
147. Muhammad, W.N.A.W., et al., *Microstructure and mechanical properties of magnesium composites prepared by spark plasma sintering technology.* Journal of Alloys and Compounds, 2011. **509**(20): p. 6021-6029.
148. Esen, Z., *TiNi Reinforced Magnesium Composites by Powder Metallurgy*, in *Magnesium Technology 2011*. 2011, John Wiley & Sons, Inc. p. 457-462.
149. Nordlien, J.H., et al., *A TEM investigation of naturally formed oxide films on pure magnesium.* Corrosion Science, 1997. **39**(8): p. 1397-1414.
150. Zwierzak, I., M. Baleani, and M. Viceconti, *Microindentation on cortical human bone: effects of tissue condition and indentation location on hardness values.* Proceedings of the Institution of Mechanical Engineers, Part H: Journal of Engineering in Medicine, 2009. **223**(7): p. 913-918.
151. Hvid, I., et al., *Compressive strength of tibial cancellous bone: Instron® and osteopenetrometer measurements in an autopsy material.* Acta Orthopaedica, 1983. **54**(6): p. 819-825.
152. Misch, C.E., Z. Qu, and M.W. Bidez, *Mechanical properties of trabecular bone in the human mandible: Implications for dental implant treatment planning and surgical placement.* Journal of Oral and Maxillofacial Surgery, 1999. **57**(6): p. 700-706.
153. Dall'Ara, E., et al., *The effect of tissue condition and applied load on Vickers hardness of human trabecular bone.* Journal of Biomechanics, 2007. **40**(14): p. 3267-3270.
154. Røhl, L., et al., *Tensile and compressive properties of cancellous bone.* Journal of Biomechanics, 1991. **24**(12): p. 1143-1149.
155. Koike, J., *Enhanced deformation mechanisms by anisotropic plasticity in polycrystalline Mg alloys at room temperature.* Metallurgical and Materials Transactions A, 2005. **36**(7): p. 1689-1696.
156. Obara, T., H. Yoshinga, and S. Morozumi, *{1122} ⟨1123⟩ Slip system in magnesium.* Acta Metallurgica, 1973. **21**(7): p. 845-853.
157. Reed-Hill, R.E. and W.D. Robertson, *Additional modes of deformation twinning in magnesium.* Acta Metallurgica, 1957. **5**(12): p. 717-727.
158. Muránsky, O., et al., *In situ neutron diffraction investigation of deformation twinning and pseudoelastic-like behaviour of extruded AZ31 magnesium alloy.* International Journal of Plasticity, 2009. **25**(6): p. 1107-1127.

159. Wonsiewicz, B.C., *Plasticity of magnesium crystals*. 1966, Massachusetts Institute of Technology.
160. Zhang, Z. and D.L. Chen, *Contribution of Orowan strengthening effect in particulate-reinforced metal matrix nanocomposites.* Materials Science and Engineering: A, 2008. **483–484**(0): p. 148-152.
161. Bohlen, J., et al., *On the influence of the grain size and solute content on the AE response of magnesium alloys tested in tension and compression.* Materials Science and Engineering: A, 2007. **462**(1–2): p. 302-306.
162. Scott, V.D. and M.H.M. Lindsay, *Dislocation vectors related to the ductility of beryllium.* Journal of Nuclear Materials, 1966. **18**(2): p. 176-186.
163. Luo, A., *Processing, microstructure, and mechanical behavior of cast magnesium metal matrix composites.* Metallurgical and Materials Transactions A, 1995. **26**(9): p. 2445-2455.
164. Bolotin, V.V., *Delaminations in composite structures: Its origin, buckling, growth and stability.* Composites Part B: Engineering, 1996. **27**(2): p. 129-145.
165. Güden, M., et al., *Effect of strain rate on the compressive mechanical behavior of a continuous alumina fiber reinforced ZE41A magnesium alloy based composite.* Materials Science and Engineering: A, 2006. **425**(1–2): p. 145-155.
166. Yoo, M.H., *Slip, twinning, and fracture in hexagonal close-packed metals.* Metallurgical Transactions A, 1981. **12**(3): p. 409-418.
167. Axen, N., et al., *Ceramic material and process for manufacturing*. 2003, Google Patents.
168. Bureau, M.N., J.G. Legoux, and J. Denault, *Implantable biomimetic prosthetic bone*. 2006, Google Patents.
169. Luo, A.A., *Magnesium casting technology for structural applications.* Journal of Magnesium and Alloys, 2013. **1**(1): p. 2-22.
170. Dezfuli, S.N., et al., *Fabrication of biocompatible titanium scaffolds using space holder technique.* J Mater Sci Mater Med, 2012. **23**(10): p. 2483-8.
171. Kulekci, M.K., *Magnesium and its alloys applications in automotive industry.* The International Journal of Advanced Manufacturing Technology, 2008. **39**(9): p. 851-865.
172. Witte, F., *The history of biodegradable magnesium implants: a review.* Acta biomaterialia, 2010. **6**(5): p. 1680-1692.
173. Staiger, M.P., et al., *Magnesium and its alloys as orthopedic biomaterials: A review.* Biomaterials, 2006. **27**(9): p. 1728-1734.
174. Liu, C., et al., *Influence of heat treatment on degradation behavior of bio-degradable die-cast AZ63 magnesium alloy in simulated body fluid.* Materials Science and Engineering: A, 2007. **456**(1–2): p. 350-357.
175. Alvarez-Lopez, M., et al., *Corrosion behaviour of AZ31 magnesium alloy with different grain sizes in simulated biological fluids.* Acta Biomaterialia, 2010. **6**(5): p. 1763-1771.

176. Hong, D., et al., *In vitro degradation and cytotoxicity response of Mg–4% Zn–0.5% Zr (ZK40) alloy as a potential biodegradable material.* Acta biomaterialia, 2013. **9**(10): p. 8534-8547.
177. NaddafDezfuli, S., et al., *Advanced bredigite-containing magnesium-matrix composites for biodegradable bone implant applications.* Materials Science and Engineering: C, 2017. **79**: p. 647-660.
178. Askeland, D.R. and P.P. Phulé, *The science and engineering of materials.* 2003.
179. Kondoh, K., et al., *In-situ synthesis of Mg2Si intermetallics via powder metallurgy process.* Materials Transactions, 2003. **44**(5): p. 981-985.
180. Haghshenas, M., *Mechanical characteristics of biodegradable magnesium matrix composites: A review.* Journal of Magnesium and Alloys.
181. Hvid, I., et al., *Compressive Strength of Tibial Cancellous Bone: Instron® and Osteopenetrometer Measurements in an Autopsy Material.* Acta orthopaedica Scandinavica, 1983. **54**(6): p. 819-825.
182. Dall'Ara, E., et al., *The effect of tissue condition and applied load on Vickers hardness of human trabecular bone.* Journal of Biomechanics, 2007. **40**(14): p. 3267-3270.
183. Mirzaali, M.J., et al., *Mechanical properties of cortical bone and their relationships with age, gender, composition and microindentation properties in the elderly.* Bone, 2016. **93**(Supplement C): p. 196-211.
184. Ślósarczyk, A., Z. Paszkiewicz, and C. Paluszkiewicz, *FTIR and XRD evaluation of carbonated hydroxyapatite powders synthesized by wet methods.* Journal of Molecular Structure, 2005. **744**: p. 657-661.
185. Umeda, J., et al., *Powder metallurgy magnesium composite with magnesium silicide in using rice husk silica particles.* Powder Technology, 2009. **189**(3): p. 399-403.
186. Carbonneau, Y., et al., *On the observation of a new ternary MgSiCa phase in Mg-Si alloys.* Metallurgical and Materials transactions A, 1998. **29**(6): p. 1759-1763.
187. Eisenmann, B., H. Schäfer, and A. Weiss, *Der Übergang vom „geordneten" Anti-PbCl2-Gitter zum Anti-PbFCl-Gitter: Ternäre Phasen ABX der Erdalkalimetalle mit Elementen der 4. Hauptgruppe (A = Ca, Sr, Ba; B = Mg; X = Si, Ge, Sn, Pb).* Zeitschrift für anorganische und allgemeine Chemie, 1972. **391**(3): p. 241-254.
188. Lee, K.H., et al., *Bredigite-structure orthosilicate phosphor as a green component for white LED: the structural and optical properties.* Optics express, 2012. **20**(6): p. 6248-6257.
189. Sanderson, R., *Chemical Bonds and Bonds Energy*. Vol. 21. 2012: Elsevier.
190. Christian, J.D., *Strength of chemical bonds.* Journal of Chemical Education, 1973. **50**(3): p. 176.

191. Gröbner, J., I. Chumak, and R. Schmid-Fetzer, *Experimental study of ternary Ca–Mg–Si phase equilibria and thermodynamic assessment of Ca–Si and Ca–Mg–Si systems.* Intermetallics, 2003. **11**(10): p. 1065-1074.
192. Mahdavian, M.M., L. Ghalandari, and M. Reihanian, *Accumulative roll bonding of multilayered Cu/Zn/Al: An evaluation of microstructure and mechanical properties.* Materials Science and Engineering: A, 2013. **579**: p. 99-107.
193. Reihanian, M., F.K. Hadadian, and M.H. Paydar, *Fabrication of Al–2 vol% Al2O3/SiC hybrid composite via accumulative roll bonding (ARB): An investigation of the microstructure and mechanical properties.* Materials Science and Engineering: A, 2014. **607**: p. 188-196.
194. Lu, W., et al., *Microstructure, corrosion resistance and biocompatibility of biomimetic HA-Based Ca-P coatings on ZK60 magnesium alloy.* Int. J. Electrochem. Sci, 2012. **7**: p. 12668-12679.
195. Kannan, M.B., *13 - Hydroxyapatite coating on biodegradable magnesium and magnesium-based alloys A2 - Mucalo, Michael*, in *Hydroxyapatite (Hap) for Biomedical Applications*. 2015, Woodhead Publishing. p. 289-306.
196. Hu, S., R. Zhang, and X. Zhang, *Study on mineral surface reacted with water at temperatures above 300°C and 23 MPa.* Research on Chemical Intermediates, 2011. **37**(2): p. 503-514.
197. Dixit, S. and S.A. Carroll, *Effect of solution saturation state and temperature on diopside dissolution.* Geochemical Transactions, 2007. **8**(1): p. 3.
198. Hagihara, K., et al., *Possibility of Mg- and Ca-based intermetallic compounds as new biodegradable implant materials.* Materials Science and Engineering: C, 2013. **33**(7): p. 4101-4111.
199. Scholz, M.S., B.W. Drinkwater, and R.S. Trask, *Ultrasonic assembly of anisotropic short fibre reinforced composites.* Ultrasonics, 2014. **54**(4): p. 1015-1019.
200. Carreño-Morelli, E., et al., *Carbon nanotube/magnesium composites.* physica status solidi (a), 2004. **201**(8): p. R53-R55.

Summary

When a bone is fractured, it loses its structural integrity which makes it unable to bear any mechanical load. Therefore, a broken bone must be supported until it regains its strength to handle the body's movement and weight.

A surgical procedure is needed to set a fractured bone. This procedure often involves repositioning the bone fragments into their natural position and then, attaching them together using internal fixation devices such as plates and screws. These fixation devices restore load-bearing capacity to bone, allowing the fractured bone to be healed by the primary bone healing mechanism.

To date, implants used for internal fixation are usually made from titanium and stainless steel, which are strong but, notorious for triggering adverse reactions such allergic responses caused by implant erosion in patients.

Therefore, permanent fixtures should be removed from the body after the fractured bone heals sufficiently, which imposes another invasive surgery on the patient.

The advent of biodegradable magnesium-based composites about two decades ago was an attempt to address the clinical complications regarding the permanent fixtures.

However, magnesium-based composites are still in their infancy, and a have a lot to achieve before being considered as fully functional materials for bone fixation purposes.

Currently, there are two major issues with magnesium composites. Firstly, most of the magnesium-based composites made to date lack sufficient mechanical integrity, making them unsuitable for load-bearing applications. The second, and the most important, issue would be the rapid degradation of magnesium when exposed to physiological solutions, causing pre-mature mechanical failure before the patient fully recovers.

The main aim of this thesis is to provide the necessary background and technical information to address these issues, and to be a reliable platform for future researches on the subject to build upon.

This thesis is organized into four main parts. In the first part, chapter 2 explores a feasible fabrication method to produce a monolithic magnesium specimen from its powder form with minimum structural dis-integrity, and analyzes its degradation behavior in a pseudo-physiological solution.

Chapters 3 and 4, as the second part of this thesis, focus on fabrication of a novel biodegradable magnesium-based composite, based on our understanding of the shortcomings of monolithic magnesium when it comes to exposure to physiological solutions.

Chapter 3, reveals a feasible method to fabricate a biodegradable magnesium-bredigite composite and explores the degradation behavior of this composite in a physiological solution.

Chapter 4, attempts at optimizing the fabrication parameters to achieve a composite with an integrated microstructure and sufficient mechanical strength.

By combining the results from chapter 3 and 4, a clear correlation between the corrosion mode and rate, and the loss of the mechanical properties of magnesium-bredigite composites during degradation in a physiological solution could be established.

It was concluded that the magnesium-bredigite composites suffer from inter-particle fracture under mechanical load, and localized corrosion upon exposure to physiological solutions, which limited the period of mechanical functionality up to a month.

Chapter 5, as the third part of this thesis, builds upon the conclusions that have been made from chapter 3 and 4, aiming at addressing the interparticle fracture and localized corrosion. In chapter 5, establishing a chemical bonding between powder particles through an in-situ oxidation process, as an additional bonding mechanism to the mechanical interlocking is proposed to tackle these issues.

It was concluded that the in-situ fabrication of the magnesium-bredigite composite was proven to be a feasible method to achieve homogeneity and integration in microstructure, mechanical compatibility to human bone, controlled degradation rate, and bioactivity at the same time.

However, On the other hand, the degradation rate of the composite, requires further improvement to preserve the mechanical functionality of the composite for a longer period of time. Further research should be directed towards improving the degradation.

Chapter 6, as the forth part of this thesis, evaluates the progress and examines the highlights of the previous chapters and provides practical guidelines for further research on the subject.

Curriculum Vitae

Sina NaddafDezfuli was born on September 4th, 1985 in New Delhi, India.

He moved to Iran in 1987, where he lived most of his life. He followed his high school education at Shiraz University High school (Shiraz, Iran), where he earned his diploma in 2003. He continued his education at Shiraz University, where he got his Bachelor of Science in Materials Science and Engineering in 2009.

Immediately after his B.Sc., he started his Master of Science study at Sharif University of Technology, where he received his M.Sc. degree with an honor in Biomedical Engineering – Biomaterials in 2011. He worked on the design and fabrication of titanium-based orthopedic implants, which was patented and awarded as the best invention by the committee of the Fajr International Inventions and Innovation Competetion in 2012.

In October 2012, Sina joined the Biomaterials and Tissue Biomechanics group in the Department of Biomechanical Engineering at Delft University of Technology to work on his PhD project on the "Biodegradable magnesium matrix composites" under the supervision of Prof. dr. Frans van der Helm and Dr. Jie Zhou, which was funded by the Dutch organization for health research and healthcare innovation (ZonMw).

List of publications

1. NaddafDezfuli, S., Huan, Z., Mol, J.M.C., Chang, J., Zhou, J., 2014. Influence of HEPES buffer on the local pH and formation of surface layer during in vitro degradation of magnesium in DMEM. Progress in Natural Science: Materials International 24, 531-538.

2. NaddafDezfuli, S., Huan, Z., Mol, J.M.C., Leeflang, S., Chang, J., Zhou, J., 2017. Advanced bredigite-containing magnesium-matrix composites for biodegradable bone implant application. Materials Science and Engineering C 79, 647-660.

3. NaddafDezfuli, S., Leeflang, S., Huan, Z., Chang, J., Zhou, J., 2017. Fabrication of novel magnesium-matrix composites and their mechanical properties prior to and during in vitro degradation. Journal of the Mechanical Behavior of Biomedical Materials 67, 74-86.

4. NaddafDezfuli, S., Brouwer, J.C., Mol, J.M.C., van der Helm, F.C.T., Zhou, J., 2018. Biodegradation and mechanical behavior of an advanced bioceramic-containing Mg matrix composite synthesized through in-situ solid-state oxidation. Journal of the mechanical behavior of biomedical materials 80, 209-221.

Acknowledgments

Since my admission to M.Sc. program, I have been dreaming of joining Delft University to pursue my doctorate. This would not have been possible without the people who granted me this chance. Therefore, it is my pleasure to thank those who made it possible, including my supervisors, Dr. Jie Zhou and Prof. Frans van der Helm, who trusted me to perform independent research.

Doing experimental research was the key element to accomplish this research. I would like to thank Sander van Asperen, and Sander Leeflang for their help and support. I would like to dedicate my special thanks to Hans Brouwer, my friend and colleague, who has always believed in me and helped me in this challenging process without hesitation.

My special regards goes to Prof. Arjan Mol and Prof. Wim Sloof who shared their precious knowledge with me, and generously provided me with necessary equipment to conduct this research.

I would not have enjoyed my time at TU Delft as much if it was not for my colleagues and friends Rosa, Jamal, Shahram, Paul, Saber, Mohammad, Dineke, Anouk, Diones, Sabrina and others.

The financial support of The Netherlands Organization for Health Research and Development (ZonMw) for this research is greatly appreciated.

And finally, I would like to thank my family. My mom and dad who were always an inspiration to me and supported me in every step of my life. I would like to thank my only brother for being the best friend for me. This thesis would not have been possible without their love and support.

Sina

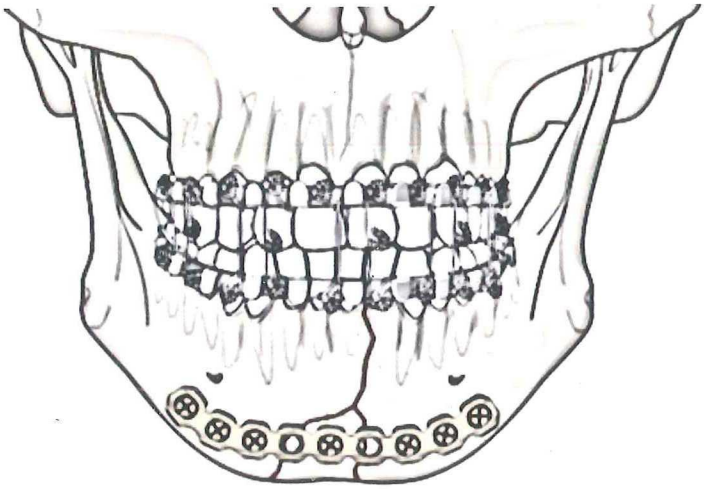

TU Delft